

Durability 2000

*ACCELERATED
AND OUTDOOR
WEATHERING TESTING*

*WARREN D. KETOLA AND
JOHN D. EVANS, EDITORS*



STP 1385

STP 1385

Durability 2000: Accelerated and Outdoor Weathering Testing

Warren D. Ketola and John D. Evans, Editors

ASTM Stock Number: STP1385



ASTM
100 Barr Harbor Drive
PO Box C700
West Conshohocken, PA 19428-2959

Printed in the U.S.A.

Library of Congress Cataloging-in-Publication Data

Durability 2000: accelerated and outdoor weathering testing

Warren D. Ketola and John D. Evans, editors.

p. cm.—(STP ; 1385)

ASTM Stock Number: STP1385

Includes bibliographical references.

ISBN 0-8031-2856-8

1. Testing. 2. Accelerated life testing. 3. Weathering. I. Ketola, Warren D., 1948–
II. Evans, John D., 1967– III. ASTM Committee G3 on Weathering and Durability.
IV. ASTM special technical publication; 1385.

TA410.D78 2000

620.1'12—dc21

00-056917

Copyright © 2000 AMERICAN SOCIETY FOR TESTING AND MATERIALS, West Conshohocken, PA. All rights reserved. This material may not be reproduced or copied, in whole or in part, in any printed, mechanical, electronic, film, or other distribution and storage media, without the written consent of the publisher.

Photocopy Rights

Authorization to photocopy items for internal, personal, or educational classroom use, or the internal, personal, or educational classroom use of specific clients, is granted by the American Society for Testing and Materials (ASTM) provided that the appropriate fee is paid to the Copyright Clearance Center, 222 Rosewood Drive, Danvers, MA 01923; Tel: 978-750-8400; online: <http://www.copyright.com/>.

Peer Review Policy

Each paper published in this volume was evaluated by two peer reviewers and at least one editor. The authors addressed all of the reviewers' comments to the satisfaction of both the technical editor(s) and the ASTM Committee on Publications.

To make technical information available as quickly as possible, the peer-reviewed papers in this publication were prepared "camera-ready" as submitted by the authors.

The quality of the papers in this publication reflects not only the obvious efforts of the authors and the technical editor(s), but also the work of the peer reviewers. In keeping with long-standing publication practices, ASTM maintains the anonymity of the peer reviewers. The ASTM Committee on Publications acknowledges with appreciation their dedication and contribution of time and effort on behalf of ASTM.

Foreword

This publication, *Durability 2000: Accelerated and Outdoor Weathering Testing*, contains papers presented at the symposium of the same name held in New Orleans, Louisiana, on 25–26 January 2000. The symposium was sponsored by ASTM Committee G3 on Weathering and Durability. The symposium co-chairmen were Warren D. Ketola, 3M Traffic Control, Materials Division, and John D. Evans, DuPont Automotive.

Contents

Overview

vii

CHARACTERIZATION

- Salt Spray Performance Evaluation: Proposed Image-Analysis-Based Test Method**—Y. J. WARBURTON AND D. L. GIBBON 1
- Comparative Study of Standard Weathering Test Methods Using Image Analysis**—F. LEE, B. POURDEYHIMI, AND J. MARTIN 15
- On the Use of Ion Scattering Spectroscopy to Predict the Outdoor Durability of Polymeric Films**—R. R. ADKINS 35
- Activation Spectra: Techniques and Applications to Stabilization and Stability Testing of Materials**—N. D. SEARLE 41

OUTDOOR

- Stationary Rack and Black Box Under Glass Exposures of Mineral Filled Polyethylene in Inland and Marine Tropical Climates**—L. P. VELEVA AND A. VALADEZ-GONZALEZ 61

ACCELERATED

- Stress Analysis and Accelerated Test Design for Interior Light Environments**—W. D. KETOLA, R. M. FISCHER, AND L. J. THOMAS 75
- Exposure Test Results for Inkjet Inks in Interior Light Environments**—R. M. FISCHER AND W. D. KETOLA 87
- Advances in Accelerated Weathering Instrumentation Technology Using Advanced Control Systems**—B. PATEL, F. LEE, AND K. SCOTT 103
- Predicting the Durability of Building Stone Using Accelerated Weathering**—S. A. BORTZ AND B. WONNEBERGER 116

Lightfastness of Artists' Pencils: Natural and Accelerated Exposure Results— P. J. BRENNAN AND E. T. EVERETT	133
SERVICE LIFE	
Calculation of the Spectral Irradiance of Solar Radiation for the Lifetime Prediction of Polymer Materials— D. KOCKOTT AND G. MANIER	151
Estimating the Durability of Roofing Systems— C. G. CASH	165
The Durability of Modern Sculptures Constructed of Glass— P. B. ADAMS AND H. B. TRE'	176

Overview

Weathering and durability issues play an important role in the performance of many products that are used both outdoors and indoors. Products used in both environments are exposed to degradation caused by light, heat, moisture and the effects of pollutants. Customer expectations for durability are increasing and today's market often requires faster introduction of new products. These factors require a better understanding of the exposure stresses in both indoor and outdoor environments, more reliable laboratory accelerated tests, and analysis techniques that provide for more precise characterization of the changes caused by exposure.

STP 1385 represents the work of a number of researchers presented at Durability 2000: Accelerated and Outdoor Weathering Testing, January 25 and 26, 2000, in New Orleans, Louisiana. This was the third in a series of symposia sponsored by the ASTM G3 Committee on Weathering and Durability in its continuing effort to promote research leading to advances and innovations in durability testing. The papers presented in STP 1385 are divided into three categories: (1) characterization of materials that have been subjected to exposure tests; (2) advances in understanding or new developments in either outdoor, indoor, or laboratory accelerated tests; and (3) service life prediction.

Material Characterization

Many products or materials are evaluated using visual inspection for changes in important appearance or other attributes caused by exposure. These visual inspections can be imprecise because of differences in assessment criteria of those conducting the evaluation. The papers by Warburton and Gibbon and Lee et al. describe the use of images analysis techniques that can significantly improve the repeatability and reproducibility of appearance characterization of a variety of materials, appearance attributes, and exposure tests. Very long laboratory accelerated or outdoor exposures are often needed to produce measurable changes in physical properties of a material. Analytical techniques that can detect changes that correspond to loss of physical properties can significantly shorten exposure times needed to evaluate different materials or material formulations. Adkins reports on the use of ion scattering spectroscopy to measure H/C and O/C ratios as a function of depth in materials exposed for 500 hours in a laboratory accelerated test. The H/C and O/C ratios correlated with physical property changes produced in long term outdoor exposures of the same materials. In many cases it is important to know which spectral regions of the light source used for exposure are primarily responsible for degradation. Searle describes monochromatic and polychromatic techniques for determining this "activation spectrum" of a material and shows it can be used for the development of more light stable materials and in the design of laboratory accelerated tests.

Developments in Outdoor, Indoor, and Laboratory Accelerated Exposure Tests

The type and rate of degradation may vary significantly with the type of climate where a product is used. Veleva and Valadez-Gonzalez report on black box under glass exposures of mineral filled polyethylene that were conducted in two different climates. This research showed that for black box under glass exposures of this material, the degradation mechanism did not change, but the rate of degradation was related to differences in specific climate

parameters. Ketola et al. and Fischer describe the development and evaluation of a laboratory accelerated test to simulate a specific indoor light environment. Results from the new test are compared to those from conventional laboratory accelerated test in order to determine which can best be used to estimate long term color stability of a series on ink-jet inks. Patel et al. describe improvements in techniques used to control irradiance, temperature, and humidity in laboratory accelerated exposure tests and show how more modern equipment can provide more consistent exposure conditions. Bortz and Wonneberger report on the development of a laboratory accelerated exposure test that has been successfully used to estimate the long-term durability of building stone. This test is based on a cyclic freeze/thaw immersion of the stone material in acidic solution that simulates the effects of exposure in polluted environments. Brennan and Everett report on results from outdoor and laboratory accelerated exposure tests that are being done as part of an effort to develop a new ASTM standard for assessing lightfastness of artists' colored pencils. In general, performance ranking produced better agreement between the tests than a rating system.

Service Life Prediction

Predicting service life of materials is the ultimate goal of any exposure program. Meaningful predictions of service life are contingent upon reliable measurements of the exposure stresses that can affect durability. Kockott and Manier describe a computer model that can be used to determine the spectral power distribution of daylight in many different locations. This program can be used to more realistically estimate the radiant exposures in critical spectral regions in a variety of climates. Cash reports on a method for estimating the durability of a variety of roofing materials based on thermal load and various construction and design parameters. Adams and Tré show how characterization of the properties of a glass and its response to accelerated environmental stresses can be used to determine that a sculpture made of the glass will remain relatively unchanged for at least 20 years.

Significant advances have been made in exposure tests and the methods used to characterize materials that have been subjected to exposure tests. Some of these advances may ultimately be incorporated into ASTM standards describing durability tests or methods for material characterization. The ASTM G3 Committee is committed to promoting this research. We hope that you find the advances reported in STP 1385 helpful in your research and encourage you to participate in the work of the ASTM G3 Committee.

Warren D. Ketola

3M Traffic Control Materials Division
St. Paul, MN
Symposium Co-chairman and editor

John D. Evans

DuPont Automotive
Troy, MI
Symposium co-chair and editor

CHARACTERIZATION

Yi J. Warburton¹ and Donald L. Gibbon¹

Salt Spray Performance Evaluation: Proposed Image-Analysis-Based Test Method

Reference: Warburton, Y. J. and Gibbon, D. L., “Salt Spray Performance Evaluation: Proposed Image-Analysis-Based Test Method,” *Durability 2000: Accelerated and Outdoor Weathering Testing, ASTM STP 1385*, J. D. Evans and W. D. Ketola, Eds., American Society for Testing and Materials, West Conshohocken, PA, 2000.

Abstract: ASTM Test Method for Evaluation of Painted or Coated Specimens Subjected to Corrosive Environments (D 1654-92) is the current industry standard. This standard assigns a number, from 0 to 10, to reflect the width of the paint delaminated as measured from a scribe line to the creepage front. At times when the width along the scribe is not uniform, it is difficult to apply this standard. The difficulty lies in the fact that the standard is attempting to describe a two-dimensional pattern with a linear parameter. A two-dimensional parameter should be more suitable, and delaminated area seemed to be an obvious choice. Image analysis is a powerful tool to aid in the evaluation of the proposed parameter. The results using percentage area correlate well and linearly with D 1654 ratings. Effects of scribe length, paint color, reproducibility, and operator-to-operator variance are also discussed.

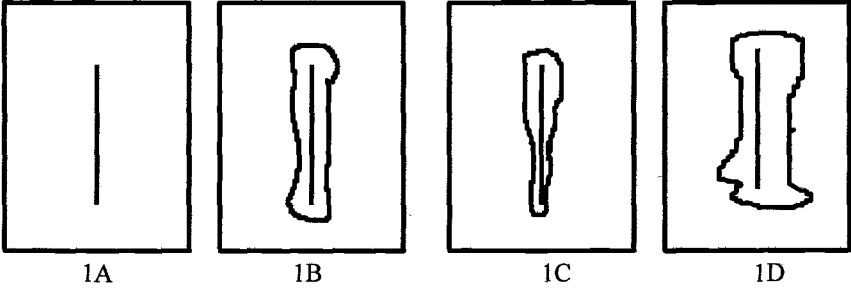
Keywords: corrosion, D 1654-92, salt fog, salt spray, B117, accelerated weathering, image analysis

Introduction

Accelerated weathering tests are routinely performed to rank and estimate the corrosion resistance of painted metal substrates. Neutral salt fog/spray, in accordance with ASTM Standard Practice for Operating Salt Spray (Fog) Testing Apparatus (B 117-94), is one of most commonly employed methods in the paint and metal pretreatment industries. For panel testing, typically a straight line is scribed at the center through the paint to expose the substrate metal before the panel is placed in the test chamber, as shown in Figure 1A. At the completion of the test, the scribe line is either scraped or blown with an air gun in accordance with ASTM Test Method for

¹ Research Associate and Research Fellow, respectively, Technology Group, Calgon Corporation, P.O. Box 1346, Pittsburgh, PA 15230.

Evaluation of Painted or Coated Specimens Subjected to Corrosive Environments (D 1654-92) to reveal delaminated areas as shown in Figures 1B to 1D.



- 1A: Scribe line before exposure test.
- 1B: Creepage pattern uniform along the scribe and symmetric across the scribe.
- 1C: Creepage pattern non-uniform along the scribe, symmetric across the scribe.
- 1D: Creepage pattern non-uniform along the scribe, asymmetric across the scribe.

Figure 1 - Illustration of Various Creepage Patterns.

D 1654-92 assigns a number, from 0 to 10 (Table 1), to reflect the width of the paint delaminated as measured from the scribe line to the creepage front.

Table 1 - Rating of Failure at Scribe.

Millimeters	Representative Mean Creepage From Scribe	
	Inches (Approximate)	Rating Number
Zero	0	10
Over 0 to 0.5	0 to 1/64	9
Over 0.5 to 1.0	1/64 to 1/32	8
Over 1.0 to 2.0	1/32 to 1/16	7
Over 2.0 to 3.0	1/16 to 1/8	6
Over 3.0 to 5.0	1/8 to 3/16	5
Over 5.0 to 7.0	3/16 to 1/4	4
Over 7.0 to 10.0	1/4 to 3/8	3
Over 10.0 to 13.0	3/8 to 1/2	2
Over 13.0 to 16.0	1/2 to 5/8	1
Over 16.0 to more	5/8 to more	0

This standard works well with a relatively uniform and symmetric creepage pattern, as shown in Figure 1B. However, in situations when either the width along the scribe is non-uniform, as shown in Figure 1C, or the creepage is asymmetric across the scribe, as shown in Figure 1D, it is difficult to apply D 1654-92 objectively. The standard calls for documentation of the representative mean, maximum, and minimum creepage from the scribe. One way of determining the mean is to average five readings along the scribe, as shown in Figure 2: for Figure 2A r_{11} through r_{15} , and for Figure 2B r_{21} through r_{25} . Figures 2A and 2B have identical means, maxima, and minima but the delaminated area in Figure 2B is 20% larger than in Figure 2A. Mathematically, since

$(r_{\max}+r_{\min}+r_1+r_2+r_3)/5=r_{\text{mean}}$, even if $\max(r_{\max})$, $\min(r_{\min})$ and $\text{mean}(r_{\text{mean}})$ are constants, there are still three variables r_1 , r_2 , and r_3 .

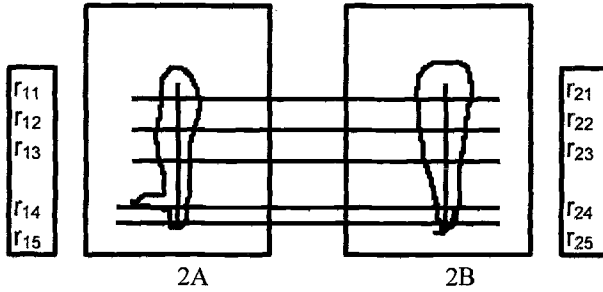


Figure 2 - Illustration of Two Creepage Patterns with Similar Mean, Max., and Min.

The difficulty of rating non-uniform and/or asymmetric patterns lies in the standard’s attempt to describe a two-dimensional pattern with a linear parameter, the width. A more suitable parameter should reflect the two-dimensional nature of the creepage pattern, for example, delaminated area, expressed either as absolute area in terms of cm^2 , or as a percentage of total test area as proposed by Warburton et al. [1]. They have found good correlation to ASTM methods. This paper further examines variables that affect the results, e.g. scribe length, background paint color, reproducibility, and operator-to-operator variance. Image analysis has also been proposed to evaluate results of gravelometer and scab test [2].

Experimental

Five sets of samples consisted of 31, 20, 5, 3, and 3 cold-rolled steel (CRS) 7.6 cm x 12.7 cm (3 in. x 5 in.) panels respectively, and one set of 5 electric boxes as shown (Table 2) below were studied.

Table 2 - Samples Tested.

Set #	Sample #	Sample Description	Scribe Length (cm)	Paint
1	31	CRS panels	5.08 ± 0.32 cm	Solvent, white
2	20	CRS panels	3.81 ± 0.32 cm	Same as set #1
3	5	CRS panels	6.35 ± 0.32 cm	Powder, beige
4	5	CRS electrical box	7.30 ± 0.32 cm	Same as set #3
5	3	CRS panels	7.30 ± 0.32 cm	Powder, dark brown
6	3	CRS panels	5.08 ± 0.32 cm	Powder, black

All samples were tested in the same salt spray chamber per B 117-94. Every sample was rated in three ways: per D 1654-92 with rating from 0 to 10, millimeter readings (e.g. 2.5 mm is a representative width measured from scribe to creepage front), and delaminated areas as percentages of total test areas. In this case, the delaminated area was expressed as a percentage of total test area because it is easier to visualize. An example was given using set #1 with the data sorted first by ASTM

rating in an ascending order and second by millimeter reading in a descending order (Table 3).

Table 3 – Results of Three Rating Methods for Set #1.

ASTM Rating	Millimeter Reading	Delaminated Area %
0	19.0	29.30
0	17.0	28.72
0	17.0	24.93
1	15.0	21.00
2	12.0	14.83
3	9.0	14.39
3	9.0	14.43
3	8.0	9.47
3	8.0	10.11
3	8.0	9.43
3	7.0	9.17
3	7.0	9.26
4	7.0	8.97
4	7.0	8.69
4	6.5	8.97
4	6.5	8.66
4	6.5	8.57
4	6.0	9.22
4	6.0	7.12
4	5.5	6.44
4	5.5	7.32
5	3.0	3.93
5	3.0	3.44
6	2.5	2.88
6	2.5	3.12
6	2.0	2.59
6	2.0	2.30
6	2.0	2.25
7	2.0	1.56
8	0.5	0.93
8	0.5	0.84

Delaminated area in units of cm^2 was determined using a 3-CCD video camera interfaced with a computer and an image analysis software package (Image-Pro® Plus, version 3.0²). Delaminated area as a percentage of total test area was calculated using a standard spreadsheet program.

² Media Cybernetics, Inc., Silver Spring, MD.

Results and Discussions

Correlation to ASTM Method

The following (Figure 3) is the graphic presentation of the above data (Table 3).

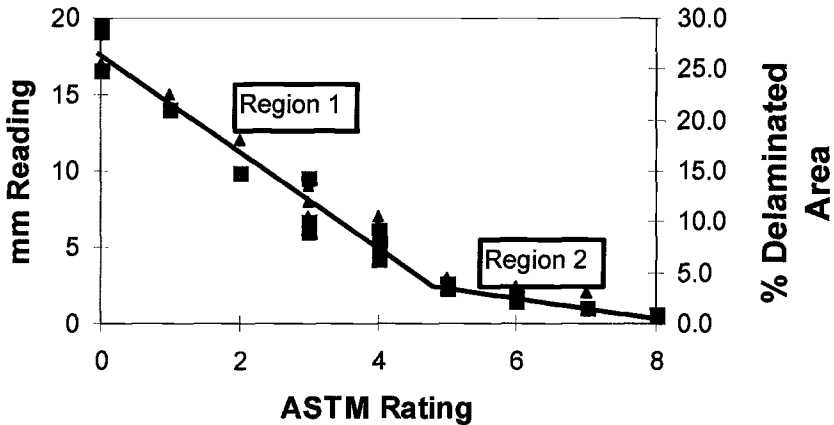


Figure 3 - Data for set #1. Squares are delaminated area % and triangles are millimeter readings. Two straight lines are drawn as a guide to the eye.

The following can be noted:

Firstly, over a broad range of ASTM ratings, from 0 to 8, there is an excellent correlation among the three methods. The lower ASTM ratings correspond to larger millimeter readings and larger percentage delaminated areas.

Secondly, there seem to be two linear regions of the correlation as shown by the two straight lines: Region 1 from ASTM rating of 0 to 5, and Region 2 from 5 to 8. For Region 1, the slope of the line correlating mm reading to % delaminated area is much higher than that of the line in Region 2. Referring to Table 1, it can be seen that for each ASTM rating of 6 and above, the mm range is very narrow, typically 0.5 to 1.0. For example, ASTM rating number of 8 corresponds to 0.5 to 1.0 mm. On the other hand, ASTM ratings of 5 and below correspond to a much larger mm range, typically 2 mm or more. For example, ASTM rating number of 2 corresponds to 10.0 to 13.0 mm, and rating number of 0 corresponds to 16.0 or over. This translates to much larger % delaminated areas for Region 1. Therefore the slope of the correlation line of Region 1 is much higher than that of Region 2.

This also explains the third trend: larger data spread for Region 1. Because the width variance is larger for this region, therefore variance of both mm reading and % delaminated area is correspondingly larger as shown in Table 4. Table 4 lists the arithmetic averages of ratings of set #1 which have three or more millimeter readings or

delaminated area percentage. It can be seen that σ_{n-1} for ASTM rating number of 6 is much smaller than that of 0, 3, or 4.

Table 4 - Averages and Sample Standard Deviations for Set #1, ASTM Rating of 0, 3, 4, and 6.

ASTM Rating	Millimeter Reading		Delaminated Area %	
	Average	σ_{n-1} *	Average	σ_{n-1}
0	17.67	1.15	27.65	2.37
3	8.00	0.82	10.89	2.42
4	6.17	0.71	8.22	0.99
6	2.20	0.27	2.63	0.37

* Sample standard deviation

Scribe Length

Data for set #2 are collected on panels painted with identical paint as set #1 with a shorter scribe length, 3.81 cm vs. 5.08 cm.

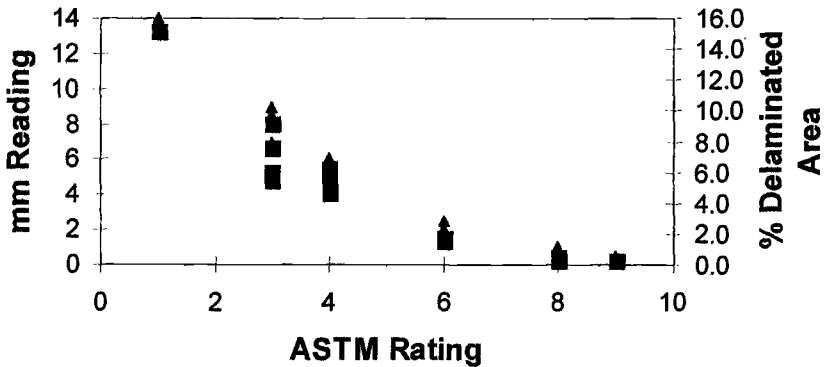


Figure 4 - Data for set #2. Squares are delaminated area % and triangles are millimeter readings.

A comparison of Figures 3 and 4 is shown in Figure 5. It can be seen that a 10% delamination for a panel with a 5.08 cm scribe corresponds to only about 6% delamination for a panel with a 3.81 cm scribe. Similar analysis and conclusions can be drawn on all other sets of data. It is, therefore, important to keep the scribe length constant within each set during the ranking.

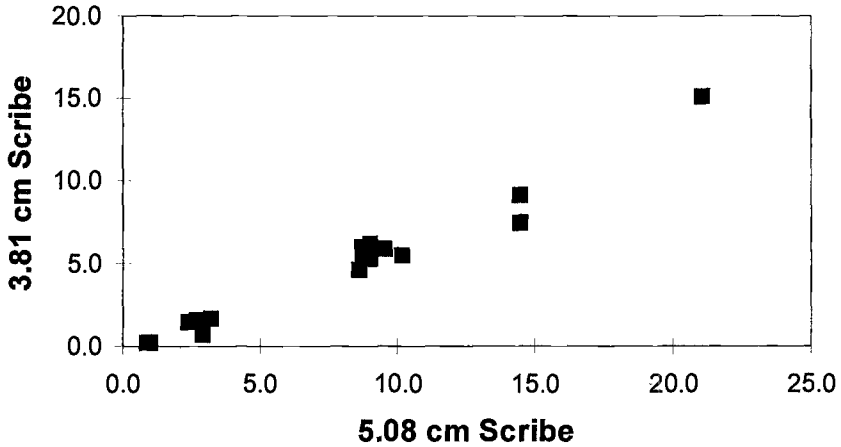


Figure 5 - % Delaminated Area Data for Set #1 and 2.

Variation of % delaminated area as a function of scribe length could be a disadvantage of using image analysis as compared to the width used in the ASTM method, which is scribe-length-independent. However, in situations where a repetitive routine operation is performed on identical samples, such as in many quality control operations, image analysis will clearly be the method of choice. It can also be seen in the following sections that the operator-to-operator variance on applying image analysis is practically zero, and this could also be a significant advantage.

As mentioned before, delaminated areas can be expressed either in terms of cm^2 or as a percentage of total test area. Percent delaminated areas are easier to visualize. However, if there is any doubt in the precise determination of the total test area (as might be in the case of a complex geometry), delaminated areas as cm^2 should be used to avoid possible ambiguity. In such a situation, however, if relative ranking of samples is the only concern, which is often the case, then both cm^2 delaminated area and percent delaminated area determined with a rough estimate of total test area can be used.

Figures 6 and 7 serve to illustrate the effect of total test area on percent delaminated area: Figure 6 is the graphic representation of data for set #3, and Figure 7 for set #4. Sets #3 and 4 are the same beige powder paint on two different substrates: set #3 are panels and set #4 are electrical boxes. For the electrical boxes, the scribe was made on the side and the total test area is considerably smaller than that of the panels. Therefore, percent delaminated area in Figure 6 is lower than that in Figure 7.

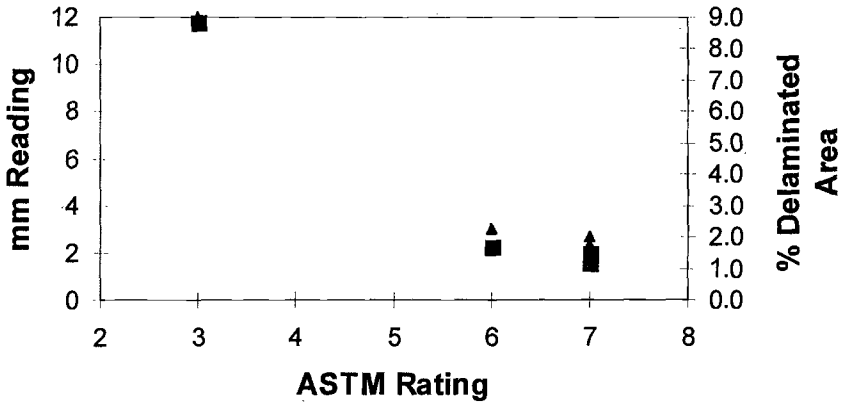


Figure 6 - Data for Set #3. Squares are delaminated area % and triangles are millimeter readings.

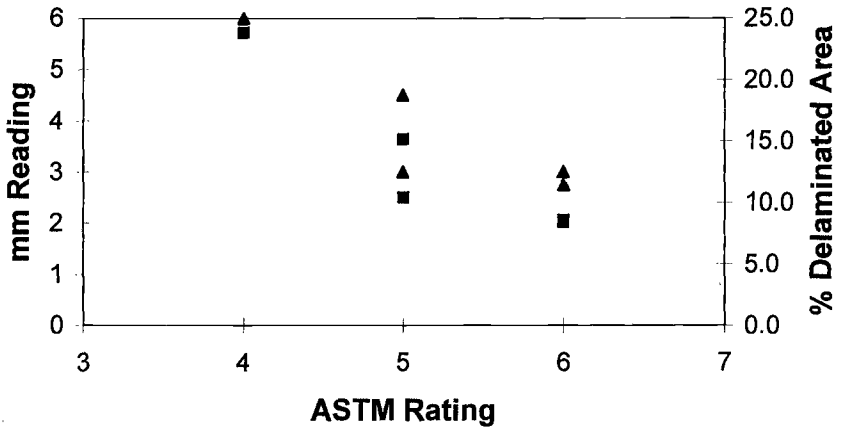


Figure 7 - Data for Set #4. Squares are delaminated area % and triangles are millimeter readings.

Sample Preparation for Image Analysis

Light vs. Dark Paints - Image analysis discriminates the delaminated areas from the paint based on the color difference of the two. Usually for CRS, the delaminated area is corroded and is easily differentiated against a light color paint as is the case with sets #1, 2, 3, and 4. The software can be programmed to automatically pick up dark objects and determine their areas. For sets #5 and 6, the same approach can be taken depending on the color differences. However, when the paint is darker than the

corroded area, bright objects should be specified. This operation can also be done by manually bringing up the color histogram and defining the color region of interest. This option provides the operator with the maximum flexibility and finest degree of discrimination. An alternative approach to preparing samples with dark paint is to wipe the delaminated area with 1:1 dilution of concentrated HCl in water to reveal the metal substrate, which is typically “white metal”. This gives a very large color difference and always works very well.

Set #5 and 6 are darker paints: dark brown and black respectively. Unlike the previous 4 sets of samples where the corroded areas are dark and background is light, these two sets of samples have less color contrast. However, the software had enough capability that picking up dark objects on a dark background was not too difficult and valid data with excellent correlation can be collected.

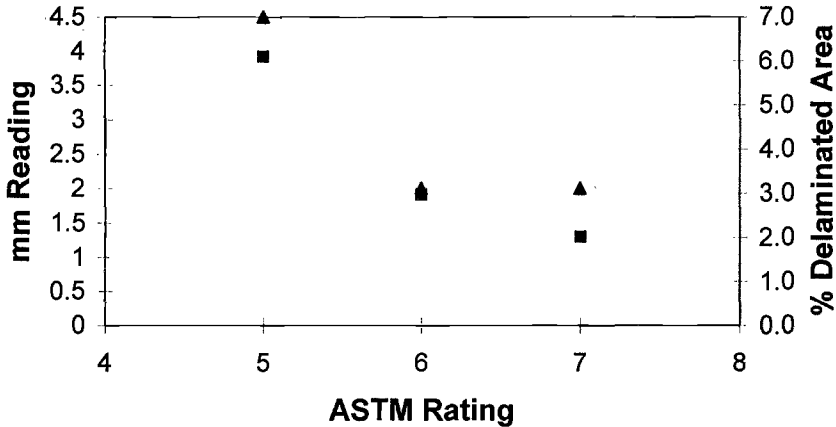


Figure 8 - Data for Set #5. Squares are delaminated area % and triangles are millimeter readings.

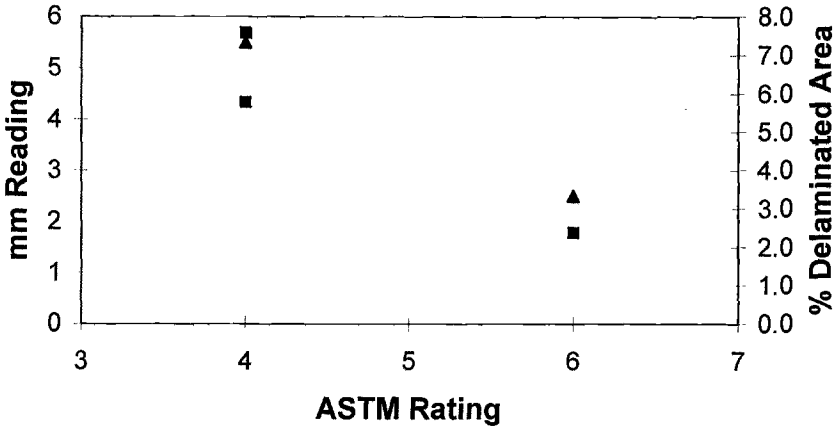


Figure 9 - Data for Set #6. Squares are delaminated area % and triangles are millimeter readings.

Rust Run-offs and Surface Discoloration - Similar consideration should be given to rust run-offs around and below the scribe and any other surface discoloration that may result from blisters underneath the paint film. These areas can be avoided either by carefully excluding them by defining the analysis area-of-interest (this is a restricted area the software will examine), or by wiping them off with diluted HCl, which readily dissolves the rust. At times, when the specimens have considerable rust run-offs, and the paint has good mechanical integrity, a very fine sand paper can be used with HCl to provide excellent results.

Several other issues are worth consideration.

Multiple Objects and Hole-Filling Function of the Image Analysis Software

Sometimes when the creepage is very narrow, the software may identify objects (e.g. rust on the scribe) as being separated, and therefore there could be more than one object, as shown in Figure 10 below.

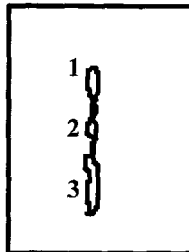


Figure 10 - Illustration of Multiple Objects.

In this case, the summation of areas of all objects should be used. This can easily be done if the software is set up to export data to a spreadsheet and the spreadsheet can be set up to perform this function.

With galvanized substrates, occasionally some of the corroded area (“white rust”) will be of lighter color than the surrounding corroded area. In such cases, the image analysis software should have hole-filling set up to account for these areas.

Reproducibility

One of the authors took two measurements of set #1 on different days and Figure 11 shows excellent reproducibility.

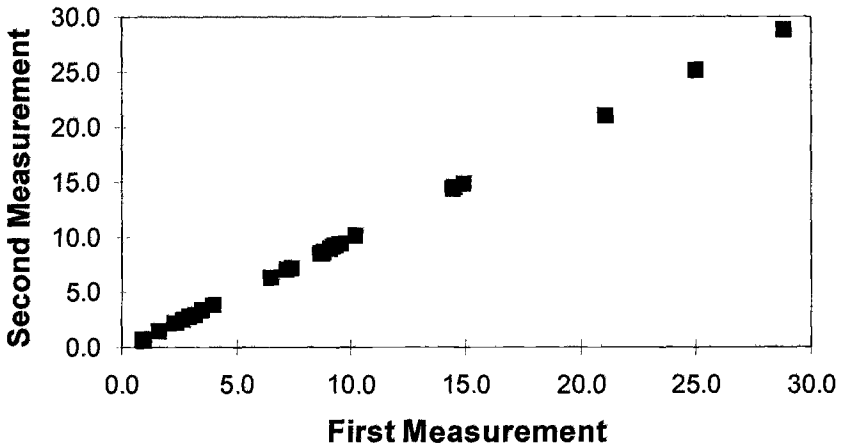


Figure 11 - *Reproducibility of Set #1.*

Operator-to-operator Variance

The image analysis functions discussed above are very basic and are offered by all image analysis software packages. The authors have taken advantage of the macro capability, which is also a standard feature of these software packages, to streamline and minimize operator error and keystrokes. Finally for each panel, it only takes six key strokes to obtain a digital image, collect, export and graph all the data.

Four users made measurements on Set #2: one is inexperienced, one has limited experience, one is very experienced, and the fourth is one of the authors. The first three were plotted against one of the authors’ measurements in Figure 12. As is clearly seen, operator-to-operator variations have virtually been eliminated. Therefore another advantage of image analysis is that minimal training and experience are required to

achieve reliable ratings. The ASTM method requires a higher degree of skill and experience.

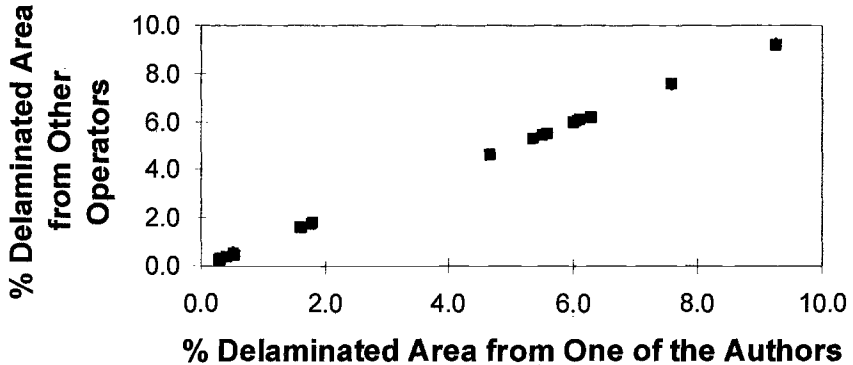


Figure 12 - *Operator-to-operator Variance Study.*

Conclusions

Delaminated area is a parameter that reflects the two-dimensional nature of a creepage pattern. It is a more quantitative and less subjective measurement of corrosion performance than the width of the creepage. When delaminated area is determined *via* an image analysis routine with appropriate software, automation can be achieved and operator-to-operator variations can be virtually eliminated.

Acknowledgments

The authors wish to thank Dr. David L. Elliott, Mrs. Nancy S. Sherwood, Mrs. Vivian I. Bikulege for their management support for this project, Ms. Pamela J. Dotter, Ms. Kimberly M. Jackson, Dr. David L. Elliott for participating in operator variance study.

References

- [1] Warburton, Y. J., Smith, J. L., and Simon, G. C., "Application of Image Analysis and Correlation to Established Methods in the Evaluation of Salt Spray Performance," *Metal Finishing*, January 1999, pp.16-22.
- [2] Duncan, D. J., and Whetten, A.R. "Image Analysis Techniques: Used to Quantify and Improve the Precision of Coatings Testing Results," *Polymeric Materials Science and Engineering*, Vol. 68, 1993, pp. 157-160.

Fred Lee,¹ Behnam Pourdeyhimi,² and Jack Martin³

Comparative Study of Standard Weathering Test Methods Using Image Analysis

Reference: Lee, F., Pourdeyhimi, B., and Martin, J. “Comparative Study of Standard Weathering Test Methods Using Image Analysis,” *Durability 2000: Accelerated and Outdoor Weathering Testing, ASTM STP 1385*, J. D. Evans and W. D. Ketola, Eds., American Society for Testing and Materials, West Conshohocken, PA, 2000.

Abstract: Human visual evaluation and photometric gloss and color measurements are the common techniques used for determining the surface deterioration in weathering and durability studies. However, the human visual inspection technique is a subjective and qualitative method and therefore lacks objectiveness as a standard method. The photometric techniques provide quantitative measurements but do not fully incorporate all aspects of surface morphology. Therefore, instrumental inspection techniques that integrate photometric response as well as surface morphology would be beneficial. In this report, the feasibility of an image analysis system as an objective and quantitative surface measurement technique is demonstrated. For the study, three different commercially available plastics were exposed to various weathering conditions conforming to five different industry standard test methods. The materials were periodically evaluated using the image analysis system, and the results were compared. In addition, conventional photometric evaluation results were compared to this new technique. Analysis of the data provided some insight into comparing the four different accelerated weathering tests.

Keywords: weathering, imaging, image processing, image analysis, photometric measurements, evaluation

¹Standards Program Manager, Atlas Electric Devices Company, 4114 N. Ravenswood Ave, Chicago, IL 60613.

²Professor, School of Textile Engineering, North Carolina State University, Raleigh, NC 27695.

³Site Manager, South Florida Test Service, Atlas Weathering Services Group, 17301 Okeechobee Rd, Miami, FL 33018.

Introduction

Materials durability studies, such as weathering, involve precise monitoring and meaningful analysis of appearance and surface defects since the quality of product is often judged by its surface appearance. Current techniques that monitor and analyze materials' surface degradation are often deficient in accurate characterization of various appearances and morphological changes [1-5]. Unfortunately, the characterization of surface appearance is an assessment of the human visual attributes that are difficult to objectively quantify. Unlike other material properties such as physical or mechanical properties, the appearance properties are tied to human psychology and further complicated by various visual illusions. As with other subjective visual assessments, the results are often sensitive to biases in an individual's perception [6]. Besides, this experience driven human technique makes proper training very difficult and thus suffers from a lack of repeatability and sensitivity of measurement.

The complex response of human perception, however, can be measured partially using photometric devices such as glossmeters and colorimeters. While the photometric devices can mainly measure the amount of light reflected from the measurement area, spectrally or non-spectrally, the content of the target area is still at a loss. For example, the cause of gloss loss, such as crazing or mildew, cannot be obtained by the photometric measurement. In other words, there are inherent disadvantages such that two morphologically different surfaces, but with the same amount of surface reflection, could be given the same gloss value. In weathering evaluation where precise understanding of morphological changes of exposed surface is crucial, this could lead to a misinterpretation of weathering effects and, furthermore, incorrect conclusions about the material's durability. This deficiency also exists in color measurement. Colorimetric measurement would not differentiate the differences caused between dirt retention versus mildew growth. Therefore, human visual inspection became necessary in weathering studies. However, human visual inspection is highly subjective and qualitative. Hence it would be desirable to develop automated instrumental methods, such as digital imaging, that incorporates two-dimensional imagery for evaluating surface morphology and measuring surface degradations including physical defects.

Digital imaging and image processing/analysis techniques have been available for many years in the scientific community. From biology to metallurgy, imaging has been routinely applied in surface characterization and for monitoring the kinetics of changes in surface/component morphology. Its ability to gather visual information in two (and pseudo-three) dimensional formats in a transferable digital file has been fully accepted. In addition, its ability to 'analyze' and 'archive' the imagery only furthers the applicability.

This paper describes an imaging technology case study based on a weathering research project that examined five different standard weathering test methods widely used throughout the materials industry for many years. In this study, an imaging technology developed by Atlas Electric Device Company was used to study the feasibility of this growing technology.

Image Capture System - Hardware

The image capture system including the enclosed optical and illumination arrangement used in this study has been developed by Atlas Electric Devices Company, Chicago, Illinois, USA, and Atlas Materials Testing Solution BV, Gelnhausen, Germany. This hardware, including the proprietary software, has been developed through the industry-wide consortium "Video Image Enhanced Evaluation of Weathering (VIEEW)" sponsored by coatings, plastics, rubber and sealants manufacturers and organized by Atlas Weathering Services Group – South Florida Test Service, Miami Florida, USA.

The hardware portion of the VIEEW system, or of any other image acquisition (capture) device, requires a unique optical arrangement for flat image forming. Unlike conventional photometric devices where a two-dimensional optical arrangement is usually adequate, an imaging system requires a three-dimensional optical arrangement where the focal plane is perpendicular to the optical axis to provide uniform and even focusing. In conjunction with the optical arrangement, a special illumination scheme is needed for optimized reflections and correct viewing of surface morphology.

It is a physical phenomena that the higher the incident angle, the better geometric reflection is obtained. Geometric reflection refers to light reflection caused by optical smoothness of the surface, not by its chromaticity. For example, gloss is a measure of the geometric reflectance, and a 20° gloss measurement provides a better distinction between high gloss surfaces than a 60° gloss reading. The ideal incident angle is therefore 0°. This angle is particularly useful in imaging for capturing surface texture and roughness. For example, when a stream of light is reflected perpendicularly (0°) from the surface, the direction of reflection is confined to 0° if the surface is optically smooth. However, when the surface is not optically smooth due to the surface irregularities, the light will be reflected from the surface at angles greater than 0° creating a light scattering effect.

This scattering effect of reflected light is most beneficial in examining surfaces in the presence of dirt, cracks, streaks, etc, which are common in weathered surfaces. In fact, these characteristics render conventional gloss measurements unreliable and manufacturers caution users on this problem. In the VIEEW system, when light is reflected at large angles caused by surface irregularity, the scattering effect appears as a darker image indicating a rough (low gloss) surface. Figure 1 is a composite of four automotive top coat images captured using the 0° incident angle system showing the off-axis scattering of scratch marks appearing as dark lines.

Imaging systems for surface inspection should also consider an additional illumination scheme that induces chromatic diffuse reflection to measure chromaticity, since color is an important surface property. When a uniform and spatially integrated Lambertian distribution is required, integrating sphere technology is commonly used as in spectral radiometers. An integrating sphere is composed of two perfect hemispheres that are coupled together to form a spherical cavity. Furthermore, the inner surface of the sphere is coated with a high reflectance substance to achieve a high degree of diffuse illumination. The VIEEW system incorporated an integrating

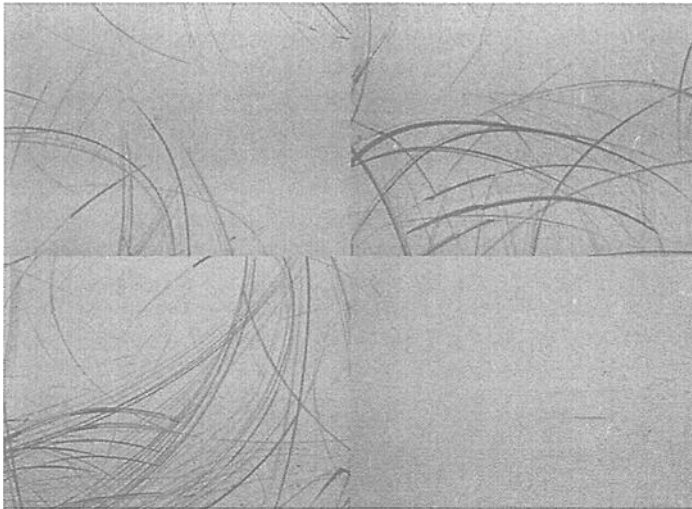


Figure 1 - *Scattering Effect Of 0° Incident Reflected Light. (Reproduced with Permission from Ref 6)*

sphere to measure relative color change similar to the visual color measurement. However, absolute color measurement is not intended and the VIEEW system is based on a black and white imaging scheme for capturing high contrast images. See Table 1 for the comparison of the two distinct modes of illumination conditions on the same coating surface. Both the geometric illumination and the chromatic illumination are calibrated using known calibration targets for repeatability and reproducibility.

Table 1 - *Chromatic and Geometric Viewing of a Partially Weathered Sample. Note the Difference in the Ability to Detect Defects. (Reproduced with Permission from Ref 6)*

Chromatic Information (Diffuse Illumination)	Geometric Information (Directional[0°] Illumination)

Image Processing/Analysis - Software

Image analysis software deals with specific defect types. In dealing with each defect, the program needs to decide what attributes are relevant and how they can best be measured. Some deal with the estimation of size, shape and distribution characteristics while others derive first order as well as second order surface texture properties to estimate physical damage. The first category, by its nature, requires a binary(B&W) image as an input, thus requiring a thresholding step to convert the image from a gray format to a black and white format. The thresholding method must be appropriate for the defects in question and often there are a steps of preprocessing needed to enhance the defects (or regions) of interest (ROI) prior to the thresholding. For the surface analysis of weathered materials where there are no predetermined morphological patterns, the pre-processing should be generic yet precise in enhancing appropriate defects. Unlike other image analysis where there are predetermined ROI, such as in the component inspection during a manufacturing process, weathering defects are material specific and change during exposure. Therefore, material and defect independent preprocessing techniques are necessary and some operator intervention is often inevitable. In aiding this process, gray image analysis (the second category) can be used to determine images with defects prior to the binary analysis for specific defects. The gray image analysis is a measure of various surface textures and measured directly from as-acquired gray images. Since the textural properties are measured directly from gray images without potential biases from the preprocessing procedures, the result is completely objective and requires no operator intervention. The details on the gray and binary analysis and their algorithms were discussed in the referenced publications [3-5,7-8]. The software (VIEEW) used in this study has been developed by Atlas Electric Devices Co. and Georgia Institute of Technology.

Materials

Three types of plastics were used for this demonstration. The three plastics were labeled as Plastics A (Polycarbonate, transparent, 3"x4"x3/8"), Plastics B (Polypropylene, blue, 3"x4"x1/8") and Plastic C (Polypropylene, white, 3"x4"x1/8") in this paper.

Standard Weathering Tests Used in This Study

All methods used in this study are industry standard tests as listed below. These test methods utilize Florida inland static weathering, indoor accelerated weathering (xenon arc light source and fluorescent UV source) and outdoor accelerated weathering (EMMAQUA[®]). The indoor accelerated weathering conditions are found in Table 2.

ASTM G7 - Standard Practice for Atmospheric Environmental Exposure Testing of Nonmetallic Materials (Outdoor Test Method)

ASTM G26 - Standard Practice for Operating Light-Exposure Apparatus (Xenon-Arc type) With and Without Water Exposure of Nonmetallic Materials
 ASTM G53 - Standard Practice for Operating Light- and Water-Exposure Apparatus (Fluorescent UV-Condensation Type) for Exposure of Nonmetallic Materials
 ASTM 4364- Standard Practice for Performing Accelerated Outdoor Weathering of Plastics Using Concentration Natural Sunlight (EMMAQUA[®] NTW)
 SAE J1960 - Accelerated Exposure of Automotive Exterior Materials Using a Controlled Irradiance Water Cooled Xenon Arc Apparatus

Table 2 - Indoor Accelerated Weathering Conditions

	ASTM G26	ASTM G53	SAE J1960
Irradiance (W/m ² ·nm@340nm) (Filter Combination)	0.35 (Boro/Boro)	N/A (UVA 340)	0.55 (Quartz/ Type S Boro)
Relative Humidity (%)	55	N/A	50
Dry Bulb Temp (°C)	47	N/A	47
Black Panel Temp (°C)	70	60 (50 Dark)	70 (38 Dark)
Cycles	90 min Light /30 min Light and Spray	4 Hours UV / 4 Hours Condensation	40 min Light / 20 min Light and Front Spray / 60 min Light / 60 min Dark and with Back spray

Evaluations

Two conventional photometric measurements and a number of different imaging techniques were conducted. The two conventional photometric measurements were CIE (L*, a*, b*) scale color measurement using Ultra Scan by Hunter Lab and 20° gloss measurement using Micro-Tri-Gloss by BYK-Gardner. In order to provide comparability of the image analysis system to the existing measurement equipment, the geometric reflectance (0°) measurements were compared with the conventional 20° gloss measurements for plastics and the chromatic reflectance measurements (using integrating sphere) were related to CIE L* values to observe lightness changes. For the gray image analysis, surface relief is presented for the plastics as a measure of surface texture caused by different physical defects. This property provides some morphological information that can be used as an indicator for further analysis in a binary format. There were primarily two types of binary analysis performed, cracking analysis and particle analysis.

The evaluation schedule is shown in Table 3. This schedule was based on computed radiant dosages equivalent to the outdoor duration of one year. At each interval, at least six replicate samples were measured.

Table 3 - *The Evaluation Schedule used in this Study*

Color and Gloss Interval Code	C0	C1	C2	C3	C4	C5	C6
Imaging Interval Code	I0	N/A	N/A	N/A	I4	N/A	I6
ASTM G7 (Months)	0	1	3		6	9	12
SAE J1960 (KJ/m ² @340nm)	0	250	500	1000	1500	2250	3000
ASTM G26 (KJ/m ² @340nm)	0	250	500	1000	1500	2250	3000
ASTM G53 (Hours)	0	250	500	1000	1500	2262	3000
ASTM D4364 (MJ/m ² @295-385nm)	0	24	48	96	144	216	288

Photometric Results

20° Gloss Data vs. 0° Geometric Reflectance

Overall, the main appearance change in plastics was observed in 20° gloss values, not in color changes. Plastics A (Polycarbonate) showed some yellowing in all exposures but not significant enough to be the main defect for this material in this study. Hence, only 20° values, along with 0° geometric reflectance values, were reported in this report. (Figures 3-5) Note that the reflectance values for Plastics A were lower than the other two plastics in comparison to the gloss values. This was due to the adjusted lower light intensity during the image capture to compensate for high reflectance of Plastics A.

It is important to provide comparability between the existing technique and the new measurement technique. To measure this comparability between the 20° gloss measurements and the 0° reflectance measurements, the measurement values were compared using Pearson's correlation coefficient as shown in Figure 2. The correlation coefficient was 0.94 indicating good agreement between two measurement sets. It was interesting to note that the discrepancies were greater at low reflectance measurements. This could suggest the interference of weather induced surface morphology (dirt, cracks and streaks, etc) in gloss measurements.

Interpretation of 20° Gloss Data

Examining the standard test methods in terms of the gloss values and the reflectance values, the two xenon test methods showed the most gloss changes at the final exposure intervals suggesting the most severe test conditions among the five methods used. (Figures 3-5) For the SAE J1960 method, this was an expected result

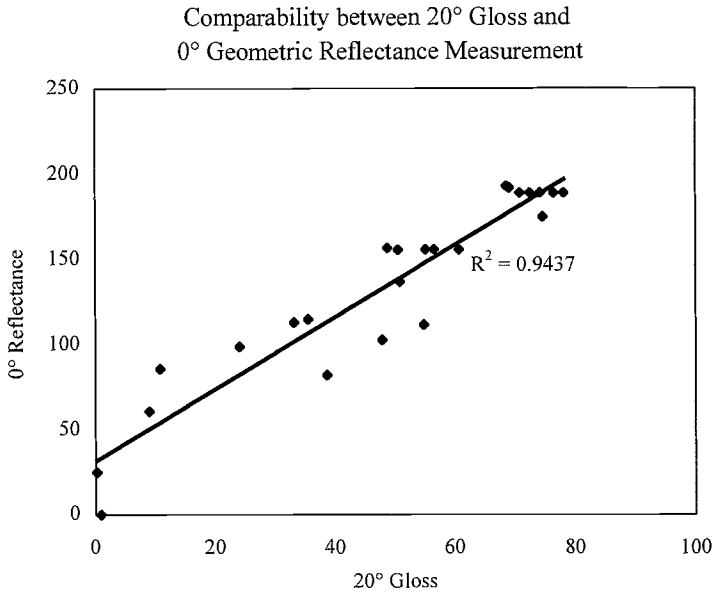


Figure 2 - Comparability between Gloss Measurement and 0° Reflectance Measurement

since this method uses the higher irradiance, higher temperature conditions and lower wavelength cut-on irradiance value allowing more damaging UV radiation. In all three materials, SAE J1960 using Quartz/Type S Borosilicate filter combination showed sudden deterioration after 1000KJ/m²@340nm. However, ASTM G26 method induced a bigger gloss loss than SAE J1960 method for Plastics A material, suggesting a reversed severity between the two xenon methods. This was an unexpected result and counter intuitive because ASTM G26 requires a lower irradiance value and a higher cut-on wavelength (less UV radiation) making the test much less severe than the SAE J1960. This unexpected results between ASTM G26 and SAE J1960 test could indicate morphological changes that could have rendered the gloss reading not representative of actual surface damage. However, these morphological changes could be only speculated from the gloss readings but not determined.

Examining the gloss results in terms of degradation trend, ASTM D4364 EMMAQUA Night Time Wetting method seemed to have followed ASTM G7 outdoor trend most closely. It was interesting to note that ASTM G53 test showed a high variability in terms of its relative severity compared to other test methods. For example, ASTM G53 method showed high severity comparable to SAE J1960 in Plastics A. However, it did not show any sign of deterioration for Plastics B.

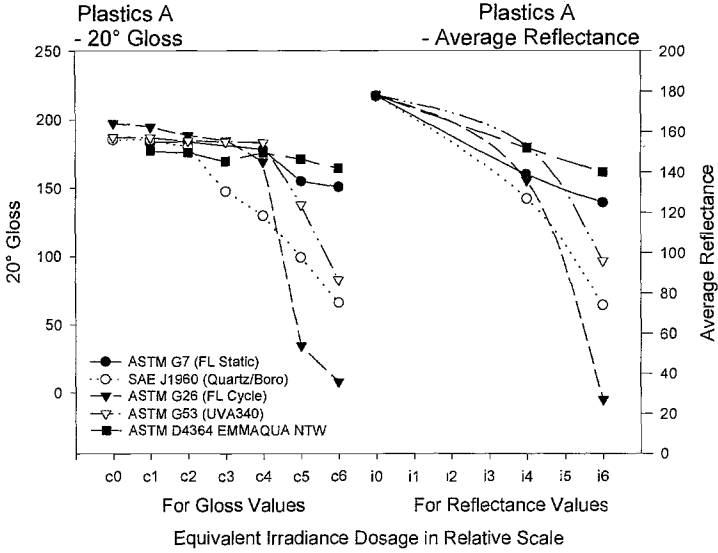


Figure 3 - 20° Gloss Data vs. Imaging Data for Plastics A

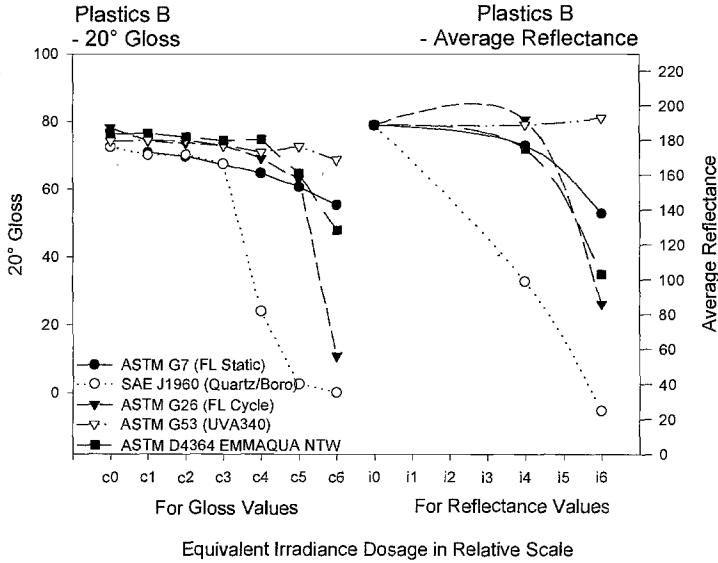


Figure 4 - 20° Gloss Data vs. Imaging Data for Plastics B

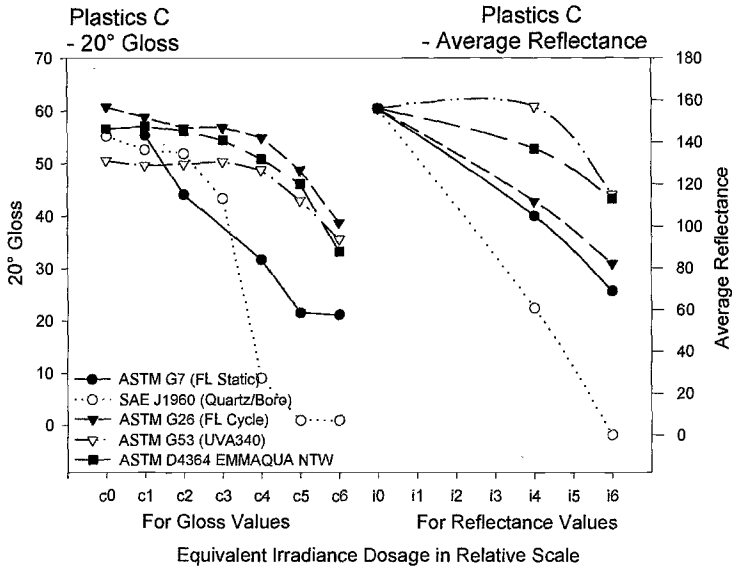


Figure 5 - 20° Gloss Data vs. Imaging Data for Plastics C

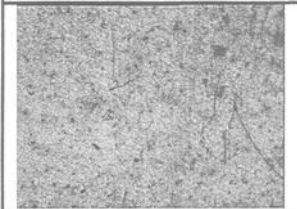
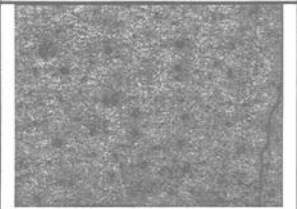
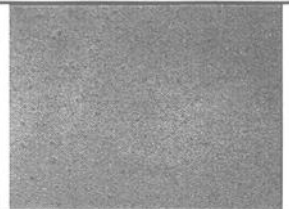
Image Analysis Results

Qualitative Discussions on the Images

One advantage of having images during weathering studies is to record surface conditions at each interval. This provides complete surface information otherwise lost. Often, a number of samples are archived for this record keeping purpose at each interval, but their aging process will continue even under non-exposure conditions. Theoretically, it would be most beneficial to have the entire aging process recorded using the imaging technology. It is a rare but known practice to video tape or photograph specimens at each interval for comparison purposes. However, it is important to caution users that different illumination conditions at each interval are making comparisons between intervals impractical.

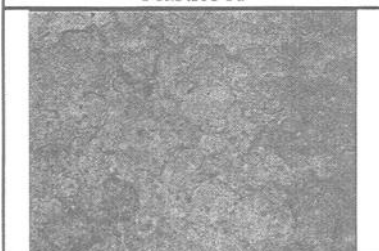
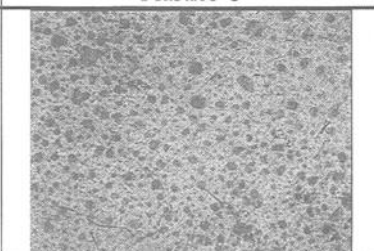
Examination of each image revealed surface texture explaining causes for gloss loss. Often, without images or actual samples, it is common to treat gloss loss as general surface deterioration. From the images of these plastics samples, it was evident that gloss loss for different test methods was indeed induced by a variety of surface textures or surface defects. SAE J1960 tested Plastics A samples showed fine directional crazes at interval I4 and these crazes developed into a network of cracks at interval I6. (Table 4) These cracks could explain the relatively low gloss loss as discussed in the previous section. Crazing was also observed in Plastics B by ASTM G26 test method. The crazes were finer and more linear than the crazes found on Plastics A.

Table 4-*Cracking and Crazing Formations*

Plastics A at I4 Interval	Plastics A at I6 Interval	Plastics B at I6 Interval
		

Plastics A and Plastics C at interval I6 of ASTM G53 method using fluorescent condensation device showed heavy water condensation marks that were not found in any other test methods (Table 5). It was clear that the water condensation spots caused a loss of gloss. The outdoor samples and other accelerated samples showed no water spots. The water spots found in this device were quite notable since all accelerated test devices used the same source of water and operated simultaneously under the same laboratory condition. It is possible that the evaporated water had contaminants which were volatile enough to be carried by the steam and during the condensation phase the contaminants remained on sample surface creating water marks [9]. The evaporative process, which the fluorescent devices use, may not completely separate water from the contaminants that can be collected in the water bath. In contrast to the spray, which has enough force to wash the surface, the droplets of condensation that may contain particles of dust or contaminants from the water remain on the surface.

Table 5-*Water Spots from Fluorescent UV devices*

Plastics A	Plastics C
	

Another view in explaining this phenomena might be related to the temperature of water vapor. Unlike the xenon arc device where the spray water temperature is comparable to the natural condition at 20 - 25°C, the saturation temperature of the water vapor used in the condensation process would be much higher due to the inherent evaporation process used in the device. During the condensation cycle in the fluorescent UV device, the controlled black panel temperature was 50°C and the

actual sample surface would be at 50°C since there is no radiation heat transfer loss. For the water vapor to condense on the 50°C sample surface, the temperature of the water vapor need be at or above the saturation temperature (dew point), or near 60° at 70% relative humidity or much higher. When the high temperature water vapor condenses on a sample surface, the elevated temperature of the vapor would have adverse effects such as increased solubility [10]. Therefore, it may be the difference in the physical processes by which the water comes into contact with the surface as well as the unnaturally high vapor temperature that caused the water spotting on Plastics A and Plastics C.

Quantitative Analysis

Two different types of image analyses (gray and binary image) were carried out to quantify the surface texture and the surface defects induced by the weather elements. The gray image analysis was done on all materials and the binary image analysis was done for only those materials that showed definitive surface defects. As briefly mentioned in the image processing/analysis section, the textural information obtained by the gray image analysis “flags” the operator to further analyze the images using the binary analysis. When flagged, the operator would make an observation as to whether the defects have clear geometrical boundaries, which then can be measured quantitatively. For example, the water marks on Plastic C by ASTM G53 have clear boundaries and their geometrical attributes can be measured along with the amount of defects on the given image area. The textural information itself provides in-depth quantitative information that is not obtainable with the human visual evaluation. For instance, the watermarks on Plastics A by ASTM G53 have no quantifiable geometric features but the texture created by the watermarks is clear and can be quantified by a textural property. From fifteen sample images of plastics, four samples showed quantifiable surface defects and were analyzed using binary image analysis.

Surface relief is the property used as a gray image textural measurement. Surface relief is a secondary parameter that can be obtained from a histogram. The histogram is a graphical interpretation of the gray level make-up of an image. This technique was discussed in detail and used to measure automotive coatings’ surface texture created by a scratch and mar test [4,8]. Textural parameters deal with the overall impression of an image. Therefore, these parameters are arbitrary index values without units. In case of the surface relief, a higher index indicates a rougher surface. Surface relief values for plastic samples are shown in Figure 6. It was evident that the images with cracks or water spots have higher surface roughness ratings.

In this study, surface relief values of 6 and higher seemed to indicate visually apparent and observable textures and the values of 4 to 6 seemed to indicate subtle textures. There were four images that showed quantifiable surface defects and these four images were calculated at 6 or higher. These four images were Plastics A by SAE J1960 at interval I4 and I6 showing crazing and cracking, Plastics B by ASTM G26 at interval I6 showing crazing and Plastics C by ASTM G53 at interval I6 showing water marks. The subtle water marks of Plastics A by ASTM G53 at interval I6 was calculated as 4.

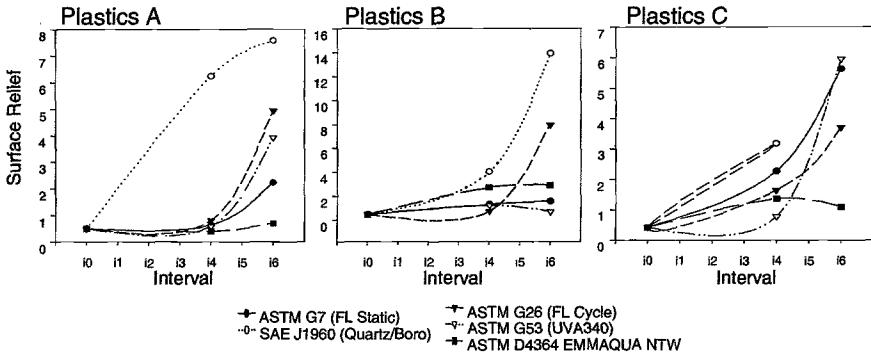


Figure 6-Surface Relief

The binary analysis was used to quantify two different characteristics of common weather induced surface defects for the four samples with the corresponding quantifiable surface defects: cracking and particles (circular defects). As mentioned, the binary analysis requires a conversion from gray images to binary images (black and white). This process is generally referred to as “segmentation”. For the weather induced surface images with surface defects, a complex filtering process was carried out prior to the segmentation in order to identify the region of interest, i.e. defects. This preliminary process is referred to as preprocessing. The preprocessing procedure formulated for the cracking images of the plastic samples is shown in Figure 7. This formulation, or recipe, included 4 steps of image-processing techniques using proprietary algorithms. The recipes were programmed internally to provide repeatable, reproducible and objective results for all images. The processing recipe for the particle analysis (not shown) is similar to that of the cracking.

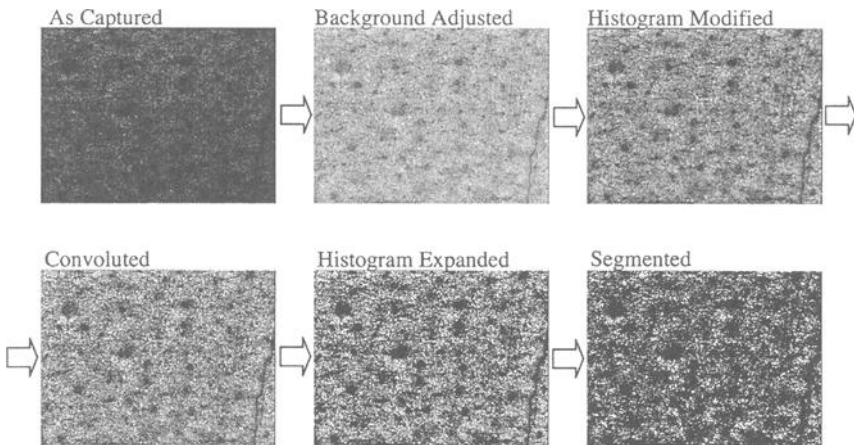
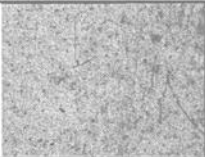
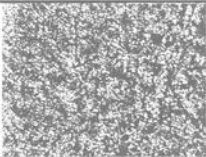
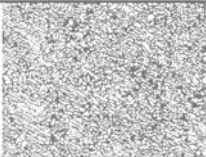
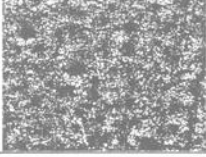
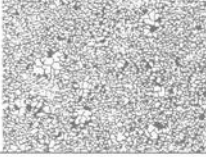
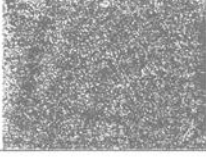


Figure 7-Image Processing of Surface Texture

Once the preprocessing was completed a binary image was obtained and geometrical information, such as quantity of cracks [8] and size of water spots, was extracted. Often, this information is sufficient in describing degree of degradation or performance ratings. At times, however, further descriptive information such as defect orientation, spatial uniformity, size distribution, shape characteristics, frequencies, etc, is needed to fully describe the defect types. In fact, this descriptive information is required in the visual evaluation. For example, there are nine different types of cracking geometry (irregular, line and short parallel, switch, crow foot, mosaic, shrinkage, short random, sigmoid) described in ASTM D660 – Standard Test Method for Evaluating Degree of Checking of Exterior Paints as a visual inspection reference.

Cracking surface defects were analyzed using a crack density parameter. The crack density indicates the amount of cracks present in a given image. As shown in Table 6, Plastics A by SAE J1960 at C4 interval showed 0.53 (53%) crack density. At C6 interval, the crack density increased to 0.63 (63%). Plastics B by ASTM G26 at C6 interval showed 0.54 (54%) crack density.

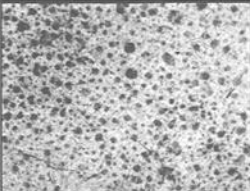
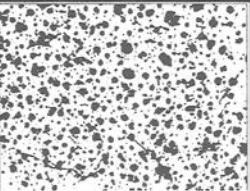
Table 6-Image Analysis: Cracking

	Gray Analysis	Binary Analysis	Binary Analysis 2
Plastics A SAE J1960 (Quartz/Boro) Duration: C4			
Image Data	Surface Relief: 6.23	Crack Density: 0.53	Crack Orientation: 123°
Plastics A SAE J1960 (Quartz/Boro) Duration: C6			
Image Data	Surface Relief: 7.57	Crack Density: 0.63	Crack Orientation: 83°
Plastics B ASTM G26 (FL Cycle) Duration: C6			
Image Data	Surface Relief: 7.93	Crack Density: 0.54	Crack Orientation: 109°

In addition to the crack density measurement, crack orientation was measured. This measurement was made because of the angular directionality. This measurement indicated that all cracks are oriented in 2nd quadrant ($90^\circ - 180^\circ$), except Plastics A by SAE J1960 at C6 which showed a random formation at a near vertical orientation.

The water spots found on Plastics C were analyzed in terms of their particle (spot) size (Table 7). The average water spot size for Plastics C was 10.2 pixels. The pixel value can be calculated into a linear dimension once the dimensional relationship is known. This dimensional calibration was not done in this study. In addition to the average size, other particle-related parameters such as size distribution, roundness, minimum size, maximum size, aspect ratio, spatial uniformity, etc. can be measured. In this study, the spatial uniformity was measured using the nearest neighbor distance (NND) technique [8]. Three parameters are obtained by the NND technique: average actual distance between centers of gravity, expected distance for uniformly random formation and corrected distance for the image of interest. If the latter two parameters are closely matched, the spatial distribution is considered to be uniform and the pattern is random, showing no periodicity. The water spots on Plastics C showed the uniformly random pattern. (Table 7)

Table 7-Image Analysis: Water Spotting

	Gray Analysis	Binary Analysis	Binary Analysis 2
Plastics C ASTM G53 (UVA340) Duration: C6			
Image Data	Surface Relief: 5.95	Average Particle Size: 110.2 pixels	Spatial Uniformity: <i>Uniformly Random</i> Ave Dist: 13.9 pixel Expected Dist: 10.9 Corrected Dist: 11.0

The parameters presented in this report are only a few chosen to demonstrate the image analysis technology from many available geometric descriptors. Often, image analysis parameters are fairly complex and contain many potential interpretations. It requires a fair understanding of the parameters as well as the materials to derive meaningful answers to image analysis data. As a common inspection tool, the data as presented in this report could be cumbersome and difficult to implement in a Q/C environment. It is the developer's on-going effort to simplify data and provide more user-friendly outputs comparable to the pictorial ratings in standard visual evaluation procedures.

New Surface Parameter

In comparing test methods or materials, statistical analyses are often used to provide mathematical relationships. Conventionally, a single evaluation parameter such as gloss is used. However, it was noted in this study that the conventional quantitative evaluation technique might not necessarily provide complete surface information. Using the gray image analysis, there were two surface parameters, reflectance and texture, obtained to describe the surface morphology. Together, these parameters contain pertinent weather induced surface information. Logically, these quantitative surface parameters could be combined into a single parameter with the relative significance of each parameter weighted. This combined parameter could then be used as a texture weighted reflectance parameter that describes weathering effects on material surface. This type of simple, mathematical relationship could be useful in enhancing basic reflectance data. One example based on this study is:

<i>Original Surface Parameter</i>	<i>Reflectance (A)</i>	<i>Surface Relief(B)</i>
<i>Relative Significance (Weight)</i>	5	5
<i>Weighted Parameter</i>	5A	5B
<i>Combined Image Parameter (X)</i>	$X = 5A + 5B$	

The combined parameter was applied to the final interval Plastics A data as shown in Figure 8. In this example, the SAE J1960 data, which was indicated by the gloss measurement as less severe than the ASTM G26 method, was rated higher by the combined image parameter. The reason was a higher surface relief rating caused by cracking. This example assumed that the surface relief and the reflectance were equally important. Depending on the materials and degradation criteria, one could formulate a variety of different mathematical relationships to provide various evaluations needs.

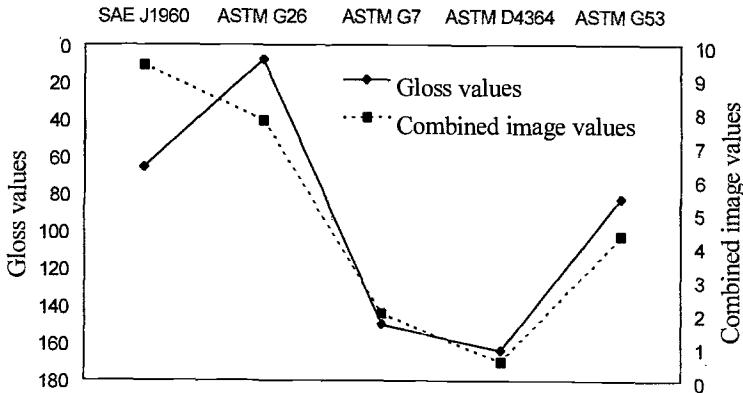


Figure 8-Combined Image Parameter vs. Gloss Values

Comparison of Standard Test Methods

One way to compare the severity of different test methods is to rank their performances at a particular interval during or after exposure. The interval at which ranking is assessed should be selected carefully because the performance trends could cross over during exposure. In this study, the comparison was made at the final interval, since the relative ranks were apparent at this interval. The combined image values, as discussed in the previous section, were used to compare the five test methods. The test methods were ranked by normalizing the values of each method to the most severe test method per each material. This normalization provides relative rankings rather than absolute rankings so that minor differences can be compared. The higher ranks indicate the more severe morphological changes, including the surface reflectance and texture.

As shown in Figure 9, the SAE J1960 xenon method ranked highest followed by the ASTM G26 xenon method. The SAE J1960 test method using Quartz/Borosilicate filter combination and a higher temperature condition was expected to be a harsh test. The ASTM G26 Florida Cycle is a modification of an ASTM G26 cycle and has an elevated temperature condition. In comparison to the ASTM G7 outdoor results, these two xenon standard tests were more aggressive than the Florida outdoor test. ASTM D4364 ranked lower than the two xenon methods and somewhat similar to the outdoor method in Plastics A and Plastics B. In terms of the degradation trend, the ASTM D4364 also followed the outdoor method in Plastics A and Plastics B, as shown in Figure 3 and Figure 4. This trend was not observed in Plastics C. The ASTM G53 results showed some variability in the relative rankings between Plastics A and Plastics B. In Plastics A and Plastics B, this fluorescent UV/condensation method ranked at 4.5 and 0.2 respectively.

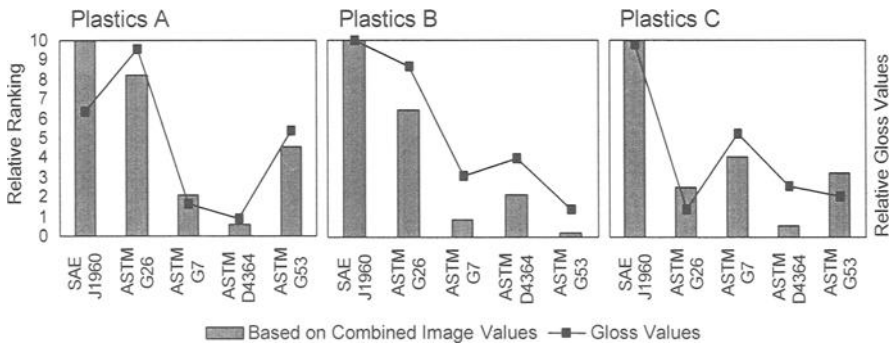


Figure 9—Normalized Severity Rankings of the Standard Test Methods

To assess the performances of the test methods, the apparent surface defects should be taken into consideration. The combined image values shown in Figure 9 suggest the influence of the apparent surface defects and the surface texture not quantified by the gloss measurements. As a result, several rankings and their relative

differences to other rankings are different from the gloss evaluation data. The difference may not look significant for this particular study that has a limited number of specimens. However, it is an important issue when a large number of specimens are evaluated and the performance criteria are stringent.

Table 8 contains a summary of observations and measurements of surface deterioration using the imaging and image analysis technique.

Table 8 – *Summary of the Effect of Five Benchmark Weathering Standard Test Methods*

	SAE J1960	ASTM G26	ASTM G7	ASTM D4364	ASTM G53
Light Source	Xenon	Xenon	Outdoor	AZ Solar	Fluorescent
Severity	1	2	3-4	3-5	3-5
Apparent Surface Defects	Cracking	Cracking	None	None	Water Spots
Comparison to the Outdoor test	More severe than outdoor	More severe than outdoor	N/A	Similar Deterioration Pattern	Cannot Determine

Summary

Understanding surface deterioration is an important factor in durability and weathering studies. Quantitative understanding of surface change is fundamental to better relate various external factors resulting in materials’ surface degradation. Conventional photometric measurements provide limited information and may lead to erroneous conclusions if the actual surfaces are not considered. As reported in this study, it is critical to properly understand causes and modes of surface degradation that are not obtainable by the conventional photometric measurement technique.

The imaging technique demonstrated in this report suggests the following benefits:

- The imaging technique can provide more appropriate viewing of weathered surfaces using different types of optical and illumination techniques.
- The geometric reflection similar to the gloss measurement is obtainable.
- The illumination technique enhances the surface texture allowing the surface morphology to be measured quantitatively.
- The image analysis technique provides quantitative measures for common surface defects.
- Multivariable image data may provide meaningful descriptions of weathered surfaces.
- The technique can minimize subjectivity in surface evaluation.

Examining the five standard test methods using the imaging technology, provided the following information:

- The current automotive standard test condition (SAE J1960) was the most severe test among the five standard conditions for all materials tested.
- The two xenon standard test conditions (SAE J1960 and ASTM G26) were more severe than the other test conditions for most of materials tested.
- The ASTM G53 florescent UV/condensation test method varied more significantly in the relative rankings compared to other test methods and rendered uncommon surface defects for some materials.

Acknowledgments

The authors would like to thank the following laboratories for exposure and evaluation of the materials. South Florida Test Service, Miami, Florida, and DSET Laboratories, Phoenix, Arizona. The authors would also like to thank Mr. Al Zielnik, General Manager, Polymer Evaluation Products, Atlas Electric Devices Co. and Mr. Matt McGreer, General Manager, Client Education, Atlas Electric Devices Co. for their knowledge and insight during the study.

References

- [1] Martin, J. W., Saunders, S. C., Floyd, F. L., and Wineburg, J. P., *NIST Building Science Series 172, Methodologies for Predicting the Service Lives of Coating Systems*, Building & Fire Research Lab, National Institute of Standards and Technology, 1994.
- [2] Martin, J. W., and McKnight, E., *Journal of Coatings Technology*, 1985, 57, 49.
- [3] Pourdeyhimi, B., and Lee, F., *European Coatings Journal*, 1995, 11, 804.
- [4] Pourdeyhimi, B., Wang, X., and Lee, F., "Evaluation of Scratch and Mar Resistance in Automotive Coatings: Nanoscratching by Atomic Force Microscope", *European Coatings Journal*, In Press.
- [5] Pourdeyhimi, B., Wang, X., and Lee, F., "Evaluation of Scratch and Mar Resistance in Automotive Coatings: Surface Reflectivity and Texture", *European Coatings Journal*, In Press.
- [6] Russ, J. C., *The Image Processing Handbook*, CRC Press, Boca Raton FL, 1994, pp. 3-5.
- [7] Lee, F., Pourdeyhimi, B., and Adamsons, K., "Analysis of Coatings Appearance and Surface Defects Using Digital Image Capture/Processing/Analysis, The International Symposium on a Systems Approach to Service Life Prediction of Organic Coatings, Breckenridge, Co, Sep 14-19, 1997.
- [8] Pourdeyhimi, B., *Image 2.0 - Image Processing and Analysis Program*, 1999.
- [9] Discussions with Dr. Norma Searle.
- [10] Discussions with Dr. George Wypych.

Ronald R. Adkins¹

On The Use Of Ion Scattering Spectroscopy To Predict The Outdoor Durability Of Polymeric Films

Reference: Adkins, R. R., “On the Use of Ion Scattering Spectroscopy to Predict the Outdoor Durability of Polymeric Films,” *Durability 2000: Accelerated and Outdoor Weathering Testing, ASTM STP 1385*, J. D. Evans and W. D. Ketola, Eds., American Society for Testing and Materials, West Conshohocken, PA, 2000.

Abstract: Ion scattering spectroscopy (ISS) has been found to have potential as a fast method of predicting the outdoor durability of polymeric films. Three sets of samples were studied by ISS. The samples had been artificially weathered for 500 hours. The ISS measurements looked at the hydrogen/carbon (H/C) and the oxygen/carbon (O/C) ratios as a function of depth. There was no apparent correlation of the ratios of the weathered samples to known outdoor performance. However, when the H/C and O/C ratios of the file samples were divided by those of the artificially weathered samples as a function of depth, there was a correlation. The proportions of the H/C ratios were found to correspond directly to the known outdoor weathering results for two of the three sets of samples. The proportions of the O/C ratios were found to correspond to known outdoor weathering in the third set and also to one of the two sets in which there was correlation with the H/C ratios.

Keywords: ion scattering spectroscopy, weathering

Introduction

The market is demanding materials with greater outdoor lifetime expectancy with faster product introductions. This has forced a greater dependency on artificial test methods to determine if a product will meet the lifetime expectancy and has also led to studies in the development and understanding of test methods.

The science of weathering is a science of the surface according to some [1]. Our studies would indicate also that changes from weathering occur first at the surface and interfaces before going into the bulk. This led to the consideration of the use of ion scattering spectroscopy (ISS) as an instrument to follow these changes. ISS is well suited to looking at the first few atomic layers of a material [2].

¹Division Scientist, Commercial Graphics Division, 3M Corporation,
Building 207-BN-03, 3M Center, St. Paul, MN 55144-1000.

Experimental Method

Samples

Three sets of samples were chosen for our initial study on the use of ISS to determine more quickly the outdoor durability of materials. Samples 1, 2, and 3 are three different urethane clear coats over the same white plasticized vinyl film. Samples 4, 5, and 6 are three urethane acrylate overlay films with differing amounts of ultraviolet absorbers (UVA) and hindered amine light stabilizers (HALS). Samples 7, 8, and 9 are three melamine/alkyd top films in which only the amounts of UVA and HALS stabilizers differ. These samples were weathered for 500 hours by a proprietary test method, based upon ASTM Standard Practice for Operating Fluorescent Light Apparatus for UV Exposure of Nonmetallic Materials (G154-98), that we feel gives a good correlation to outdoor weathering. The samples had been weathered in Florida and Arizona for four years and the outdoor performance of these three sets of materials is known to be:

$$\begin{aligned} 1 &\approx 2 > 3 \\ 5 &> 4 \approx 6 \\ 8 &> 7 \approx 9 \end{aligned}$$

Ion Scattering Spectroscopy

The samples were studied by ISS at Advanced R&D in Stillwater, MN. All samples were analyzed under identical conditions using a KRATOS/3M Model 535 BX combined ISS/SIMS System equipped with a Balzers 160 L/sec turbomolecular pump on the sample insertion chamber. All data were obtained automatically using an Advanced R&D Computer Data System. The samples were measured for the H/C and O/C ratios as a function of depth (sputtering time). The depth (A) of the sputtering with time is not linear so that the axes for depth are not linear.

Results and Discussion

There was no apparent relationship between the hydrogen/carbon (H/C) and oxygen/carbon (O/C) ratios of the samples and known outdoor weathering performance when looking at only the ratios of the weathered samples. However, when the H/C and O/C ratios of the file samples were divided by the corresponding ratios of the weathered samples as a function of depth, correlations to known outdoor performance did emerge.

Figure 1 graphs the proportions of the H/C ratios of the file samples to the artificially weathered samples for Samples 1—3 while Figure 2 displays the proportions of the O/C ratios of these samples as a function of depth. In Figure 1, there is a distinct difference between Sample 2 and Samples 1 and 3 at a depth below the surface of 5 A and more. This relationship, however, does not correspond to the known outdoor weathering performance as noted above. Furthermore, the proportions of Figure 1 are not approaching 1.0 that would be expected at a depth of the bulk that has not been affected by the weathering. Figure 2 presents the proportions of the O/C ratios. Here, at a depth greater than 8 A, the results correspond to the known outdoor performance. Samples 1

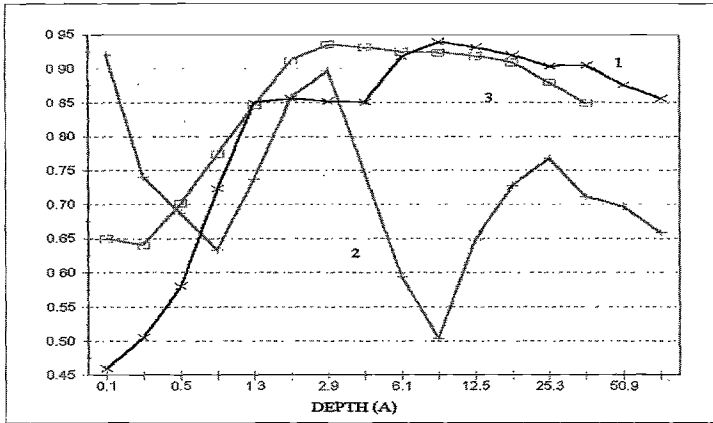


Figure 1. The Proportions of the H/C Ratios of the File Samples to the Weathered Samples as a Function of Depth for Samples 1—3.

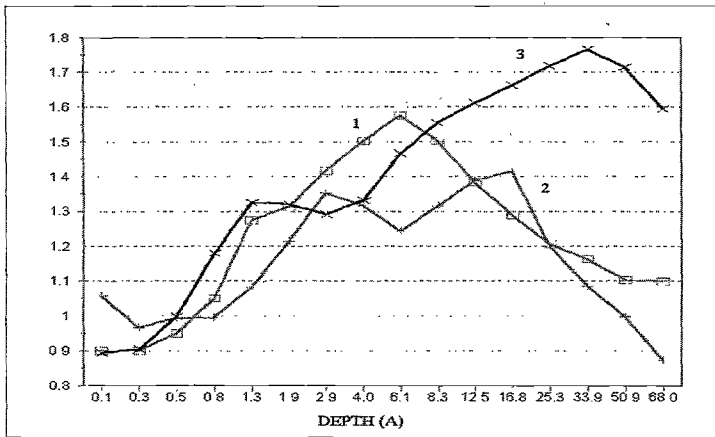


Figure 2. The Proportions of the O/C Ratios of the File Samples to the Weathered Samples as a Function of Depth for Samples 1—3.

and 2 are the same and distinctly different from Sample 3. The results show also that at a depth of around 50 A the proportions are at or near 1.0 for Samples 1 and 2 whereas for Sample 3 the depth would be much greater before the proportion approaches 1.0.

Figures 3 and 4 are the corresponding figures for Samples 4, 5, and 6, the three urethane acrylate overlay films. In Figure 3, from a depth near the surface to about 50 A, the results correspond to known outdoor performance (see above) with Sample 5 being distinctly different from Samples 4 and 6 which are comparable. The proportions of the H/C ratios for Sample 5 remain at or near 1.0 over a depth of the 100 A suggesting no effect by the weathering cycle. The proportions of the H/C ratios for Samples 4 and 6, however, do not appear that they would approach 1.0 unless at a depth much greater than

the 100 A. The O/C proportions in Figure 4 correspond also to known outdoor performance at a depth greater than 25 A. Here, however, all proportions are near 1.0 so there is some question as to what is being measured.

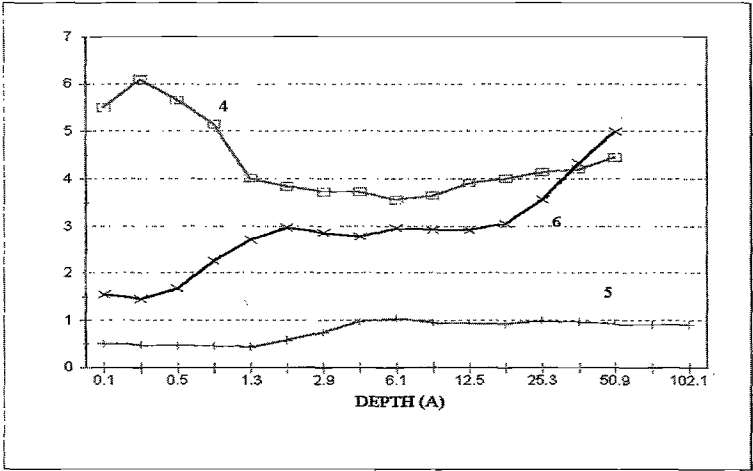


Figure 3. The Proportions of the H/C Ratios of the File Samples to the Weathered Samples as a Function of Depth for Samples 4—6.

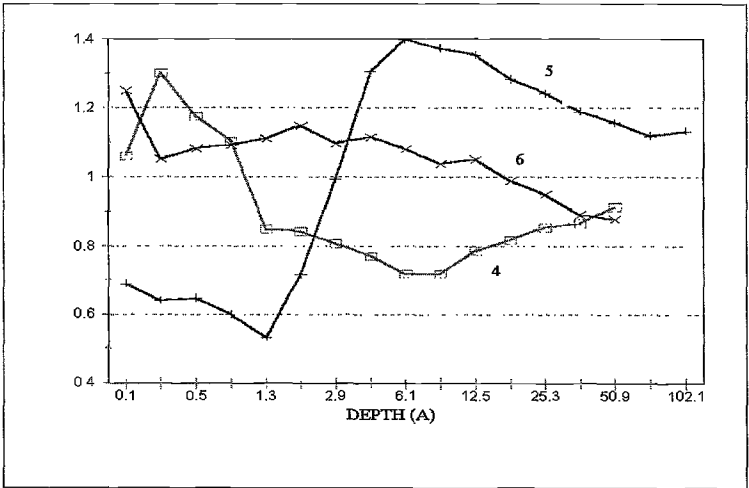


Figure 4. The Proportions of the O/C Ratios of the File Samples to the Weathered Samples as a Function of Depth for Samples 4—6.

Figures 5 and 6 are the corresponding figures for Samples 7, 8, and 9, the melamine/alkyd films. From a depth of around 4 A and deeper, the proportions of the H/C ratios in Figure 5 correspond to known outdoor performance. With these three

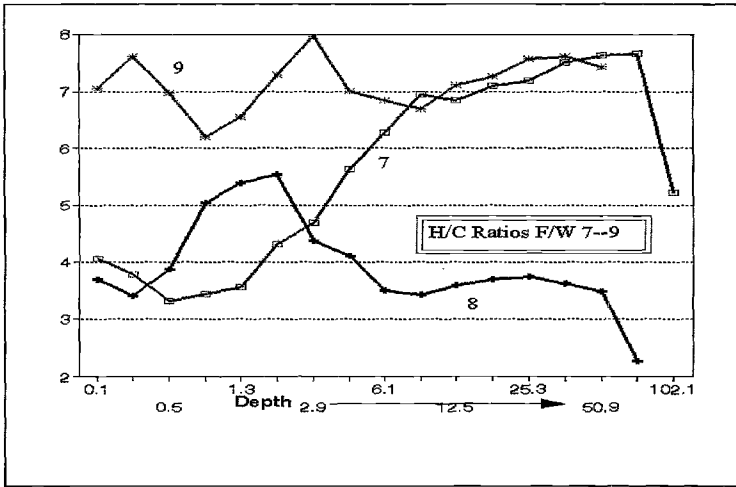


Figure 5. The Proportions of the H/C Ratios of the File Samples to the Weathered Samples as a Function of Depth for Samples 7-9.

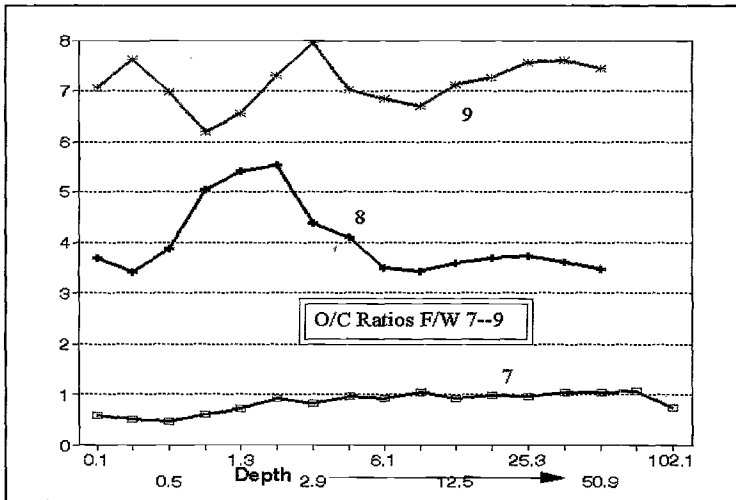


Figure 6. The Proportions of the O/C Ratios of the File Samples to the Weathered Samples as a Function of Depth for Samples 7-9.

samples, the proportions of the H/C ratios will not approach 1.0 until a depth significantly greater than 100 Å. This would suggest that these samples have been affected more by the artificial weathering than the other two sets of samples. In Figure 6, the results indicate that all three samples are different. This is not the case from known outdoor weathering results.

Conclusions

This study has been a preliminary one, at best. Future studies would be needed to see why there are correlations with known outdoor weathering with the H/C ratios in some samples and with the O/C ratios with others. Whether this is a reflection of different mechanisms of degradation among the polymeric films or a reflection of the degradation of the different stabilizer packages cannot be said at this time. The above correlations were observed after 500 hours of artificial weathering. No studies were done to determine the least amount of artificial weathering necessary before the correlations became apparent.

The results are encouraging for further work as we feel that these results have shown that ISS could be used to investigate the weathering performance of the top layer of a construction by looking at the proportions as a function of depth of either the H/C or O/C ratios. A comparison of the ratios of just the weathered samples did not give any indication of the relative performance of the samples within the three series of samples tested.

References

1. Johnson, B. W. and McIntyre, R., "Analysis of Test Methods for UV Durability Predictions of Polymer Coatings," *XXth International Conference in Organic Coatings Science and Technology, Proceedings 20*, 205, 1994.
2. Taglauer, T., "Low-energy Ion Scattering and Rutherford Backscattering," Chapter 6 in *Surface Analysis, The Principal Techniques*, John C. Vickerman, Ed., John Wiley and Sons, New York, 1997.

Norma D. Searle¹

Activation Spectra: Techniques and Applications to Stabilization and Stability Testing of Materials

Reference: Searle, N. D., "Activation Spectra: Techniques and Applications to Stabilization and Stability Testing of Materials," *Durability 2000: Accelerated and Outdoor Weathering Testing*, ASTM STP 1385, J. D. Evans and W. D. Ketola, Eds., American Society for Testing and Materials, West Conshohocken, PA, 2000.

Abstract: The activation spectrum of a material represents the relative amount of damage caused by individual spectral regions of the source to which the material is exposed. Experimental techniques used to determine activation spectra include (1) narrow-band radiation utilizing interference filters or a grating or prism spectrograph and (2) polychromatic radiation with sharp cut-on UV/visible transmitting glass filters to define the relative effects of radiation by individual spectral regions during exposure to all wavelengths longer than the cut-on of the filter. The spectral effects of radiation on a material are determined by measurement of spectral changes, i.e., by UV, visible or infrared spectroscopy, and, if sample size permits, by changes in physical properties.

Applications of activation spectra include the development of light stable materials, the design of meaningful light stability tests, timing of exposures based on actinic radiation and prediction of service life by providing a means of determining effective dosage. Examples are given to demonstrate many of the applications of activation spectra and comparison is made with action spectra which represent the wavelength sensitivity of a material independent of the spectral emission properties of the radiation source.

Keywords: activation spectra, action spectra, sharp cut-on filters, spectrograph, interference filters, actinic radiation, wavelength sensitivity

Introduction

The effects of ultraviolet (UV) and visible radiation on a material are wavelength dependent because of the spectral selectivity of both the absorption of the incident radiation by the material and the quantum efficiencies of degradation. The rate of degradation as well as the mechanism and type of degradation of many materials depend on the incident wavelengths [1-3]. The activation spectrum of a material is a graphic representation of the relative amount of damage caused by individual spectral regions of the source to which the material is exposed. It is often also referred to as the spectral sensitivity or

¹Consultant, Plastics and Chemicals, 114 Ventnor F, Deerfield Beach, FL 33442-2415.

wavelength sensitivity of a material. It differs from an action spectrum in that it represents the spectral effects of a specific light source on a material, while an action spectrum is the source-independent wavelength sensitivity of a material [3-5].

Activation Spectra Techniques

Two main techniques have been used to determine the changes produced in a material by individual spectral regions of a light source. One is based on isolating narrow bands of radiation either with interference filters or with a prism or grating spectrograph. The other is based on the use of UV/visible transmitting sharp cut-on glass filters to define individual spectral regions during exposure to polychromatic radiation. While the isolated narrow band technique, particularly the spectrographic technique, provides higher resolution wavelength sensitivity spectra, the cut-on filter technique more closely simulates natural polychromatic exposures since samples are irradiated simultaneously by all wavelengths longer than the spectral region being evaluated.

Narrow Band Techniques

Interference Filters – The determination of activation spectra of polymeric materials using interference filters to isolate portions of the incident actinic radiation was demonstrated by G. Kampf et al. [6]. Each filter is used for exposure of a separate specimen to an individual spectral band. All specimens are exposed for the same length of time. The change in property caused by each spectral band is plotted as a function of either the wavelength at the peak of the spectral band or the spectral range of the band at half the peak height. Figure 1 shows both types of plots for the activation spectrum of polyamide-6 based on formation of yellow color by global solar radiation.

The smooth curve connects points representing the peak wavelengths of the six spectral bands isolated by the six interference filters. The bar graphs represent the spectral ranges of the bands. The activation spectrum shows that the 320 nm spectral region of terrestrial solar radiation causes the most intense yellowing, while the 400 nm region is most effective in photobleaching the yellow colored products present prior to exposure.

The action spectrum is shown by the curve that connects the open circles. It represents the yellowing caused by exposure to the same radiant energy by each of the spectral bands and therefore does not reflect the differences in intensities among the spectral bands. Since the energy of the photons associated with each wavelength increases with decreasing wavelength, the shorter the wavelength the greater the damaging effect on the polymer. Thus, in contrast to the activation spectrum, which reflects the sharp decrease in intensity of solar radiation below 320 nm [3], the action spectrum shows increase in sensitivity with decreasing wavelength in this region. The two types of spectra differ in both appearance and the type of information they provide. They are also experimentally different in that measurement of the intensity of the radiation in each spectral band is required for an action spectrum, but not for an activation spectrum.

The interference filter technique is applicable to any type of exposure normally used for the materials. Since a specimen the size of the filter can be irradiated by each spectral band, it allows determination of spectral sensitivities by physical property changes such as tensile strength, elongation and impact strength as well as by spectral changes. How-

ever, this technique is not widely used because of the instability of the filters to ultra-violet radiation and humidity.

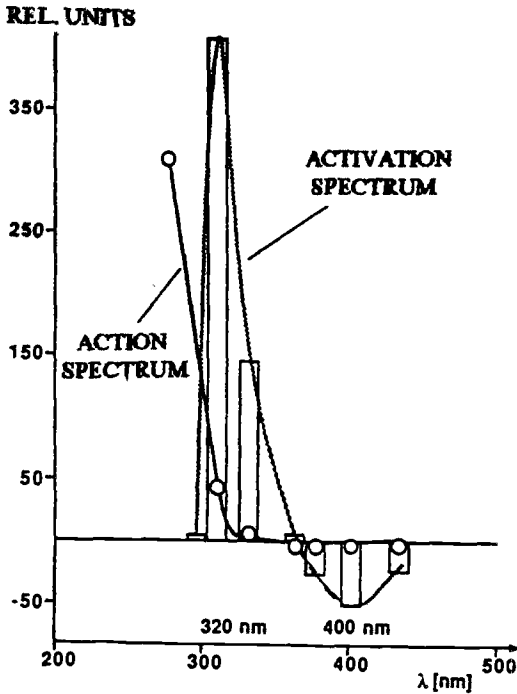


Figure 1 – Activation and Action Spectra of Polyamide-6 Yellowing;
Light Source for Activation Spectra: Global Solar Radiation

Spectrograph – In the spectrographic technique [7-10], the radiation is spectrally dispersed into individual spectral bands by either a prism or grating and projected onto a single specimen placed in the focal plane of the spectrograph. Each band irradiates a different section of the specimen, thus producing a degradation “spectrum”. The spectrograph provides a full range of spectral bands in contrast with the limited number of bands normally covered by the use of interference filters. However, the light source used for activation spectra by this technique is usually limited to one that can be focussed on the entrance slit. Both sunlight and borosilicate filtered xenon arc radiation have been used. The sample is irradiated in the focal plane at the exit window until the changes produced are sufficient to provide a well-defined activation spectrum. Because each spectral band irradiates only a very narrow section of the sample, depending on the size of the spectrograph, detection of degradation may be limited to spectral changes.

In the quartz prism spectrograph used for activation spectra by Hirt and co-workers [7-9], the spectral region between 280 nm and 410 nm was spread across about a 1 cm wide section of the specimen. The dispersion ranged from 10 nm/mm at the short wavelength end to 30 nm/mm at the long wavelength end. Specially designed adapters for

UV/visible and infrared spectrophotometers were used to determine the absorption of a specific wavelength in 0.5 mm sections of the sample before and after exposure. For example, to determine the relative amount of yellowing or bleaching caused by each of the spectral bands, absorption of 400 nm was measured with the UV/visible spectrophotometer set for this wavelength. The change in absorption measured was then plotted as a function of wavelength of irradiation to produce the activation spectrum.

Calibration of the sample position for wavelength of irradiation was accomplished by substituting a photographic plate for the sample at the exit window in the identical position of the sample and exposing it to the spectrally dispersed emission lines of a low pressure mercury arc focused on the entrance slit. The positions of the mercury lines on the plate were determined by densitometry.

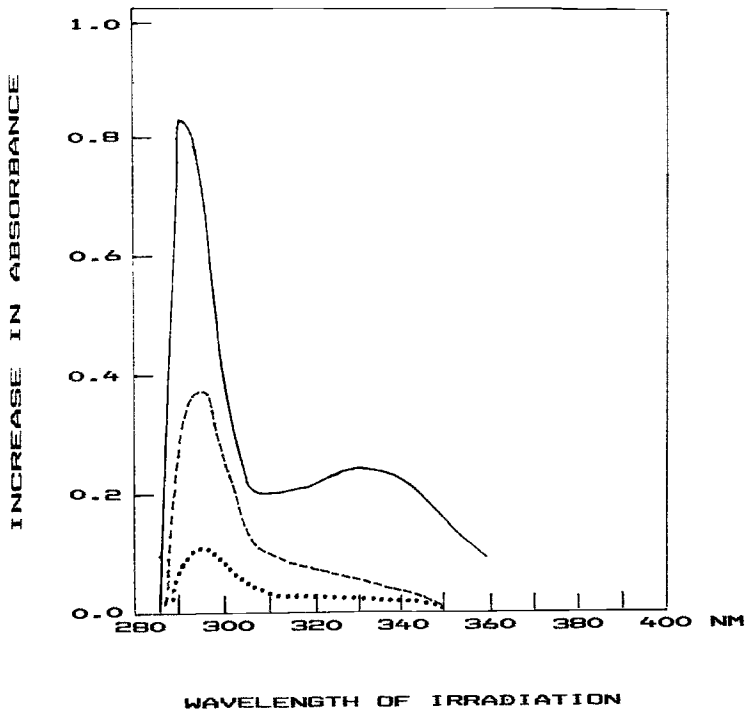


Figure 2 – Activation Spectra of Polycarbonate: Increase in Absorbance at 300 nm (—) 350 nm (- -) and 400 nm (···); Light Source: borosilicate glass filtered xenon arc

Figure 2 shows the activation spectrum of a 0.1 mm film of bisphenol-A polycarbonate obtained with this equipment using the borosilicate filtered xenon arc as the exposure source. The spectral effects were based on increase in absorbance at 300 nm, 350 nm and 400 nm. The activation spectrum shows that two distinctly separate spectral regions of this source cause both increase in UV absorption and yellowing. The largest change is

caused by wavelengths in the 295-300 nm region in spite of the fact that the intensity of the source in this region is only about $1/15^{\text{th}}$ the intensity in the longer wavelength actinic region. The latter ranges from about 310 to 350 nm with wavelengths of about 330 nm having maximum effect.

Studies of polycarbonate have revealed two different mechanisms of degradation as well as differences in absorption properties of polycarbonate in these spectral regions [2, 11-14]. Wavelengths shorter than 300 nm are strongly absorbed by the main structural components of polycarbonate. The energy of the photons absorbed causes one of the polycarbonate bonds to break, followed by photo-Fries rearrangement of polycarbonate and formation of strongly yellow colored degradation products. Wavelengths between 310 and 340 nm, absorbed by impurities and defects formed primarily as a result of thermal oxidation during processing, initiate photooxidation processes. The latter also led to yellow colored degradation products.

L. D. Johnson et al. [10] used a grating spectrograph with spectrum dispersion at the sample plate of 2 nm/mm and a 5 X 7 inch photographic plate as the sample holder. Film samples were taped to the plate. Fiber samples were wound around the plate in the direction perpendicular to the dispersed spectral radiation, thus exposing a section in the center of each fiber to essentially monochromatic light of known wavelength. Sample position was related to wavelength of incident light as described above using a low pressure mercury arc line source and standard photographic procedures. Similar spectral sensitivities to xenon arc radiation were obtained for yellowing of a film of aromatic polyamide and loss in tensile strength of the fiber, indicating that the same initiating species is involved in both effects.

In the Okasaki large grating spectrograph (OLS) built at the National Institute for Basic Biology in Okasaki, Japan [5] spectral bands between 250 nm and 1000 nm are projected onto a 10 meter long focal curve with a dispersion of 0.8 nm/cm. Thus, individual samples large enough for various types of physical property tests are irradiated by each spectral band. Although activation spectra can be obtained, the studies on polymers were mainly designed to produce action spectra.

Polychromatic Technique – Sharp Cut-On Filters

In the polychromatic technique, spectral bands are defined by the difference in transmission of pairs of sharp cut-on UV/visible transmitting glass filters. A set of 12 to 15 specially designed filters is used to define 10 spectral bands between about 270 and 400 nm, some of which overlap. Figure 3 shows the spectral transmission curves of 9 of the short wavelength filters in one of the sets [15]. Filter 1 is used to determine the effect of exposure to the full radiation of the source minus the portion specularly reflected by all the filters. The 5% transmission wavelength of the filter is considered the cut-on wavelength. Each progressively shorter wavelength filter transmits increasingly more short wavelengths and a larger portion of the total UV than the next longer wavelength filter. All filters transmit most of the visible and infrared radiation.

Figure 4 shows the 6 spectral regions of irradiation defined by Filters 2 through 9. Each spectral band represents the incremental portion of the ultraviolet transmitted by the shorter wavelength filter of the pair. The spectral band peaks at the wavelength of maximum difference in transmission of the pair of filters. The spectral range of the band at

approximately half the peak height i.e., at delta 20% transmission, is defined as the spectral region of irradiation.

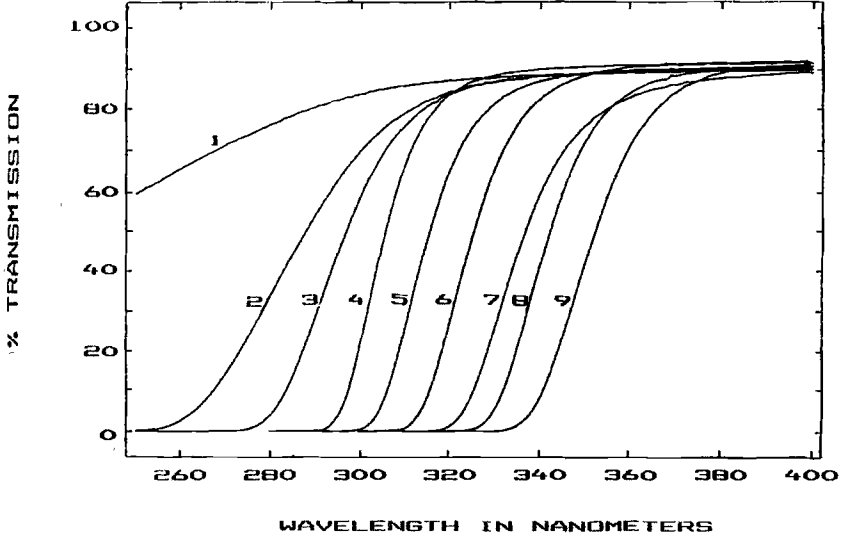


Figure 3 – Spectral Transmission Curves of Sharp Cut-on Glass Filters

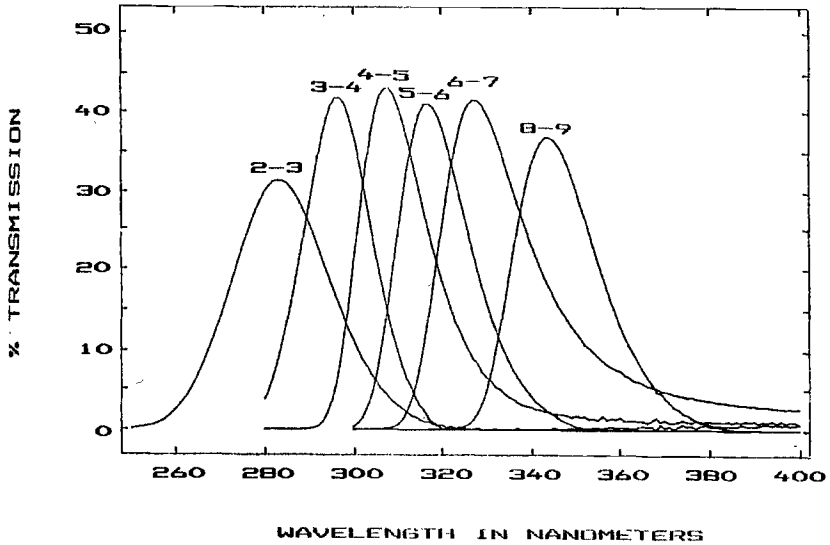


Figure 4 – Spectral Bands Defined by Filter Pairs in Figure 3

An activation spectrum is determined by exposing a replicate specimen of the material behind each of the filters. All specimens are exposed for the same length of time, sufficient to produce measurable degradation in most of the specimens and a statistically significant difference in degradation in the two specimens exposed behind most pairs of filters. The difference in degradation is attributed to the additional degradation in the specimen exposed behind the shorter wavelength filter of the pair.

An activation spectrum by the sharp cut-on filter technique is illustrated in Figure 5. It is based on formation of yellow color on exposure of a 0.70 mm film of Bisphenol-A polycarbonate to borosilicate filtered xenon arc radiation. The wavelength sensitivity profile is similar to that of the activation spectrum in Figure 2 obtained by the spectrographic technique. Yellowing is caused by two spectral regions, with the shorter wavelengths having the more severe effect. Thus, the spectrographic and filter techniques provide similar information. Wavelength shifts between the two may be due to material differences such as formulation as well as thickness and spectral band widths.

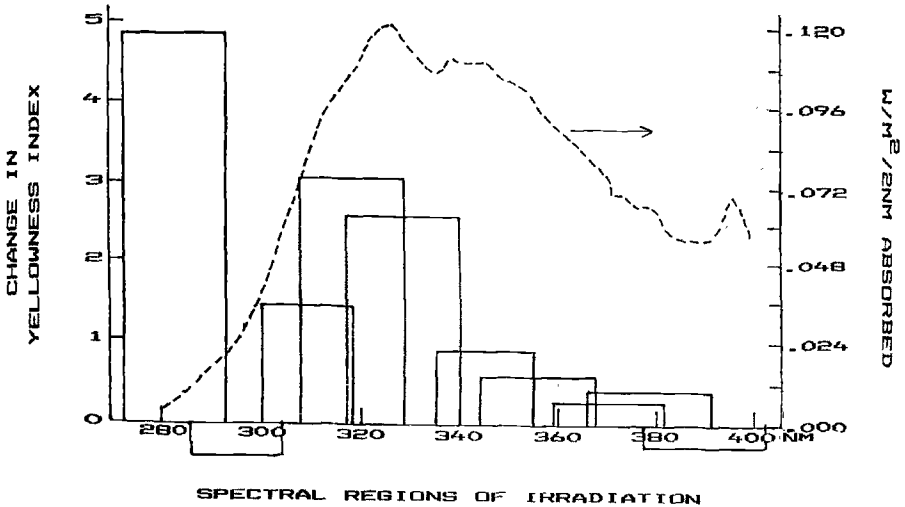


Figure 5 – Activation Spectrum of Polycarbonate Yellowing With Spectral Energy Absorbed Superimposed. Light Source: Borosilicate Glass Filtered Xenon Arc

The data in Figure 5 is plotted in bar graph form with the width of the bars representing the spectral range of each band and the height representing the change caused by the spectral band. Alternatively, the data can be plotted as a function of peak wavelength of the spectral band to produce the activation spectrum as a smooth curve, similar to that shown for the spectrographic technique.

As with the interference filters, physical property as well as spectral changes can be used as the criterion of degradation since the size of the specimen exposed to each of the spectral bands can be as large as the filter. The latter are commonly 5.2 cm (2 in.) square, but can be as large as 15.2 cm (6 in.) square. Depending on the size of the specimens required by the measurement technique, each of the filters may be used for multiple specimens.

The advantage of filters over a spectrograph for activation spectra is that they are applicable to any exposure source, while the spectrograph is only applicable to a light source that can be focussed on the entrance slit. The sharp cut-on filter technique is also more representative of the polychromatic nature of exposures under service conditions.

The Activation Spectrum – Determining Factors

The activation spectrum of a material is determined by: (1) the spectral absorption properties of the material, (2) the emission properties of the light source, (3) the quantum efficiencies of the degradation processes initiated by the absorbed wavelengths, and (4) the type of degradation measured.

Relation Between (1) and (2)

The spectral absorption properties of a material identify the fraction of the incident radiation at each wavelength that a material is capable of absorbing. Only light absorbed can have any effect on a material. The mere incidence of light on the surface cannot cause any damage if it is not absorbed. Therefore, the relation between the absorption properties of the material and the emission properties of the light source is fundamental to the interaction of the radiation with the material and thus to the activation spectrum.

The dependence of the activation spectrum of a material on the light source is illustrated by Figures 6 and 7 which show the activation spectrum of a thin film of polyarylate exposed to solar radiation and the fluorescent UVB source, respectively [16]. Yellowing by solar radiation is due primarily to wavelengths between 335 nm and 365 nm. Wavelengths shorter than 330 nm and longer than 380 nm have considerably less effect in yellowing the film of polyarylate. In contrast, yellowing of the film by fluorescent UVB lamps is caused mainly by wavelengths between 310 nm and 340 nm. Obviously, this type of radiation does not represent the spectral effects of solar radiation in the photochemical yellowing of polyarylate.

Quantum Efficiencies of Absorbed Wavelengths

Although absorption of radiation is a prerequisite to photodegradation, the spectral energy absorbed by the material from the light source is not in itself sufficient to define the activation spectrum. The relative amount of damage as a function of wavelength is dependent on the quantum efficiencies of degradation by the absorbed photons associated with each wavelength. The relation between the energy of each type of photon absorbed and the bond strengths of the material largely determine the potential damage by each of the wavelengths.

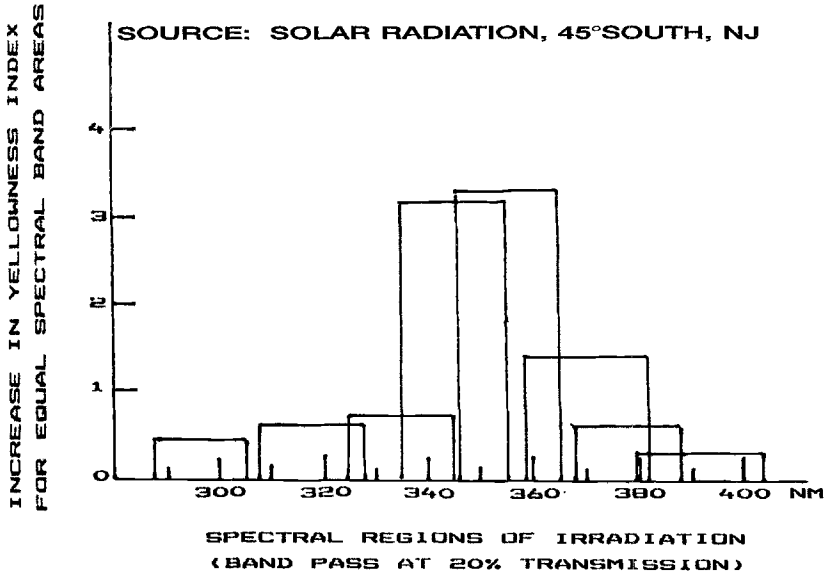


Figure 6 – Activation Spectrum of a 0.075 mm Film of Polyarylate Exposed to Solar Radiation

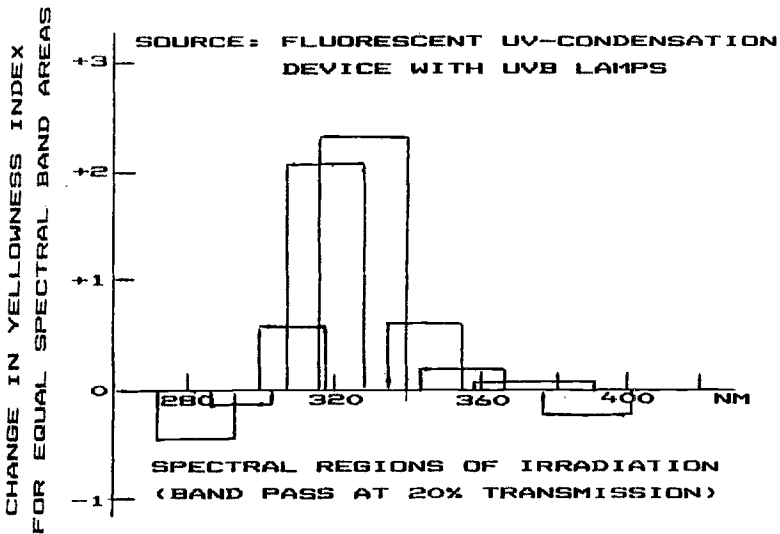


Figure 7 – Activation Spectrum of a 0.05 mm Film of Polyarylate Exposed to Fluorescent UVB Radiation

The fact that the activation spectrum is not defined solely by the spectral energy absorbed is illustrated in Figure 5 where the spectral radiation absorbed by the polycarbonate film from the light source is superimposed on the activation spectrum. The amount of radiation absorbed at each wavelength was calculated by multiplying the spectral irradiance of the light source by the spectral absorption properties of the film. Although the amount of radiation absorbed by the polycarbonate film between 325 nm and 345 nm is about tenfold more than the amount of radiation shorter than 300 nm absorbed by the film, the most intense yellowing is caused by the latter wavelengths.

The higher quantum efficiencies of polycarbonate degradation by the shorter wavelengths results from the differences in the photochemistries described in a previous section. It is known that the shorter wavelength, higher energy photons cause more severe degradation because they are capable of breaking more types of bonds, but the amount of damage cannot be predicted. Photodegradation involves complex reaction processes which are still not fully understood for most materials. Therefore, the activation spectrum must be determined experimentally.

Type of Degradation Measured

Since in many materials the mechanism and type of degradation differs with wavelength, the activation spectrum will shift with type of degradation measured. As an example, loss in impact strength of ABS and carbonyl formation in polyethylene is caused by longer wavelengths than those that cause yellowing in these polymers [17,18]. In some materials, tensile strength is mainly affected by short wavelengths, while longer wavelengths are primarily responsible for changes in elongation. The effect of wavelength on type of degradation is often due to differences in the depth of penetration of wavelengths into the material. In TiO₂ and ZnO pigmented systems and aromatic type polymers, short wavelengths are very strongly absorbed and therefore cannot penetrate significantly into the inner layers. Thus, degradation by these wavelengths is confined to surface layers. However, the longer, more weakly absorbed wavelengths are able to penetrate more deeply and thus cause bulk effects. For this reason, the activation spectrum will depend on whether surface or bulk properties are measured.

Applications of Activation Spectra

Stabilization of Materials

Light Screening Requirements – The activation spectrum of a material identifies the spectral region(s) of a specific light source responsible for its degradation and thus the type of light screening required and the potential for protection by an ultraviolet absorber. For example, the polyarylate activation spectrum in Figure 6 shows that an appropriate ultraviolet absorber would be capable of screening most of the wavelengths in solar radiation that cause yellowing of a 0.075 mm (3 mil) film. However, a 1.5 mm (60 mil) plaque of polyarylate is shown by the activation spectrum in Figure 8 to require protection against wavelengths that are not adequately screened by an ultraviolet absorber.

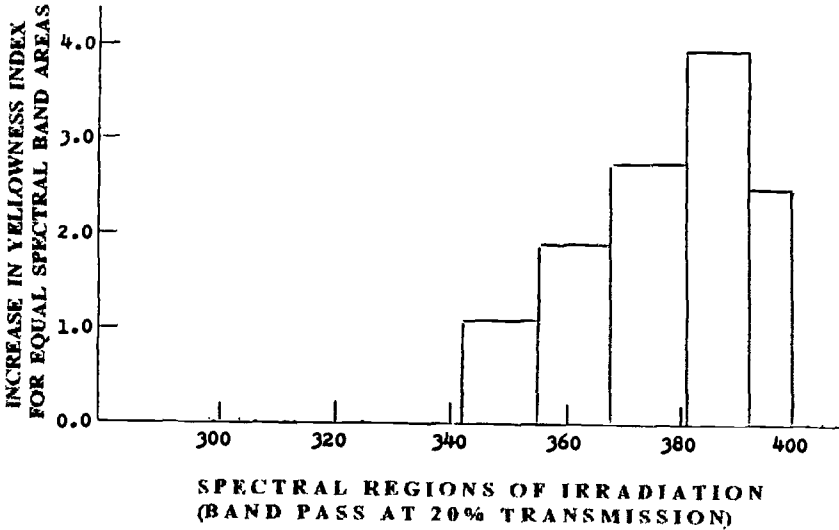


Figure 8 – Activation Spectrum of a 1.5 mm Plaque of Polyarylate Exposed to Borosilicate Glass Filtered Xenon Arc Radiation

Any additive capable of effectively screening the long wavelength UV radiation that causes yellowing in the polyarylate plaque would itself impart yellow color to the material. This information would have been useful in avoiding costly and time consuming investigations which had been carried out in an attempt to stabilize the thicker form of the polyarylate with UV absorbers.²

Evaluation of Screening Effectiveness – The relative screening effectiveness of different types of ultraviolet absorbers can be estimated from the match of their absorption properties to the activation spectrum of the material. The closer the match, the more effective the protective additive will be in screening the harmful radiation, assuming other factors such as dispersion, compatibility and migration are adequate.

The activation spectrum of the stabilized material identifies spectral regions that may require additional screening. This is illustrated in Figure 9 which shows activation spectra of a 3.2 mm thick aromatic polyester plaque both in the unstabilized form and stabilized with an orthodihydroxybenzophenone type UV absorber [3]. Comparison of the two spectra shows that while the additive protects the polymer against most of the wavelengths in the borosilicate filtered xenon arc that cause yellowing, it does not completely protect it against the shortest actinic wavelengths. On prolonged exposure of the stabilized material, yellowing is caused by wavelengths between 290 nm and 325 nm

²Personal communication

lifetimes when exposed under environmental conditions. Activation spectra provide information useful in selection of the appropriate laboratory accelerated test device by determining whether the harmful wavelengths in the artificial weathering source match those in the natural source. For example, comparison of Figures 6 and 7 shows a significant difference between the wavelengths in the fluorescent UVB lamps and solar radiation responsible for yellowing a thin film of polyarylate.

The importance of identifying and simulating the harmful wavelengths in the source to which the material is exposed under use conditions is that differences in harmful wavelengths can also cause differences in mechanism and type of degradation. This can result in distortion in stability ranking of materials compared with their ranking under use conditions. In addition, laboratory accelerated test data is only applicable to prediction of lifetimes under use conditions if the mechanisms and types of degradation are the same under both types of exposure.

Differences in wavelengths responsible for degradation can also result in invalid data on the effectiveness of an ultraviolet absorber or other type of stabilizer in protecting the material against the natural source. For example, the activation spectra in Figures 6 and 7 show that the fluorescent UVB lamps cannot be reliably used to test the effectiveness of an ultraviolet absorber in protecting the polyarylate film against solar radiation. This source would rate as effective an additive that only screens wavelengths shorter than 340 nm, whereas the additive would offer very little protection to the polyarylate film against the longer wavelengths of solar radiation that are responsible for the yellowing.

Use of Full Spectrum Actinic Exposure – The importance of closely simulating the full spectrum of actinic wavelengths of the natural source by the laboratory accelerated test

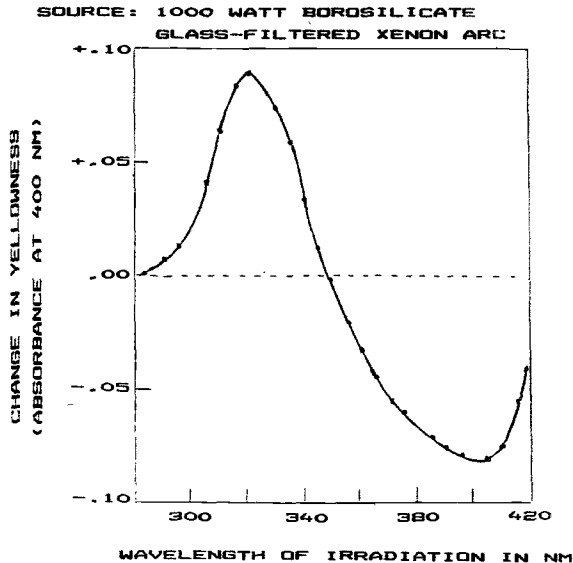


Figure 10 – Activation Spectrum of Photochemically Yellowed Aromatic Polyester

source is supported by activation spectra showing the antagonistic effects of different spectral regions. For example, bleaching by long wavelength UV and short wavelength visible radiation of the yellowing caused by short wavelength UV radiation occurs in many polymeric materials. It is illustrated in Figure 10 which shows the activation spectrum of a photochemically yellowed 3.2 mm thick sample of an aromatic polyester [3].

On exposure to borosilicate glass filtered xenon arc radiation, wavelengths between 350 nm and 450 nm bleach the yellow color which had been formed on exposure to a fluorescent UVB source, while wavelengths shorter than 350 nm cause further yellowing. Bleaching by long wavelength UV radiation also occurs in unirradiated polymeric materials. This is illustrated in Figure 1 for polyamide-6 and in Figure 11 for an aromatic polyester. Bleaching of yellow colored thermal oxidation products formed during processing [19] is particularly evident in the thicker forms of aromatic type polymeric materials. Other antagonistic effects in polymers by different spectral regions include scission of chemical bonds by short wavelength UV versus crosslinking by long wavelength UV and interference between other types of reactions [1, 20].

Thus, the net effect of the radiation source depends on the relative intensities of the long versus short wavelengths. Therefore, simulation of the spectral power distribution of long wavelength UV and visible radiation of the natural source is as important as simulation of the short wavelengths for colorless as well as for colored materials.

Form of Test Samples – The spectral sensitivities of polymeric materials vary not only with type of polymer, but also with thickness. The shift in activation spectrum depends on the absorption properties of the polymer and type of light source. The shift in activation spectrum to longer wavelengths with increase in thickness of an aromatic type poly-

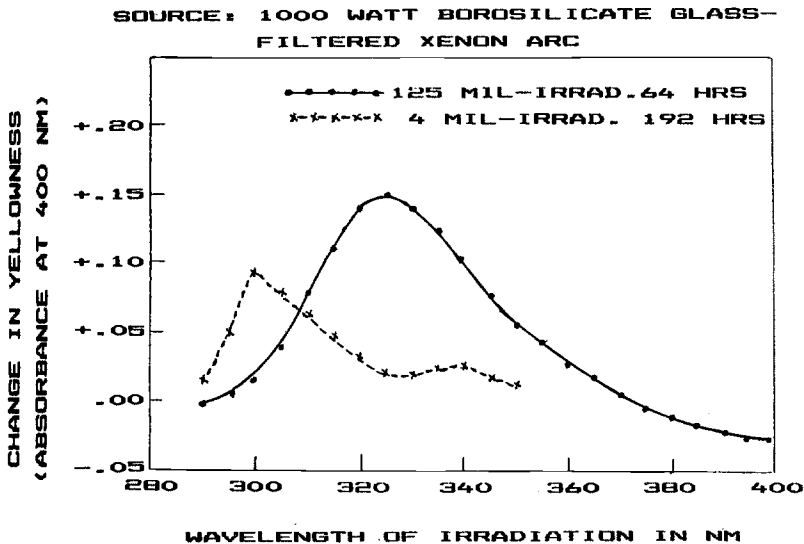


Figure 11 – *Effect of Thickness of Aromatic Polyester on the Activation Spectrum*

mer when exposed to borosilicate glass filtered xenon arc radiation is shown in Figure 11 [3]. The activation spectra were obtained by the spectrographic technique. The peak of the activation spectrum shifts from 300 nm for the 0.1 mm (4 mil) film to 325 nm for the 3.2 mm (125 mil) specimen and the wavelength sensitivity broadens to include significant effects by long wavelength UV.

The shift in wavelength sensitivity is due to a combination of factors: (1) the main absorption band of the polymer, which broadens with thickness, extends into the spectral region of the light source, (2) the increase of source intensity with wavelength coincides with the long wavelength broadening of the absorption band, and (3) because of the logarithmic nature of the absorption process, thickness has a greater effect on the amount of light absorbed in the long wavelength region where polymer absorption is weak. At short wavelengths, where the polymer absorption is strong, thickness has a smaller effect on increase in percent of light absorbed. In aliphatic type polymers, the main absorption band is outside of the spectral region of solar radiation. Therefore, thickness has a negligible effect on their absorption properties in this spectral region and thus on their wavelength sensitivity to solar radiation. A cursory glance at the figure suggests that the thicker sample is less sensitive to short wavelengths than the thin sample, but closer examination shows that the exposure time for the thicker specimen was one third of that for the thin film. At equal exposure times, the effect of short wavelengths should be the same for both.

The importance of testing these materials in the form in which they will be used in practice is strongly supported by the shift in activation spectrum with thickness. It shows that the screening requirements and thus the type of ultraviolet absorber needed for the thicker forms of these polymers differs from that needed for thin films or for the surface layers. A UV absorber that screens only short wavelengths could not adequately protect the inner layers of the thicker specimens. Due to differences among materials in the effect of thickness on their wavelength sensitivities, the form in which materials are tested can also change their stability ranking. Further, the shift in damaging wavelengths with thickness can alter the mechanism and type of degradation in the inner layers compared with effects on surface layers since these are often wavelength dependent. Prediction of lifetimes under natural conditions by short term accelerated laboratory tests is only valid if the degradation mechanism is the same under both types of exposure. Thus, whether testing is for the purpose of evaluating the performance of additives or predicting stability ranking or lifetimes under use conditions, materials should be tested in the form in which they will be used in practice.

Timing of Actinic Radiant Exposure and Prediction of Lifetimes – Correlations between laboratory accelerated and outdoor weathering tests as well as between natural weathering tests under different site and seasonal conditions are reported [21-23] to be improved when radiant exposures are compared in terms of total UV radiation rather than time or total solar radiation. It was suggested (21, 22) that "timing" of exposures based on only the portion of the UV radiation shown by the activation spectrum of the material to be responsible for the degradation is necessary to further improve correlations.

Since all wavelengths in this region are not equally effective, a further refinement would be to time exposures based on "effective" irradiance. The activation spectrum can be used to determine the effective fraction of the incident actinic radiation. It is first normalized by equating the wavelength of maximum sensitivity to the irradiance of the

source at that wavelength. The ratio of the integrated area of the activation spectrum to the integrated area under the spectral irradiance curve of the source in the actinic region gives the effective portion of the latter. The ratio multiplied by total dosage gives the effective dosage. The relation between the latter and material damage can be used for prediction of lifetimes.

References

- [1] Lemaire, J., Gardette, J-L., Rivaton, A., and Roger, A., "Dual Photochemistries in Aliphatic Polyamides, Bisphenol-A Polycarbonate and Aromatic Polyurethanes – A Short Review", *Polymer Degradation and Stability*, Vol. 15, 1986, pp. 1-13.
- [2] Rivaton, A., "The Bisphenol-A Polycarbonate Dual Photochemistry", *Die Angewandte Makromolekulare Chemie*, Vol. 216, 1994, pp. 147-153.
- [3] Searle, N. D., "Wavelength Sensitivity of Polymers", *International Conference on Advances in the Stabilization and Controlled Degradation of Polymers*, Vol. 1, A. V. Patsis, Ed., Technomic Pub. Co., Lancaster, PA, 1989, pp. 62-74.
- [4] Trubiroha, P., "The Spectral Sensitivity of Polymers in the Spectral Range of Solar Radiation", *International Conference on Advances in the Stabilization and Controlled Degradation of Polymers*, Vol. 1, A. V. Patsis, Ed., Technomic Pub. Co., Lancaster, PA, 1989, pp.236-241.
- [5] Torikai, A., "Wavelength Sensitivity of Photodegradation of Polymer Materials", *Trends in Photochemistry and Photobiology*, Vol. 3, 1994, pp. 101-115.
- [6] Kampf, G., Sommer, K., and Zirngiebl, E., "Studies in Accelerated Weathering: Part I. Determination of the Activation Spectrum of Photodegradation in Polymers", *Progress in Organic Coatings*, Vol. 19, 1991, pp. 69-77.
- [7] Hirt, R. C., Searle, N. Z., and Schmitt, R. G., "Ultraviolet Degradation of Plastics and the Use of Protective Ultraviolet Absorbers", *SPE Transactions*, Vol. 1, No. 1, 1961, pp. 21-25.
- [8] Searle, N. Z. and Hirt, R. C., "Ultraviolet Spectroscopic Techniques for Studying the Photodegradation of High Polymers", *Preprint*, Divisions of Polymer Chemistry and Organic Coatings and Plastics, American Chemical Society, Vol. 22, No. 2, 1962, pp. 56-61.
- [9] Hirt, R. C. and Searle, N. Z., "Wavelength Sensitivity and Activation Spectra of Polymers", *Preprint SPE RETEC*, 1964, pp. 286-302.
- [10] Johnson, L. D., Tincher, S. C., and Bach, H. C., "Photodegradative Wavelength Dependence of Thermally Resistant Organic Polymers", *Journal Applied Polymer Science*, Vol.13, 1969, pp.1825-1832.

- [11] Factor, A. and Chu, M. L., "The Role of Oxygen in the Photoageing of Bisphenol-A Polycarbonate", *Polymer Degradation and Stability*, Vol. 2, 1980, pp. 302-223.
- [12] Munro, H. S. and Allaker, R. S., "Wavelength Dependence of the Surface Photo-Oxidation of Bisphenol-A Polycarbonate", *Polymer Degradation and Stability*, Vol. 11, 1985, pp. 349-358.
- [13] Factor, A., "Mechanism of Thermal and Photodegradation of Bisphenol-A Polycarbonate", *Advances in Chemistry Series*, American Chemical Society, Washington, D. C. , 1996, pp. 59-76.
- [14] Rivaton, A., "Recent Advances in Bisphenol-A Polycarbonate Photodegradation", *Polymer Degradation and Stability*, Vol. 49, 1995, pp. 163-179.
- [15] Andrady, A. L., Searle, N. D., and Crewdson, L. F. E., "Wavelength Sensitivity of Unstabilized and UV Stabilized Polycarbonate to Solar Simulated Radiation", *Polymer Degradation and Stability*, Vol. 35, 1992, pp. 235-247.
- [16] Searle, N. D., "Effect of Light Source Emission on Durability Testing", *Accelerated and Outdoor Durability Testing of Organic Materials*, ASTM STP 1202, W. D. Ketola and D. Grossman, Eds., American Society for Testing and Materials, West Conshohocken, PA, 1994, pp. 52-67.
- [17] Searle, N. D., "Spectral Factors in Photodegradation: Activation Spectra Using the Spectrographic and Sharp Cut Filter Techniques", *International Symposium on Natural and Accelerated Weathering of Organic Materials*, Sept. 28-29, 1987, Essen, FRG, D. Kockott, Ed., Atlas SFTS BV, Lochem, The Netherlands, 1988.
- [18] Searle, N. D., Maecker, N. L., and Crewdson, L. F. E., "Wavelength Sensitivity of Acrylonitrile-Butadiene-Styrene", *Journal of Polymer Science: Part A: Polymer Chemistry*, Vol. 27, 1989, pp. 1341-1357.
- [19] Edge, M., et. al., "Characterisation of the Species Responsible for Yellowing in Melt Degraded Aromatic Polyesters – I: Yellowing of Poly(ethylene terephthalate)", *Polymer Degradation and Stability*, Vol. 53, 1996, pp. 141-151.
- [20] Heacock, J. A., Mallory, F. B., and Gay, F. P., "Photodegradation of Polyethylene Film", *Journal of Polymer Science: Part A-1*, Vol. 6, 1968, pp. 2921-2934.
- [21] Zerlaut, G. A., "Accelerated Weathering and Precision Spectral Ultraviolet Measurements", *Permanence of Organic Coatings*, ASTM STP 781, American Society for Testing and Materials, West Conshohocken, PA, 1982, pp. 10-34.

- [22] Zerlaut, G. A., Rupp, M. W., and Anderson, T. E., "Ultraviolet Radiation as a Timing Technique for Outdoor Weathering of Materials" Paper 850378, *Proceedings of SAE International Congress*, Detroit, Feb. 1985.
- [23] Singleton, R. W. and Cook, P. A. C., "Factors Influencing the Evaluation of the Actinic Degradation of Fibers Part II: Refinement of Techniques for Measuring Degradation in Weathering", *Textile Research Journal*, Vol. 39, 1969, pp. 43-49.

OUTDOOR

L. P. Veleva¹ and A. Valadez-Gonzalez²

Stationary Rack and Black Box Under Glass Exposures of Mineral Filled Polyethylene in Inland and Marine Tropical Climates

Reference: Veleva, L. P., and Valadez-Gonzalez, A., “Stationary Rack and Black Box Under Glass Exposures of Mineral Filled Polyethylene in Inland and Marine Tropical Climates,” *Durability 2000: Accelerated and Outdoor Weathering Testing, ASTM STP 1385*, J. D. Evans and W. D. Ketola, Eds., American Society for Testing and Materials, West Conshohocken, PA, 2000.

Abstract: During the past few years the accelerated weathering in natural condition tests has been attracting the attention of several researchers. From 1996 to 1998, CaCO₃-filled HDPE samples were exposed to degradation on a stationary rack (SR) in a field test and in a “Black Box” (BB), the accelerated natural one, carried out according to ASTM G 24, G 7 and D 4141, in the tropical humid climate of the Peninsula of Yucatan (Mexico), in two typical environments: *marine-coastal* (MC) and *rural-urban* (RU). The daily analysis of the Temperature/Relative Humidity (T/RH) complex and based on its Time of Wetness (TOW) values showed that there is a significant difference between both test environments. Periodically the polymeric specimens were evaluated using FTIR, DSC and solution viscometry to establish the photo degradation kinetic process. The results show that the *BB accelerated test* does not change but accelerates the degradation mechanism of the tested polymer in both environments. Also, this acceleration is higher for the RU than the MC environment.

Keywords: polymer mechanism degradation, mineral filler polymer, tropical humid climate, accelerated test, black box test, field test, time of wetness.

Introduction

The material degradation process can be studied by: (a) *field tests in natural conditions*, or (b) *accelerated tests* carried out in different *artificial*

¹Research Professor, Applied Physics Department, Centro de Investigación y de Estudios Avanzados (CINVESTAV-IPN), Unidad Mérida, C. P. 97310, Mérida, Yucatán, México.

²Associate Professor, Polymer Department, Centro de Investigación Científica de Yucatán (CICY), C. P. 07310, Mérida, Yucatán, México.

atmospheres. Group (b) provides rapid results in a shorter time than (a), but these tests are not reliable because they cannot represent the complex natural climatic parameters and sometimes change the mechanism kinetics of the degradation process.

Reversals in stability ranking of organic materials have often been reported between laboratory accelerated and outdoor tests. It was concluded, for example, that an accelerated test source which differs from sunlight can alter the mechanism and type of degradation, as well as the stability ranking of materials compared with the effects of outdoor exposure [1]. For many polymeric materials, the type of light source used in durability testing is a critical factor, determining the predominant mechanism of their degradation. In this case the prediction of lifetime under natural exposure conditions based on accelerated testing is not possible. It was demonstrated also that the variation of some substantial weathering parameters, such as temperature, moisture, spectral radiation, must be taken into account in an accelerated tests [2]. Depending on the material tested, any of these three factors can actually be more important than the UV radiation. To obtain improved weathering test results the specimen temperature data should be used along with the solar radiation data to more completely model exposure [3]. It was showed that high irradiance does not necessary means faster failure rates for light colored material and their degradation rate may be best accelerated by exposing at higher chamber temperature, i.e., take advantage of significant thermal acceleration.

In the past few years, the test group of the called *accelerated test in natural conditions* is bringing attention. The accelerated outdoor weathering has a history and new developments recently introduced promise to allow further improvements to this test [4]. Standards efforts have contributed significantly to their development and application in practice, which could allowed better correlation on a wider variety of materials. This group test could be a valuable tool for screening materials for use in a given environment, however for the results to have any real validity, there must be evidence that a correlation exists in the actual atmosphere of interest, e.g., there is not change in the degradation material mechanism.

The data presented in this study are part of a wider investigation of HDPE (unfilled and mineral filled) properties, by accelerated and natural test exposure. In our previously investigation [5] we presented the degradation mechanism process of this material after exposure in accelerated weathering UV chamber tester and the influence of the inclusion of CaCO₃ as a filler material. However, the real material behavior study, when it is exposed in tropical humid climate of the Peninsula of Yucatan (southeast of Mexico), is the necessary base for the prediction of its lifetime.

Experimental

Materials

A commercial extrusion grade HDPE (Quantum Petrothene, from Quantum Chemical Corporation) with 0.9537 g/cm³ density (ASTM D 792-66.13) and 0.32 g/10 minutes Melt Flow Index (ASTM D 1238-82.13 at 190°C and a load of 2160 g) was used. The HDPE as received was pulverized in a Brabender mill to get a powder with a mean

particle size average of 2 mm. Calcium Carbonate, CaCO₃ (Tecnica Mineral SA of C.V.) with a 0.1 mm average particle size and 2.70 g/cm³ of density was used as mineral filler. It was dried at 105°C, during 24 h in a convection oven, and then was treated with 0.5% w/w of KRTTS (Isopropyl Triisostearoyl Titanate, from Kenrich Petrochemicals Inc.).

Sample preparation

The 50% w/w mixture of HDPE and CaCO₃ was performed in a plasticating extruder with a 24 length/diameter (L/D) ratio, 30 mm barrel diameter, 2:1 compression ratio, two heating zones and a flat die was used as a compounder. The calcium carbonate filled HDPE composite was extruded at 45 r. p. m. After that the extruded materials were hot-press laminated to obtain 0.5 mm thick laminates. The specimens (4 x 4 cm) used in this study were cut from these laminates.

Analytical measurements

The HDPE filled with calcium carbonate (CaCO₃) samples were periodically evaluated during one year to establish their photo degradation rate. It was established from the IR absorbency spectra, obtained with a NICOLET 460 FTIR spectrometer. The spectra were recorded using the diffuse reflectance (DRIFTS) mode with a DGTS detector, 1 cm⁻¹ resolution and 200 scans. The reported indexes were calculated from three specimens as the ratio (Abs₁₇₁₅cm⁻¹/Abs₂₀₂₀cm⁻¹) for the carbonyl index and the ratio (Abs₃₄₄₅cm⁻¹/Abs₂₀₂₀cm⁻¹) for the hydroperoxide index. The 2020 cm⁻¹ peak was taken as a reference in the calculations since it does not vary with the exposure time [6].

The thermal properties of the samples were obtained from a PERKIN ELMER DSC-7 Differential Scanning Calorimeter. The details of the calculations are reported elsewhere [5].

The viscosity-Molecular Weight Average (M_v) of the samples was determined by means of solution viscometer using the Mark-Houwink-Sakurada equation [7-8]:

$$[\eta] = K\bar{M}_v^a$$

where K, *a* are constants for a given polymer, at a given temperature in a given solvent. The viscometry data were obtained using a Cannon-Ubbelohde capillary viscometer at 100°C using xylene as a solvent, accordingly to ASTM D 1601-78.

Sample Exposure

Triplicate samples were exposed to natural weathering on a conventional stationary rack (SR), at the site latitude angle (22°) and to accelerated test in natural conditions using a Black Box (BB) under glass (at 5° angle), according to procedures of ASTM G 24 - 97,

G 7 - 83 and D 4141 - 82. Both equipment were fixed facing the equator. The BB was built from Al (with dimensions according to ASTM G 7) and painted black, which permits the absorbency of a lot of heat. The BB was covered with a window glass (3 mm), pre-aged in the test atmospheres before the ignition of the tests. According to the "Q Panel Company" study, the window glass filters much of the UV in sunlight (separating the UV-A from the responsible for most photochemical changes UV-B) and below about 310 nm is completely filtered out [9]. Perforations were made on the BB bottom to allow free ambient air circulation over the samples. Figure 1 presents a general view of the BB in use.

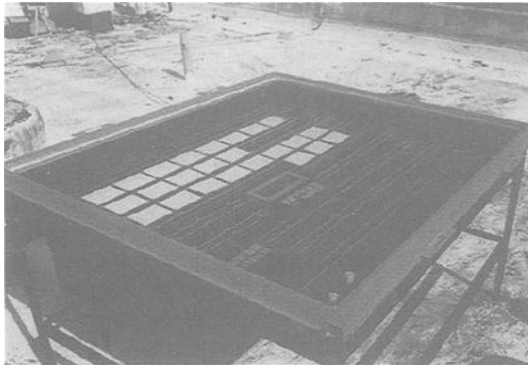


Figure 1 - Black Box (BB) in use, located at the rural-urban test station of CINVESTAV-IPN (Merida).

Test sites characterization

The study was carried out at the tropical humid climate of Yucatan Peninsula (Mexico), in two typical environments: marine-coastal (MC, at Progreso Port, 50 m from the seashore) and rural-urban (RU, at Merida, 30 km from the coast). There are two markedly different seasons in the tropical humid climate: dry (in the winter months, when the coastal airborne salinity increase significantly) and rainy (summer period, with a very low atmospheric contamination). The airborne salinity (chlorides) and SO₂ were evaluated monthly, according to ISO 9225, using the wet candle and sulphation plate methods, respectively. The RU test site is very low polluted and has characteristics of rural site (with a lot of vegetation) and it is located in the city Merida. Table 1 presents some annual climatic parameter values, during the test period 1996-1998.

It can be seen, in practice, no difference in their annual values. However, according to our study [10], the daily analysis of the Temperature-Relative Humidity

(T/RH) complex and based on its TOW³ value showed that there is a significant difference between both test environments.

Table 1 - Annual Average Values of T and RH, and Pluvial Precipitation in Merida (RU) and Progreso (MC) Test Sites During 1996-1998

Year	Pluvial Precipitation, mm		Relative Humidity, %		Temperature, °C	
	RU	MC	RU	MC	RU	MC
1996	950	320	78	79	26.0	25.9
1997	1100	550	77	79	26,4	26,3
1998	1300	700	75	78	26,8	26,1

For example, in the MC site, due to the presence of the sea (the biggest thermodynamics source), the T and RH daily values are practically constant (75-85% and 22-28°C). However, in the RU atmosphere the T increases drastically at noon (until 38-41°C and RH 40%) and falls at night, when the RH reaches 100%. That is why the annual RU TOW value is approximately 4800 h (usually done at night) and the MC one is double (8500 h). It is very important also to recognize that at MC site 64-73% of the TOW is spent in the temperature range 20-25°C; in the RU site 54-64% of the TOW occurs in the lower temperature range 20-25°C. Therefore, the RU and MC test sites determine distinct polymer degradation rates. In a such way, the "Black Boxes" exposed at both atmospheres created different environments also. During the exposure period, the T (°C) sample and the TOW which occurs on the material surface were registered, with appropriate sensors and electronic systems (Figure 2) for continuous monitoring [11-13], using ASTM sensor according to the ASTM G 84

Figure 3 (a) and (b) show examples of the daily changes of TOW and T (environmental and polymer sample exposed at SR and in BB). During the exposure period was measured by pyranometer the received daily total energy. It can be assumed that the BB environment created in the RU test site is more aggressive (accelerated) for the polymer samples than the MC one because of higher T values and TOW (due to condensation on the crystal inside) at noon.

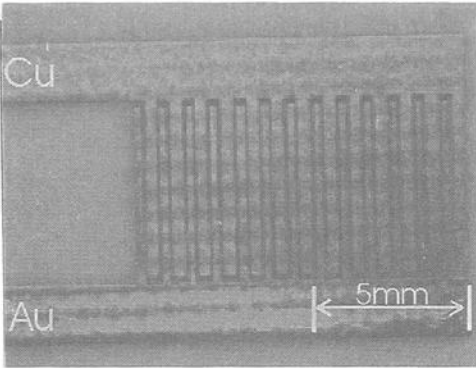
Results

The FTIR spectroscopic analysis showed that as the exposure time increases the absorbency intensity of the carbonyl band (1715 cm^{-1}) and the hydroperoxide band (3445 cm^{-1}) grows, which indicates material degradation [14-17]. Typical HDPE and CaCO_3 .

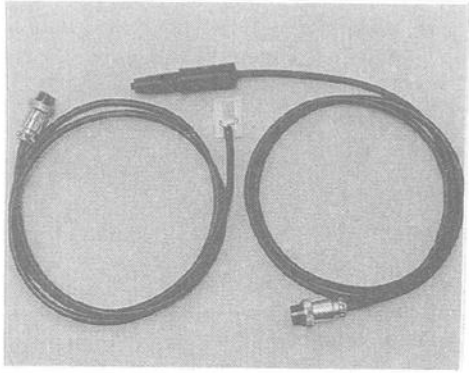
³ The Time of Wetness (TOW) is the time during which a wet film occurs on the material surface. There is a critical RH value when TOW appears: at $T > 0^\circ\text{C}$ and $\text{RH} > 80\%$ for no chloride contaminated atmosphere, according to ISO 9223, and 50-60% for coastal regions as our TOW sensors showed).

filled HDPE degradation carbonyl compounds were readily identified (ketone, ester and carboxylic acids) and used to describe the polymer degradation mechanism process [5]. Figure 4 (a) and (b) present the changes on the Hydroperoxide Index against the exposure time for the samples exposed in the RU and MC environments.

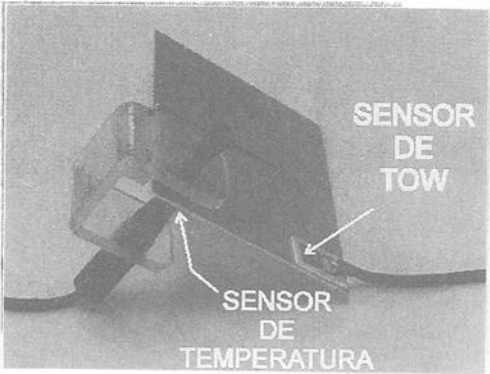
In the RU test site, the Hydroperoxide Index growth seems to be stabilized in both BB and SR whereas in the MC test site this is not the case., e.g. the Hydroperoxide Index shows a steady growth in both environments



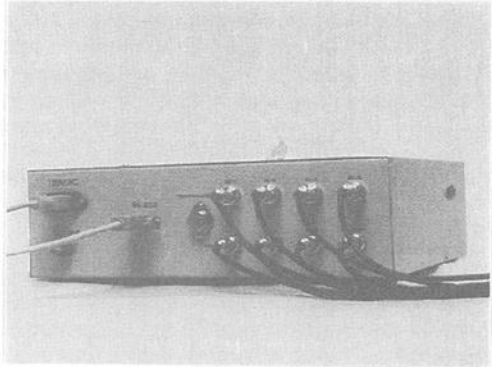
a) TOW sensor



(b) TOW and T-sensors



(c) Disposition of the sensors on the surface samples.



(d) View of the monitoring electronic system

Figure 2 - Sensors and monitoring electronic system in use.

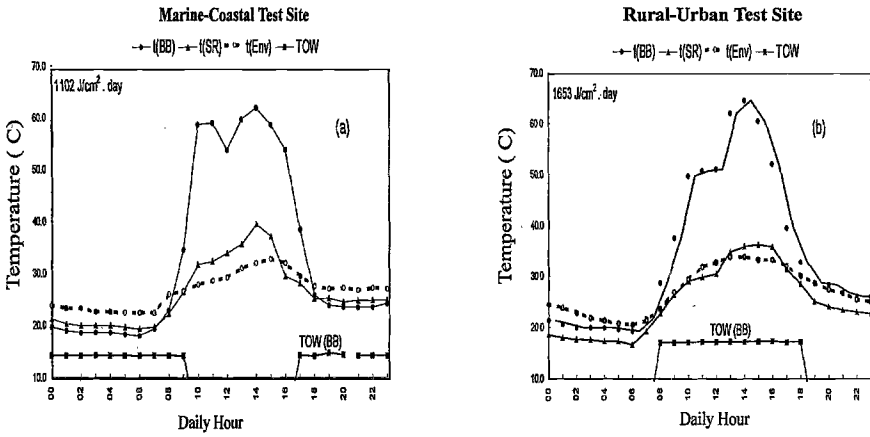


Figure 3 - Daily changes of T and TOW created in the BB and SR, exposed at MC (a) and RU (b) humid tropical test sites.

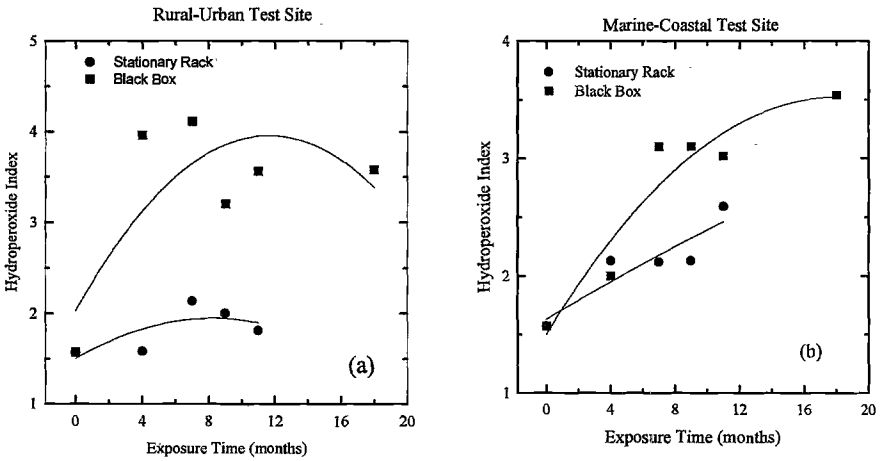


Figure 4 - Changes in the Hydroperoxide Index in the SR and BB for samples exposed at: (a) The Rural-Urban (RU) and (b) the Marine-Coastal (MC) test sites

Figure 5 (a) and (b) show the evolution of the Carbonyl Index during the exposure time in both environments.

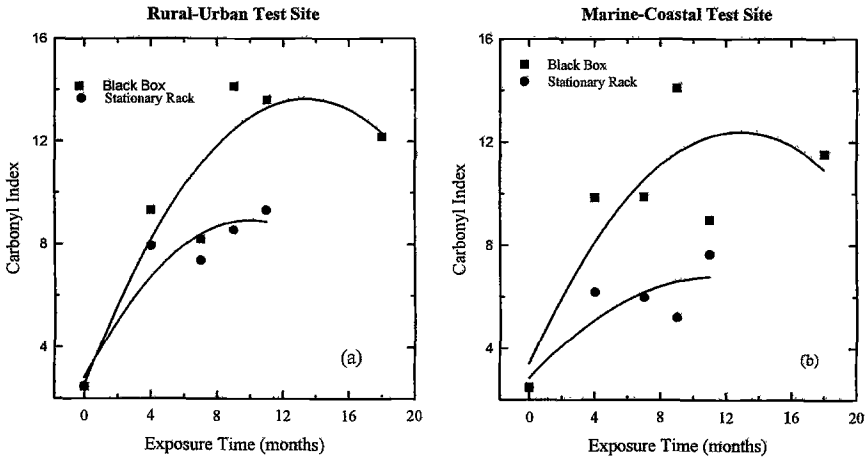


Figure 5 - Changes in the Carbonyl Index in the SR and BB for samples exposed at: (a) The Rural-Urban (RU) and (b) the Marine-Coastal (MC) test sites.

It can be seen in these pictures that Carbonyl Index is always greater in the BB than SR in both test sites and that it shows similar results for BB. In another hand, it should be noted that the increment in the Carbonyl Index in the SR is greater in the RU test site than in the MC one.

The changes in the Crystallinity of the exposed samples with the exposure time in the SR an BB at the RU and MC test sites are shown in Figure 6 (a) and 6 (b).

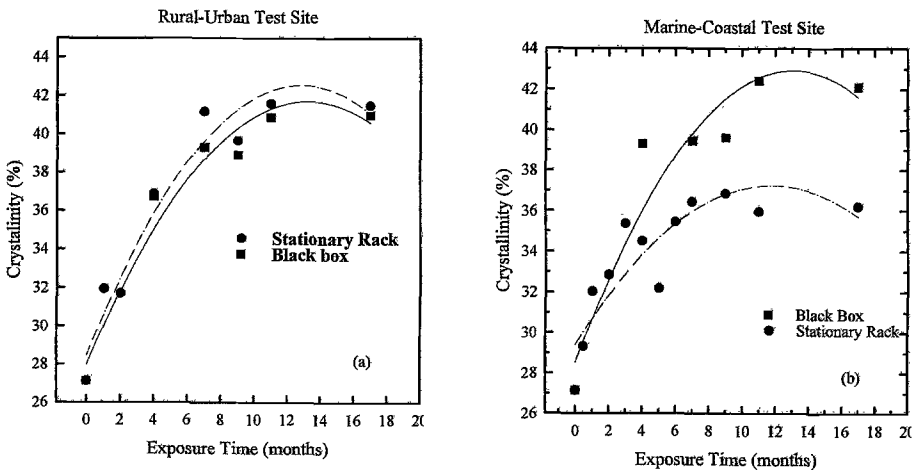


Figure 6 - Changes in the Crystallinity content in the SR and BB for samples exposed at: (a) The Rural-Urban (RU) and (b) the Marine-Coastal (MC) test sites.

It can be seen that the crystallinity of the samples grows exponentially during the first ten months of exposition and after that it is stabilized. It should be noted that at the RU test site there are no meaningful differences between the BB and SR, however in the MC test site the crystallinity content of the samples is around 15% higher in the BB than in SR.

The changes in the viscosity-Average Molecular Weight, M_v , of the exposed samples with the exposure time at the SR and BB in the RU and MC test sites are shown in Figure 7 (a) and 7 (b), respectively.

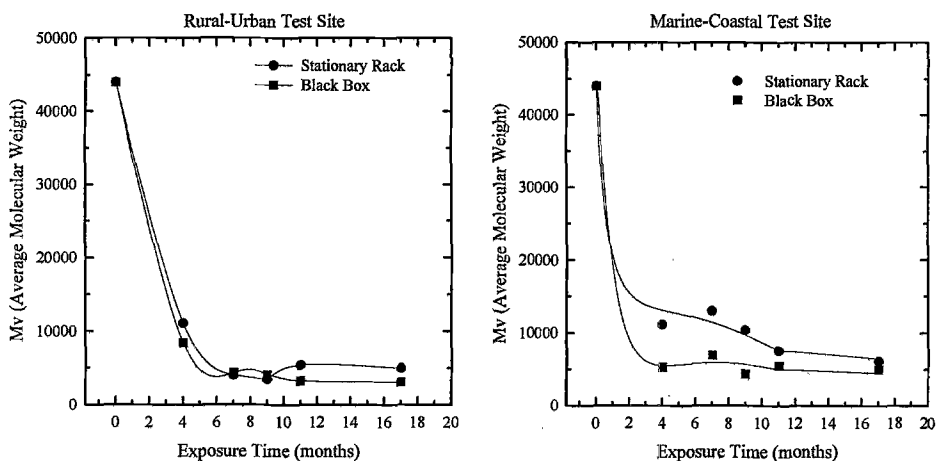


Figure 7.- Changes in the Average Molecular Weight (M_v) in the SR and BB for samples exposed at: (a) the Rural-Urban (RU) and (b) the Marine-Coastal (MC) test sites.

It can be seen that in a broad sense, the molecular weight of the samples drops dramatically during the first three months of exposition in both the BB and the SR at RU and MC test sites. However, in the case of the MC test site, there are some slightly differences between BB and SR, the M_v of the samples does not drop as fast as in the BB at the SR.

Discussion

The data obtained in this study, by means of FTIR, DSC and solution viscometry, show that the calcium carbonate filled HDPE experiments a typical two stage photo degradation mechanism in both environments (RU and MC) and field tests (SR and BB). It was previously pointed [5] pointed out that the presence of the mineral filler promotes the formation of carbonyl compounds, e.g. ketone, carboxylic acid and ester groups, during the material processing stage. The formed ketone group decomposes, following the Norrish II mechanism, and as a consequence the chain

breakup gives up, evidenced by the molecular weight drop [18-19]; at the same time the amorphous phase of the HDPE experiments an oxidation, indicated by the growth of the hydroperoxide and carbonyl groups and the crystallinity of the samples. The increment of the crystallinity could be attributed to the chain oxidation of the amorphous HDPE phase and formation of new crystals, induced by reactions of crosslinking and chain scission [20]. In the second stage, once the amorphous phase susceptible to oxidize has been exhausted, the functional carbonyl and the hydroperoxide groups are stabilized, which means that they apparently do not continue reacting. This findings are similar to those obtained when the material was exposed in a accelerated UV chamber [5], i.e. the mineral filler seems to act as a protect barrier to the UV light in the HDPE. Also, it was reported previously [21-22] that the presence of some mineral fillers (sand and CaCO_3) in polyolefins block the UV radiation and inhibit the polymer oxidation, promoting their longer life.

The natural accelerated test does not change the aging mechanism of the tested polymer. However, there is an acceleration of this process when the samples are exposed in the BB, even though there is the absence of UV radiation (cut by the window crystal). This acceleration is bigger for the RU environment than the MC one. The reason observed for more accelerated aging in the RU test site is the above mentioned difference in the T/TOW complex of both atmospheres created in the BB as a consequence of the environmental micro climate there. For example, the T values of the polymer surface exposed in the RU-BB are 25-30°C higher than those of the polymer exposed on the SR. In the MC-BB atmosphere the samples have only 15-20°C greater temperature than the polymer on the SR.

However, the sample exposed to the MC atmosphere (BB and SR) suffer higher TOW than those in the RU environment. This means that the moisture effect on the degradation rate is small and the principal parameters that control the degradation polymer process is the material obtained heat during the exposure which an indicator is the material temperature.

Conclusions

The "*Black Box under glass*" accelerated test, carried out in *natural conditions* in a humid tropical climate apparently does not change the polymer degradation mechanism of mineral filled HDPE. The acceleration is greater for the samples exposed in the rural-urban environment due to its specific T/TOW complex: greater temperature in the presence of lower time of wetness than those in the marine-coastal environment. It seems to be that the polymer suffers significant thermal accelerated degradation, principally due to IR sunlight heating of the material, even in almost absence of UV light radiation cut by the window glass.

The data obtained in this study, by means of FTIR, DSC and solution viscometry, show that the calcium carbonate filled HDPE experiments a typical two stage photo degradation mechanism in both environments (RU and MC) and field tests (SR and BB). Once the amorphous phase is oxidized, the functional carbonyl and the hydroperoxide groups are stabilized, due to the UV light protect barrier formed by the mineral filler.

Acknowledgments

The authors wish to acknowledge the Mexican Consejo Nacional de Ciencia y Tecnología (CONACYT), Contract 2667-PA for financial support in conducting various phases of this investigation and to J. M. Cervantes-Uc and L. Varguez-Garcia for their technical assistance and analysis of the samples.

References

- [1] Searle, N. D., "Effect of Light Source Emission on Durability Testing," *Accelerated and Outdoor Durability Testing of Organic Materials*, ASTM STP 1202, W. D. Ketola and D. Grossman, De., American Society for Testing and Materials, West Conshohocken, PA, 1994, pp. 54-67.
- [2] Grossman, D. M., "Errors Caused by Using Joules to Time Laboratory and Outdoor Exposure Tests," *Accelerated and Outdoor Durability Testing of Organic Materials*, ASTM STP 1202, W. D. Ketola and D. Grossman, De., American Society for Testing and Materials, West Conshohocken, PA, 1994, pp. 68-86.
- [3] Fisher, R. M. And Ketola, W. D., "Surface Temperature of Materials in Exterior Exposures and Artificial Accelerated Tests," *Accelerated and Outdoor Durability Testing of Organic Materials*, ASTM STP 1202, W. D. Ketola and D. Grossman, De., American Society for Testing and Materials, West Conshohocken, PA, 1994, pp. 88-111.
- [4] Robbins, J. S., "A Review of Recent Developments in the Use of ASTM Standard Practice G 90 for the Testing of Nonmetallic Materials ," *Accelerated and Outdoor Durability Testing of Organic Materials*, ASTM STP 1202, W. D. Ketola and D. Grossman, De., American Society for Testing and Materials, West Conshohocken, PA, 1994, pp. 169-182.
- [5] Valadez-Gonzalez, A., Cervantes-Uc, J. M., Veleva L., *Polymer Degradation and Stability*, Vol. 63, 1999, pp. 253-260.
- [6] Albertsson, A.C., Griffin, G.J.L., Karlsson, S., Nishimoto K. and Watanabe Y., *Polymer Degradation and Stability*, Vol. 45, 1994, pp. 173-178.
- [7] Rabek, J.F. , "*Experimental Methods In Polymer Chemistry. Physical Principles and Applications*", J. Wiley & Sons., 1980, Chichester.
- [8] Chirinos-Padron, A. J., Azocar, J. and Muñoz, A., *Journal of Polymer Science, Chemistry*, Vol 21, 1987, pp.2701.
- [9] Grossman, G.W, *Journal of Coatings Technology*, Vol. 49, 1977, pp. 45-54.

[10] Veleva, L., Pérez, G., and Acosta, M., *Atmospheric Environment*, Vol. 31, 1997, pp. 773-776.

[11] Veleva, L., Casanova, G., Bante, J., and Kantun, F., *Material Research Congress* (Cancun, Mexico, September 1997), Abstracts, 1997, pp. 31.

[12] Veleva L., and Alpuche M., *195th Int. Electrochem. Soc. Meeting* (Seattle, USA, May 2 - 6), Extended Abstracts, 1999, No. 83.

[13] Mex. Patent #18033, April 29, 1998.

[14] Lacoste J. and Carlsson D.J., *Journal of Polymer Science: Part A: Polymer Chemistry*, Vol. 30, 1992, pp. 493-500.

[15] Tidjani A. and Arnaud R., *Polymer Degradation and Stability*, Vol.39, 1993, pp. 285-292.

[16] Severini F., Gallo R., Ipsale S. and Ricca G., *Polymer Degradation and Stability*, Vol 41, 1993, pp. 103-107.

[17] Tidjani A. and Arnaud R., *Polymer*, Vol. 36, 1995, pp. 2841-2844.

[18] Ciccetti O., *Advances in Polymer Science*, Vol. 7, 1970, pp. 70.

[19] Schnabel W., *Polymer Degradation. Principles and Practical Applications*, New York, Hanser International, 1981.

[20] Hamid S.H. and Amin M.B., *Journal of Applied Polymer Science*, Vol. 55, 1995, pp. 1385-1394.

[21] Sanchez-Solis A. and Estrada M.R., *Polymer Degradation and Stability*, Vol 52, 1996, pp. 305-309.

[22] Jiangqi P., Hongmei, Q.J., Cen J. And Zhenmin M., *Polymer Degradation and Stability*, Vol 33, 1991, pp. 67-75.

ACCELERATED

Warren D. Ketola,¹ Richard M. Fischer,² and Linda J. Thomas³

Stress Analysis and Accelerated Test Design for Interior Light Environments

Reference: Ketola, W. D., Fischer, R. M., and Thomas, L. J., “Stress Analysis and Accelerated Test Design for Interior Light Environments,” *Durability 2000: Accelerated and Outdoor Weathering Testing, ASTM STP 1385*, J. D. Evans and W. D. Ketola, Eds., American Society for Testing and Materials, West Conshohocken, PA, 2000.

Abstract: A procedure for development of a simple, small-scale laboratory accelerated test based on the same light source used in the actual indoor application is described. This simple laboratory accelerated test can be used to evaluate durability of paints, coatings, or colorants used in art or graphic displays exposed to the interior lighting source. The steps used to develop the test include characterization of the light and thermal stresses for actual use conditions and applying the results to design an accelerated test. Examples for developing tests based on two different interior light sources are shown. Procedures for characterizing spectral power distribution, for calculating an irradiance acceleration factor, and for determining the uniformity of light and thermal stresses of the accelerated test are described. Results from measurements made using these procedures are used to establish the conditions for a practical small-scale laboratory accelerated test.

Keywords: light, color, exposure testing, indoor

Introduction

There are many different types of light sources used in interior environments, each of which has different spectral power distribution characteristics. When these light sources are used to illuminate graphic displays or objects of art, color fade or shift may occur.

¹ Division Scientist, 3M Traffic Control Materials Division, 3M Center, Building 235-3E-60, St. Paul, MN 55144-1000

² Division Scientist, 3M Weathering Resource Center, 3M Center, Building 235-BB-44, St. Paul, MN 55144-1000

³ Senior Laboratory Technician, 3M Weathering Resource Center, 3M Center, Building 235-BB-44, St. Paul, MN 55144-1000

ASTM Practice For Determination of Lightfastness and Weatherability of Printed Matter (D 3434), ASTM Methods for Lightfastness of Pigments Used in Artists' Paints (D 4303), and ASTM Practice for Determining the Lightfastness of Ink Jet Prints Exposed to Indoor Fluorescent Lighting (F 1945) describe several laboratory accelerated tests that can be used to determine color stability. However, the light sources used in these procedures may not be applicable when a different light source provides the primary or sole source of illumination in indoor applications. In these cases, a simple laboratory accelerated test based on the light source used in the actual indoor application is needed. This paper describes a procedure that can be used to develop such a test. The first step in this procedure is the characterization of the spectral power distribution (SPD) of the light source and specimen surface temperatures in typical "worst case" conditions used in actual service. Spectral power distribution measurements are needed to determine whether the light sources used in conventional laboratory accelerated exposure devices are relevant to the light source used for the interior display. Spectral power distribution measurements at several distances from the light source are used to establish the relationship between irradiance and distance from the source. With this information, it is possible to calculate the distance from the light source to the sample plane of a test chamber needed for the desired irradiance acceleration factor. The next phase of test design involves characterization of the uniformity of the irradiance and surface temperatures within the sample plane for the proposed accelerated test. Results of these measurements for two different tungsten lamp light sources are used to illustrate this process for accelerated test design. Once appropriate test conditions are established, accelerated exposures can be used to rapidly determine whether products used in applications where they are exposed to the light source will have acceptable lifetimes.

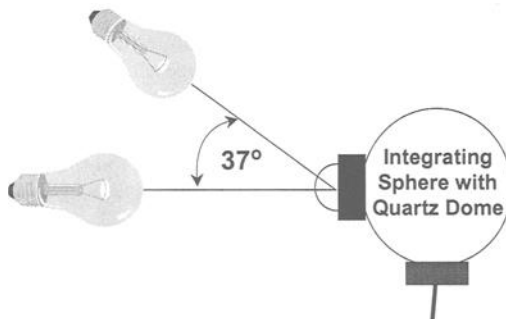


Figure 1: *Orientations of lamp and integrating sphere used for determination of spectral power distribution*

Experimental Method

Two lamps that were used to illuminate wall mounted graphic art displays were tested. These lamps were a Sylvania Tru-Aim Brilliant Halogen Lamp (50MR 16Q/40/FL/B) and a Sylvania Designer 16 Capsylite PAR lamp (59036 N5P 75W 120V white). Irradiance was measured at 2 nm increments from 250 to 800 nm using an Optronics OL754 spectroradiometer equipped with a 4-inch diameter integrating sphere with quartz dome (OL 752-S).

The spectroradiometer was calibrated with an Optronics OL752-10E 200 watt tungsten lamp traceable to NIST. Irradiance measurements were made with the entrance port of the integrating sphere in two positions relative to the beam axis of the lamps. The integrating sphere was oriented so that the angle between the beam axis of the lamp and a

line normal to the apex of the quartz dome was 37° to simulate “worst case” field conditions. The entrance port of the integrating sphere was also aligned with the beam axis of the lamp to simulate the condition that would be used in a laboratory accelerated test. Figure 1 shows the orientations of the lamp and integrating sphere. Spectral power distribution measurements were made with the integrating sphere 143 cm from the lamp (the distance representative of actual “worst case” field use) and at several other distances in order to determine the relationship between irradiance and the lamp/detector distance.

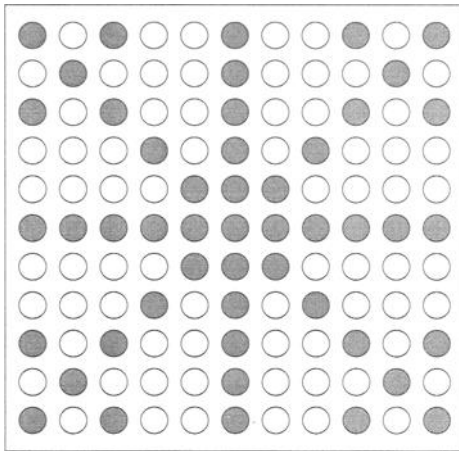


Figure 2: *Positions used for determination of irradiance uniformity*

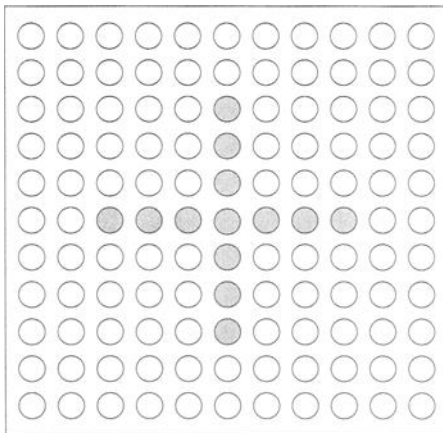


Figure 3: *Positions used for measuring temperature uniformity*

An International Light radiometer (model IL1730 with SED033 sensor) was used to determine irradiance uniformity within the sample plane at various distances from each lamp. An aluminum sheet with a series of 2.5 cm diameter holes spaced 5 cm on center was used as a positioning guide for these measurements. The lamp axis was aligned with the center hole of the grid prior to starting measurements. Figure 2 shows the measurement positions used to determine irradiance uniformity.

Surface temperature measurements were determined using 30 gauge Type T thermocouples connected to a CONTROL-ONE™ multichannel temperature recorder. Temperature measurements were made with the sample plane positioned at several distances from the lamp. For surface temperature measurements, the sample plane was covered with either white or black Scotchcal™ vinyl film. A thermocouple was attached to the specimen plane at the position where the beam axis of the lamp intersected the plane and at three positions to the left and right of center along orthogonal lines passing through the center measurement position. The distance between each thermocouple was 5 cm. Positions used for temperature measurement are shown in Figure 3.

The thermocouples were attached to the surface of the black or white Scotchcal™ using a small piece of the same film. Surface temperature data were collected every 8 seconds over a 30 minute period for each

measurement condition. The average temperature measured during this period was used for analysis.

Irradiance and surface temperature data were analyzed using either EXCEL™ (Microsoft Incorporated, Seattle, WA) or MINITAB™ Statistical Software (Minitab Incorporated, State College, PA).

Results and Discussion

The spectral power distribution for the Sylvania Designer 16 and Tru-Aim Brilliant lamps is shown in Figure 4. For comparison purposes, the spectral power distribution for a xenon-arc with window glass filters controlled to produce 0.30 W/m^2 at 340 nm and a fluorescent cool white lamp are also shown in Figure 4. The window glass filtered xenon arc and fluorescent cool-white lamps are commonly used to evaluate durability and lightfastness of materials used in indoor environments. It is clear that the spectral power distribution for the two Sylvania lamps is much different from that for the xenon lamp or for the fluorescent cool-white lamp. The xenon arc is very rich in UV radiation compared to either of the Sylvania lamps, while the Sylvania lamps have relatively higher intensity in the long wavelength visible radiation. The fluorescent cool-white lamp has lower irradiance in the UVA region, between 400 and 500 nm , and above 600 nm . Examination of Figure 4 shows that using the xenon arc or fluorescent cool white lamps

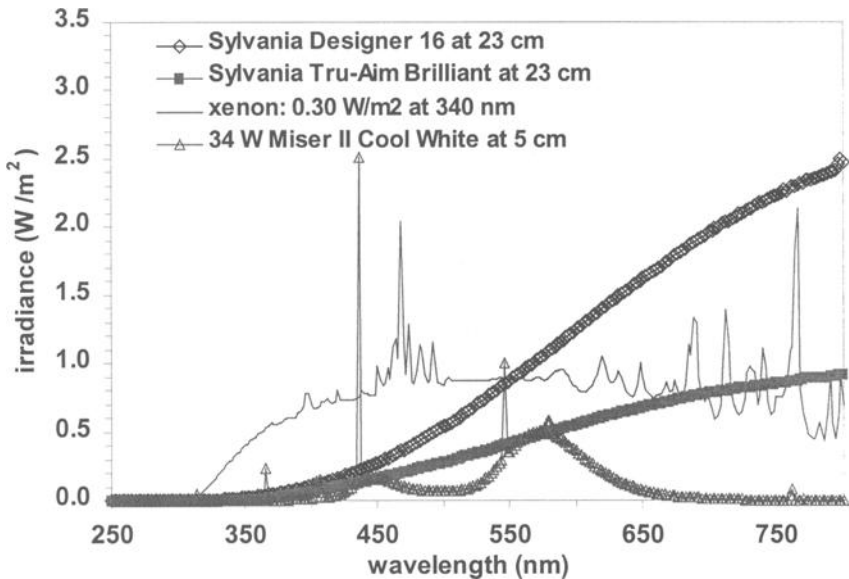


Figure 4: Spectral power distribution of Sylvania Designer 16 and Tru-Aim Brilliant lamps compared to that for xenon-arc with window glass filters and fluorescent cool-white lamp.

to simulate the effects of exposure to either of the Sylvania lamps would likely lead to errors because of the large spectral mismatches.

The spectral power distribution of each lamp was determined with the quartz dome of the integrating sphere aligned with the beam axis of the lamp and at 37° to the beam axis of the lamp. Table 1 shows the ratio of irradiance measured at 37° to the irradiance measured with the integrating sphere aligned with the beam axis. The data show that the Designer 16 lamp produced a much narrower beam of light than the Tru-Aim Brilliant lamp. For the Tru-Aim Brilliant lamp, the “angle/aligned” irradiance ratio begins to fall off at larger lamp/detector distances.

Table 1 – Ratio of irradiance for detector at 37° to beam axis of the lamp to irradiance for detector aligned with the beam axis

Lamp	Bandpass (nm)	Ratio of irradiance at 37° to irradiance with quartz dome aligned with the beam axis of the lamp at indicated lamp/detector distances				
		23 cm	46 cm	73 cm	107 cm	143 cm
Designer 16	300-400	0.70	0.58	0.62	0.63	0.61
	400-700	0.75	0.63	0.64	0.64	0.62
Tru-Aim Brilliant	300-400	0.85	0.88	0.89	0.83	0.73
	400-700	0.84	0.87	0.85	0.84	0.75

Table 2 -- Fit to parameters for power law equation (irradiance = Ax^b) for irradiance in W/m² as a function of distance to lamp in cm

Lamp	Bandpass (nm)	Coefficients for power equation of the form: Irradiance = Ax ^b		
		A	b	R ² for regression
Sylvania	340	5.76	-1.98	0.997
Designer 16	300-400	1606	-1.96	0.998
	400-700	124944	-1.93	0.999
	300-800	222898	-1.92	0.999
Sylvania	340	0.45	-1.97	0.999
Tru-Aim Brilliant	300-400	775	-1.98	0.999
	400-700	61393	-1.98	0.999
	300-800	102863	-1.98	0.999

Irradiance measured at several distances was fitted to a power law equation. The results from this analysis are shown in Table 2. The data in Table 2 are for measurements made with the entrance port of the integrating sphere aligned with the beam axis of the lamp. The R² for regression shows that for both lamps, the irradiance/distance data fit a power law equation very well. In each case, the results came

very close to the classic “inverse square law” equation for irradiance as a function of distance to a light source.

The integrated UV irradiance from 300-400 nm compared to the integrated irradiance from 400-700 nm was 1.15% for the Designer 16 lamp and 1.26% for the Tru-Aim lamp. The integrated irradiance from 400-700 nm measured with the integrating sphere oriented at 37° to the beam axis was 2.53 W/m² at a distance of 143 cm from the Sylvania Tru-Aim Brilliant lamp. For the Sylvania Designer 16 lamp, the 400-700 nm irradiance was 5.09 W/m² at the same conditions. These results represent the “worst case” irradiance for actual in-service conditions. Assuming a linear relationship between irradiance and degradation rate, the in-service irradiance can be multiplied by a desired acceleration factor to determine the irradiance necessary for the laboratory accelerated test. The equations for irradiance as a function of distance shown in Table 2 for each lamp were used to calculate the distance from the lamp to the sample plane needed to produce the desired irradiance in a laboratory accelerated test. Results from these calculations are shown in Table 3.

Table 3 -- Calculation of lamp sample plane distance for laboratory accelerated test

Lamp	in-service	irradiance acceleration factor	desired	distance from lamp to sample plane (cm) ¹
	400-700 nm irradiance (W/m ²)		400-700 nm irradiance (W/m ²)	
Sylvania	2.52	10	25.2	51.1
Tru-Aim		15	37.8	41.6
Brilliant		20	50.4	36.0
		25	63.0	32.2
		50	126.0	22.7
Sylvania	5.09	10	50.9	56.7
Designer 16		15	76.4	46.0
		20	101.8	39.6
		25	127.3	35.3
		50	254.5	24.7

¹ Beam axis of lamp normal to sample plane

Determination of the distance from the lamp to the sample plane is a major step in designing the laboratory accelerated test. However, ASTM Practice for Exposing Nonmetallic Materials in Accelerated Test Devices that Use Laboratory Light Sources (G 151), requires determination of the uniformity of irradiance and temperature within the sample plane. Irradiance uniformity was determined by measuring irradiance at a series of positions around where the beam axis of the lamp intersects the sample plane. Measured irradiance was normalized to the irradiance determined where the beam axis intersects the sample plane. These data were analyzed in two ways. First, a regression analysis was conducted using either the “LINEST” function in EXCEL or using a response surface regression in Minitab™. In all cases, the results showed that the only

significant terms ($p = 0.000$) for determining the normalized irradiance were the x^2 and y^2 coordinates describing the measurement position relative to the point where the beam axis of the lamp intersects the sample plane. This relationship fits the general equation describing a circle [1], and indicates that the irradiance was uniformly distributed around the spot where the beam axis intersected the sample plane.

Table 4 -- Relationship between normalized irradiance within the sample plane as a function of distance from the Sylvania Designer 16 lamp axis normal to the sample plane

lamp / sample plane distance	Coefficients for power equation of the form: Irradiance = Ax^b		R^2 for fit of power law equation
	A	b	
23 cm	4616	-2.9583	0.868
46 cm	1260	-1.8899	0.964
76 cm	823	-1.4120	0.958
107 cm	617	-1.1390	0.967
143 cm	475	-0.9294	0.951

The normalized irradiance was also plotted as a function of the distance from where the beam axis intersected the sample plane. Table 4 shows that a power law equation describes the relationship between the normalized irradiance and distance in any direction from where the beam axis of the Sylvania Designer 16 lamp intersects the sample plane. Table 5 shows that the equations that best fit the normalized irradiance data for the Sylvania Tru-Aim lamp.

Except for lamp positions close to the sample plane, the irradiance decreases linearly with distance from the center spot.

Table 5 -- Relationship between irradiance at any position within the sample plane as a function of distance from the center point where the beam axis of the Sylvania Tru-Aim Brilliant lamp intersects the sample plane¹

Distance from lamp to sample plane (cm)	Best fit equation	Equation (I_n is irradiance normalized to 100 at center, and x is distance from center in cm)	R^2 for regression
23	Power law	$I_n = 8978x^{-2.7926}$	0.962
46	Linear to 25 cm	$I_n = -4.610x + 116.7$	0.982
	Quadratic	$I_n = 0.115x^2 - 7.882x + 116.7$	0.980
76	Linear to 25 cm	$I_n = -2.057x + 111.7$	0.974
	Quadratic	$I_n = -0.0212x^2 - 1.904x + 108.2$	0.978
107	Linear to 25 cm	$I_n = -1.626x + 107.6$	0.889
	Quadratic	$I_n = -0.0146x^2 - 1.181x + 104.9$	0.937
142	Linear to 25 cm	$I_n = -1.062x + 104.4$	0.814
	Quadratic	$I_n = -0.0118x^2 - 0.705x + 102.2$	0.895

¹ Beam axis of the lamp is perpendicular to the sample plane

ASTM G 151 states that specimen repositioning is not required within the sample plane where the irradiance is at least 90% of the peak irradiance. ASTM G 151 requires that the exposure area be limited to an area where irradiance is at least 70% of the peak irradiance. The size of these exposure areas can be determined by solving the equations in Tables 4 or 5, or by interpolating from a graph of the normalized irradiance data plotted as a function of distance from the center spot of peak intensity. Table 6 shows the diameter for the circles where irradiance is at least 90% of peak intensity and where irradiance is at least 70% of peak intensity. It is clear from Table 6 that the usable exposure areas for the Designer 16 lamp are much smaller than for the Tru-Aim Brilliant lamp. The Designer 16 lamp uses a built in reflector to focus the light output, while the Tru-Aim Brilliant lamp has a more conventional “floodlight” design.

Table 6 -- Diameter for exposure areas where irradiance is at least 90% and 70% of peak irradiance

lamp	Distance from lamp to sample plane (cm)	Diameter for circle where irradiance is at least 90% of peak	Diameter of circle where irradiance is at least 70% of peak
Sylvania Designer 16	23	7.6 cm	8.2 cm
	46	8.1 cm	9.2 cm
	76	9.6 cm	11.5 cm
	107	10.8 cm	13.5 cm
	143	12.0 cm	15.7 cm
Sylvania Tru-Aim Brilliant	23	10.4 cm	11.4 cm
	46	11.6 cm	20.2 cm
	76	17.3 cm	33.3 cm
	107	21.7 cm	46.3 cm
	143	27.2 cm	64.8 cm

The exposure area diameter data for the Sylvania Tru-Aim Brilliant lamp shown in Table 6 is graphed in Figure 5. The diameter of both the “90%” and “70%” exposure areas is a linear function of distance between the lamp and sample plane. This provides for determination of the optimum and allowed exposure areas for any lamp / sample plane distance. When the specimen plane is close to the lamp, the “90%” and “70%” areas are indistinguishable.

ASTM G 151 also sets performance requirements for temperature uniformity within a laboratory accelerated exposure device. The devices need to maintain the temperature of a black or white temperature sensor within ± 3 °C of the desired set point and the temperature of a black or white panel temperature sensor needs to be within $\pm 5\%$ of the desired temperature at any position within the exposure area. Since the irradiance uniformity measurements showed that the area of uniform exposure was circular, temperatures were measured where the beam axis intersected the sample plane and every 5 cm in along perpendicular lines intersecting this position (Figure 3). In order to determine the “in use” temperature, an initial set of measurements was made with the lamp oriented at 37° to a line perpendicular to the plane of measurements with the lamp

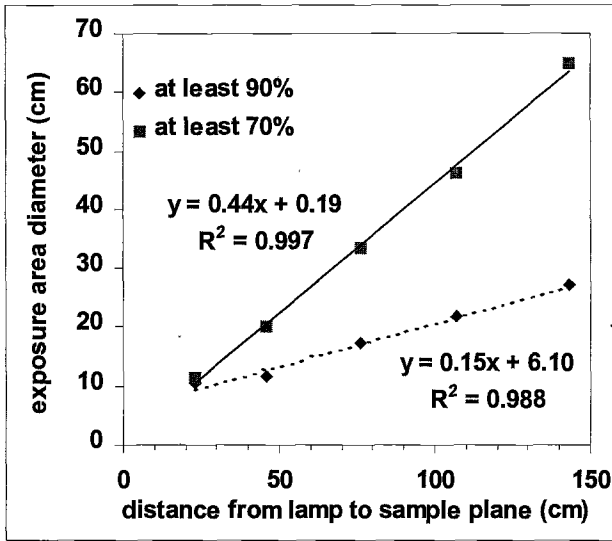


Figure 5: Diameter of exposure areas with at least 70% and 90% of peak irradiance for Sylvania Tru-Aim lamp

at a distance of 143 cm from the plane. The results for the “in use” temperatures are shown in Table 7. For the Designer 16 lamp, the data clearly shows a “hot spot” where the beam axis intersects the measurement plane. Within a 10 cm diameter circle around the center, surface temperatures are 5-7 °C higher than ambient for the black background and 2-4 °C higher than ambient for the white background. These are high temperatures for the

large distance (143 cm) from the lamp. For the Tru-Aim lamp, the spread of temperatures within the area measured was generally low and did not indicate a “hot spot” where the beam axis intersected the measurement plane. The temperatures measured at the two leftmost (horizontal) and two top positions (the -15 and -10 cm positions in Table 7) showed the most variability, with temperatures at the extreme left or top position below ambient for both black and white. These differences are likely due to

Table 7 -- Surface temperatures determined for “in-use” exposures to Sylvania Designer 16 and Tru-Aim lamps

Lamp	back-ground	orientation	Ambient (°C)	Surface temperature (°C) at indicated distance from center position						
				-15 cm	-10 cm	-5 cm	0 cm	5 cm	10 cm	15 cm
Designer 16	black	0°	22.8	25.5	27.1	28.0	29.7	28.2	26.0	25.0
	black	90°	22.8	26.4	28.8	28.1	30.1	28.9	26.9	25.8
	white	0°	22.8	23.7	26.5	25.9	26.4	26.3	25.3	24.4
	white	90°	22.9	23.4	26.2	25.3	25.3	25.0	24.6	23.8
Tru-Aim	black	0°	23.0	22.3	25.7	23.9	24.5	24.3	24.4	24.2
	black	90°	22.9	22.8	26.3	24.3	24.6	24.2	24.2	24.1
	white	0°	24.0	20.9	24.4	22.7	22.7	22.7	23.0	22.7
	white	90°	23.2	21.3	24.8	23.1	23.1	22.8	22.9	22.8

air currents over the measurement area. In any case, the average “worst case” field temperature measurements for the Tru-Aim lamp averaged less than 2 °C higher than ambient for the black background and were actually slightly lower than ambient for the white background. This may have been caused by different in air flow over the surfaces when the temperatures were measured.

In order to determine the size of the exposure area that will fall within the limits defined by ASTM G 151, it is necessary to measure surface temperatures within the sample plane at the distance needed to get the desired irradiance acceleration. Ideally, exposure temperatures in the laboratory accelerated test be should close to those for “in-service” conditions in order to use irradiance as the primary accelerating factor. The temperatures measured within this exposure area can then be compared to those in actual use to estimate whether it is practical to expose materials at the temperatures produced and avoid unrealistic thermal degradation. The data in Table 3 indicates that for an irradiance acceleration of 10:1 for the Designer 16 lamp, the specimens needed to be placed at a distance of 56.7 cm from the lamp. In a laboratory accelerated exposure device, the sample plane is typically perpendicular to the beam axis of the lamp. Table 7 showed that surface temperatures were already 5-7 °C higher than ambient for the Designer 16 lamp for a field condition where the lamp was at a distance of 143 cm and offset from the perpendicular. Attempts to measure surface temperatures with the Designer 16 lamp positioned at 56.7 cm from the specimen plane were abandoned because the temperatures were obviously high enough to produce significant thermal degradation. Development of a laboratory accelerated test for this lamp would clearly require significant cooling of specimens. This introduced a design parameter the authors felt was beyond the objective of development of a simple small-scale laboratory accelerated exposure test.

Table 8 -- *Surface temperatures for white and black materials exposed at several distances from Sylvania Tru-Aim lamp*

background color	distance from lamp (cm)	Surface temperature (°C) at indicated distance from center position						
		-15 cm	-10 cm	-5 cm	0 cm	5 cm	10 cm	15 cm
white	76	27.1	25.6	25.1	27.8	26.6	26.2	26.1
white	46	29.7	30.9	32.2	35.7	33.9	31.4	28.9
white	23	26.0	29.0	50.3	66.3	58.5	32.3	25.7
black	76	31.0	30.1	30.9	34.2	31.3	32.1	29.9
black	46	33.9	37.6	43.1	48.5	43.6	43.3	35.0
black	23	27.2	33.4	75.8	95.7	73.5	43.2	27.4

Surface temperatures measured at several lamp / sample plane distances for the Sylvania Tru-Aim lamp are shown in Table 8. For the “in-use” field condition, there was only a very small temperature difference between the maximum surface temperature and ambient temperature in the area illuminated by the lamp. However, when the lamp was

placed 23 cm from the sample plane, surface temperatures for dark colors reached a point where thermal degradation effects would be very likely without substantial specimen cooling. For the 46 cm distance, specimen surface temperatures may still be in the range where unrealistic thermal degradation effects will be minimal. At 46 cm, the ratio of irradiance at the sample plane to that for in-service conditions with the Tru-Aim lamp is 12.5:1. For specimens exposed at 46 cm, the exposure area that falls within the ASTM G 151 limits is a circle with a diameter of 6 cm for black and 11 cm for white. At 76 cm, where the irradiance ratio is 4.6:1, surface temperatures are typically 5-10 °C above ambient for any color and fairly uniform within the area where surface temperatures were measured. The area falling within ASTM G 151 limits for temperature is a circle approximately 20 cm in diameter for black and 30 cm in diameter for white. Table 9 summarizes the conditions for these two accelerated tests using the Tru-Aim lamp. For each of the accelerated tests, acceleration of degradation compared to actual use conditions will be produced by both an increase in irradiance and in exposure temperatures.

Table 9 – Comparison of surface temperature (°C) and 400-700 nm irradiance (W/m²) for in-use condition and for two laboratory accelerated tests with the Tru-Aim lamp

Color	in use conditions		lamp / sample plane distance = 76 cm		lamp / sample plane distance = 46 cm	
	temperature	irradiance	temperature	irradiance	temperature	irradiance
White	23	2.53	28	11.6	36	31.5
Black	24	2.53	34	11.6	48	31.5

Conclusions and Future Work

This paper describes a straightforward procedure for the design of a simple laboratory accelerated exposure test for an interior light environment. This procedure consists of the following steps:

1. Determine spectral power distribution of light source and evaluate whether there is an appropriate match to the spectral power distribution of light sources used in laboratory accelerated exposure tests described in existing standards.
2. Measure spectral power distribution at typical “worst case” field condition.
3. Measure spectral power distribution of the light source at several distances to determine effect of distance on irradiance and to calculate an irradiance acceleration factor for the laboratory accelerated test.
4. Determine uniformity of irradiance within the sample plane at lamp/sample plane distances being considered for desired irradiance acceleration. Define exposure area that conforms to requirements of ASTM G 151.
5. Measure surface temperature of dark and light colors in typical “worst case” field conditions.
6. Measure surface temperature of dark and light colors at lamp/sample plane distances being considered for desired irradiance and assess whether the

temperatures are likely to produce unrealistic thermal degradation without sample cooling. .

7. Determine uniformity of surface temperatures within the sample plane to define the exposure area that conforms to requirements of ASTM G 151.

The steps described above were used to define conditions for a laboratory accelerated exposure test for two different lamps used for interior lighting. The test design is based on using a single lamp and avoiding the need for additional specimen cooling. For the lamps used, the exposure areas that meet the irradiance and temperature uniformity requirements of ASTM G 151 are relatively small. However, if small specimens can be used to determine the effects of important appearance attributes such as color, the test may be quite useful.

Experiments are underway to evaluate the laboratory accelerated exposure test conditions defined in this paper. This work will determine whether use of a linear irradiance acceleration factor is valid. Additional work is needed to determine how changes in spectral distribution or total lamp output that are caused by lamp aging will affect the rate of degradation. This information will be critical if results of this type of testing are to be used to estimate service life.

The steps outlined here are also applicable to design of a larger-scale laboratory accelerated test involving use of multiple lamps. With the lamps evaluated in this work, it is likely that such a device would require that the specimens be cooled to avoid unrealistic surface temperatures during exposure.

References

- [1] Meserve, B. E., Pettofrezzo, A. J., Meserve, D. T., "Principles of Advanced Mathematics", L.W. Singer, Chicago, 1964, p 365.

Richard M. Fischer¹ and Warren Ketola²

Exposure Test Results for Inkjet Inks in Interior Light Environments

Reference: Fischer, R. M. and Ketola, W. D., “Exposure Test Results for Inkjet Inks in Interior Light Environments,” *Durability 2000: Accelerated and Outdoor Weathering Testing, ASTM STP 1385*, J. D. Evans and W. D. Ketola, Eds., American Society for Testing and Materials, West Conshohocken, PA, 2000.

Abstract: A procedure for development of a simple, small-scale laboratory accelerated test based on the same light source used in the actual indoor application is described by Ketola et al., [1] “Stress Analysis and Accelerated Test Design for Interior Light Environment” as part of this STP 1385. The test parameters identified in that work were used to evaluate and compare the durability of “inkjet” inks in both actual exposure and accelerated conditions. The inks were also exposed to more traditional weathering tests that may also be used to evaluate the light stability of materials used indoors. Test results point out the importance of matching the spectral power distribution of the real environment for obtaining the most accurate durability assessment. An approach for estimating service life for these inks is also described.

Keywords: light, color, exposure testing, indoor, weathering, durability, service life

Introduction

The primary purpose of this work is to evaluate the utility of the accelerated indoor light test described by Ketola [1]. Inkjet inks were chosen for this study because of the poor color stability that was observed for these materials in an office/laboratory setting. This permitted a reasonably short time period for evaluating accelerated test performance and, more importantly, comparing these results to “real world” exposures. Most often the materials exposed to normal display lighting in a museum or art gallery would be quite light stable compared to the inkjet inks. If similar light sources are used in advertising displays in stores or office environments, these inks may often be the graphic medium of choice. For comparison purposes the inkjet inks were also exposed to a fluorescent accelerated exposure test, sunlight through window glass and a direct sunlight simulation.

¹ Division Scientist, 3M Weathering Resource Center, 3M Center, Building 235-BB-44, St. Paul, MN 55144-1000

² Division Scientist, 3M Traffic Control Materials Division, 3M Center, Building 235-3E-60, St. Paul, MN 55144-1000

Experimental

The ink specimens were obtained from three different inkjet printers as described in Table 1. Three primary colors were selected (cyan, magenta, and yellow) along with a reddish orange that results from the combination of magenta and yellow. The inks were printed in an approximate 5 cm by 5 cm square with each color occupying a quadrant (Fig. 1).

Table 1 – *Generic Description of Inkjet Printers used to Generate Exposure Specimens.*

Printers	Type	Cost	Use
A	Inkjet	<\$300	Home
B	Inkjet	>\$500	Home/small office
C	Thermal Wax	>\$1000	Office

Orange	Cyan
Yellow	Magenta

Figure 1 – *Inkjet Exposure Grid Comprised of Three Primary Colors and One Mixture.*

The inks were printed on plain paper and polyethylene terephthalate (PET) transparency film using MicrosoftTM Word 97 with default print settings appropriate for the two substrates. The plain paper swatches were adhered to 3 mm thick by 10 cm square clear polycarbonate plaques using an acrylic pressure sensitive adhesive. The PET film/ink specimens were attached to white-painted aluminum panels (1 mm by 7 cm by 20 cm) using polyvinylidene fluoride tape.

Color measurements were made with a Spectrosensor II integrating sphere colorimeter from Applied Color Systems. UV/visible absorption spectra were collected with a Shimadzu UV 2401 PC spectrometer.

Spectral power distributions for the light sources were measured at 2 nm increments from 250 to 800 nm using an Optronics OL754 spectroradiometer equipped with a 4 inch diameter integrating sphere with quartz dome (OL 752-S). Broad band illuminance levels (lux) were determined using an International Light radiometer (model

IL1730 with SED033 sensor). Specimen exposure temperatures were determined with an Omega OS42A infrared thermometer. The exposure conditions for the various environments are described in Table 2.

Table 2 – List of Exposures Tests Used for Comparing Inkjet Ink Durability.

<p><u>Real Display</u> Sylvania Tru-Aim™ Brilliant Halogen (12V, 50W, Part # 50MR16Q/40/FL/B) 53° angle from light source beam to specimen plane 142 cm exposure distance Specimen Temp ~ 23°C Illuminance ~ 715 lux (2.5 W/m², 400-700 nm)</p>
<p><u>Accelerated Display</u> Sylvania Tru-Aim™ Brilliant Halogen (12V, 50W, Part # 50MR16Q/40/FL/B) 90° angle from light source beam to specimen plane 46 cm exposure distance Specimen Temp ~ 29-33°C Illuminance ~ 11240 lux (31 W/m², 400-700 nm)</p>
<p><u>Simulated Direct Sunlight</u> Atlas 6500W Xenon arc Specimen under quartz glass (3.2 mm) Specimen Temp - 50-55°C Irradiance - 0.35W/m²@340 - Borosilicate inner and outer filters (282 W/m², 400-700 nm)</p>
<p><u>Simulated Sunlight through Window Glass</u> Atlas 6500W Xenon arc Specimen under window glass (6.4 mm) Specimen Temp - 50-55°C Irradiance - 0.35W/m²@340 - Borosilicate inner and outer filters (264 W/m², 400-700 nm)</p>
<p><u>Fluorescent</u> Q-Panel – QUV Sylvania 34W Miser II Specimen Temp ~ 27°C Irradiance - Normal QUV (58 w/m², 400-700 nm)</p>

The sunlight simulation exposures were performed in a water-cooled xenon arc running ASTM G26 G26-96 Standard Practice for Operating Light-Exposure Apparatus (Xenon-Arc Type) With and Without Water for Exposure of Nonmetallic Materials, method A, which calls for a water spray (with light) for 18 minutes in every two hour exposure cycle. The ink/plain paper specimens were protected from the water spray by placing them behind quartz- and window glass- covered holders shown in Figure 2. The window glass on the holder also prevents some short wavelength light (below 330 nm) from impinging on the specimens. The quartz specimen cover does not significantly alter xenon arc light output. The ink/PET specimens were exposed only in the real and accelerated display environments.

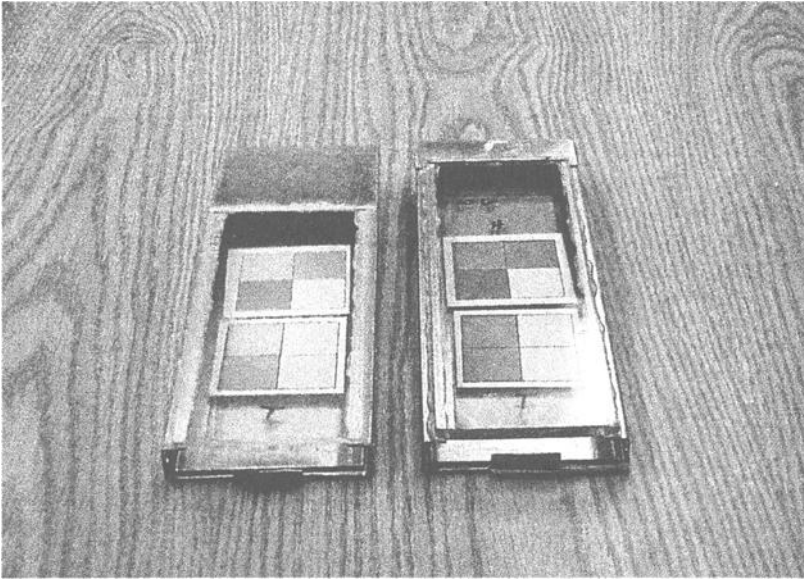


Figure 2 – *Quartz and Window Glass Covered Specimen Holders Used to Protect the Inkjet Specimens from Water Spray and Appropriately Filter the Light from the Xenon Arc Light Source (with Borosilicate Inner and Outer Filters).*

Results

Total Colorshift

During the brief “Real Display” exposures only the B and C printer inks demonstrated significant change in total colorshift (Fig 3). The excellent durability for A inks is especially prominent during xenon arc (ASTM G26) – quartz exposure (Fig. 4). For ease of viewing and simplification of discussion, only results for printers B and C will be shown. In all exposures, inkjet inks from printer A were the most durable. The magenta and orange inks from printer C had the greatest ΔE during the first few hours of exposure (see Figures 5-9 for a comparison of ΔE tendencies for Ink sets B&C in all the exposure environments described in Table 2).

The magnitude of ΔE or test severity was least in the Real Display exposure (Fig 5). The cyan, orange, and magenta inks for printer C have the most rapid total colorshift. Printer B inks start to “catch up” at the end of the 350 hour exposure period. A 50 hour accelerated display exposure causes roughly the same degree of ΔE as 350 hours of exposure in the real display (Fig. 6). Beyond 50 hours exposure, the B inks are, in general, less color stable than the C inks. The ΔE during fluorescent lighting exposure (Fig. 7) is very similar to the accelerated display results (Fig. 6) in both performance order and magnitude.

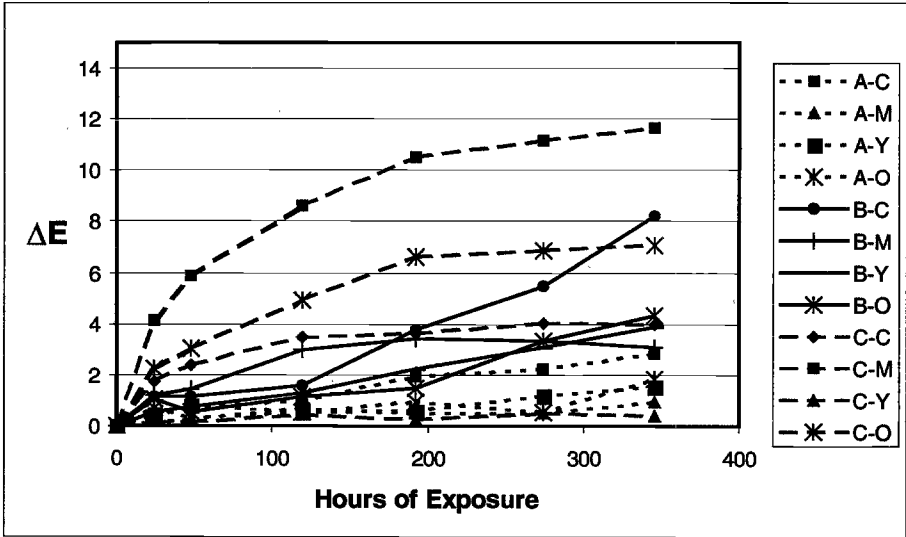


Figure 3 – Total Colorshift Results from Real Display Exposure (142 cm) for All Three (A, B, and C) Inkjet Printer Specimens. (C- Cyan, M-Magenta, Y-Yellow, and O-Orange, e.g., A-C is the cyan ink from printer A).

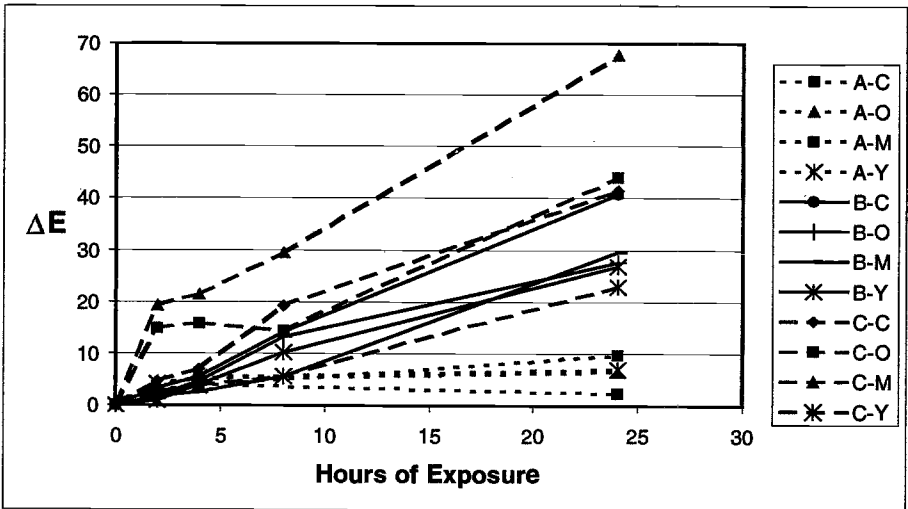


Figure 4 – Total Colorshift Results from Xenon Arc – Quartz Exposure for All Three (A, B, and C) Inkjet Printer Specimens (C- Cyan, M-Magenta, Y-Yellow, and O-Orange).

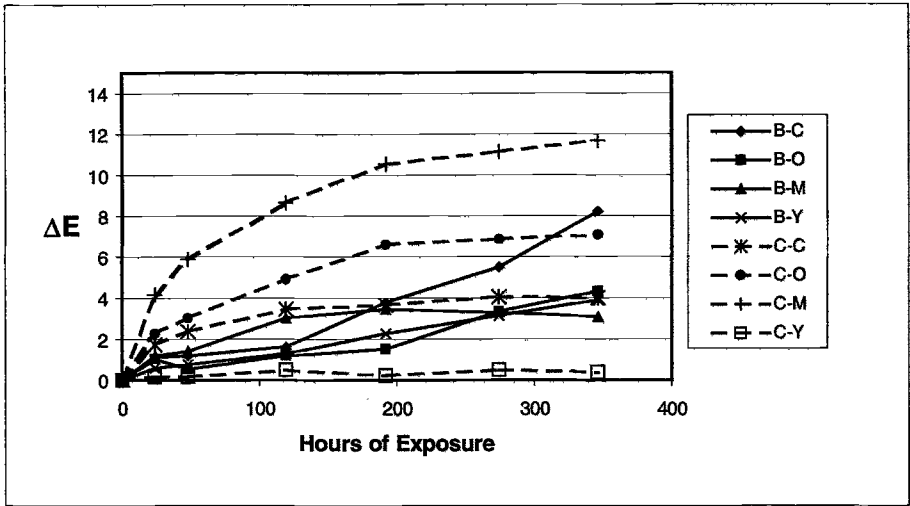


Figure 5 - Total Colorshift Results from Real Display Exposure (142 cm) for B and C Inkjet Printer Specimens.

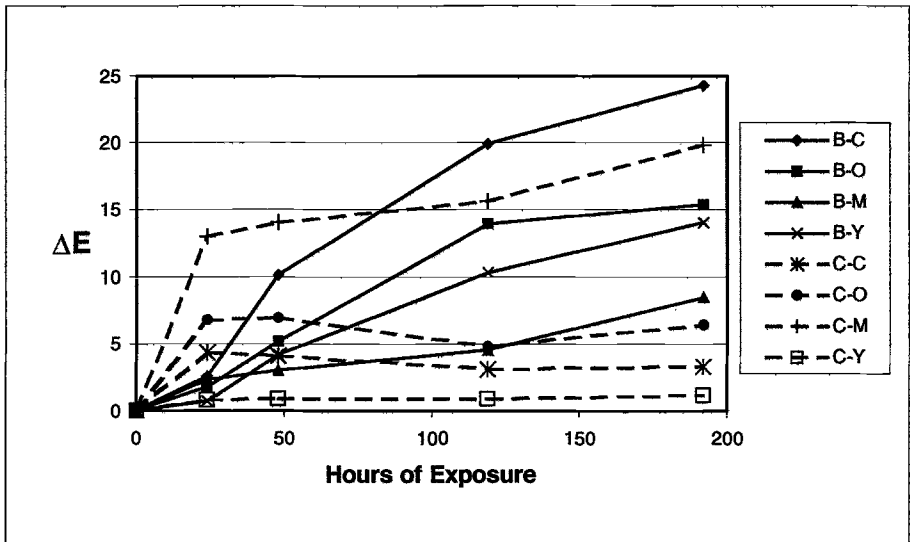


Figure 6 - Total Colorshift Results from the Accelerated Display Exposure (46 cm) for B and C Inkjet Printer Specimens.

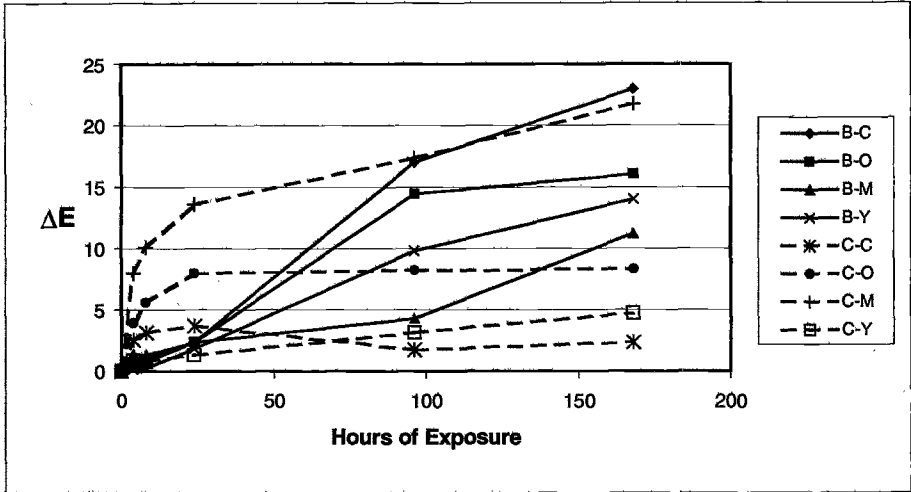


Figure 7 - Total Colorshift Results from the Fluorescent Lighting Accelerated Exposure For B and C Inkjet Printer Specimens.

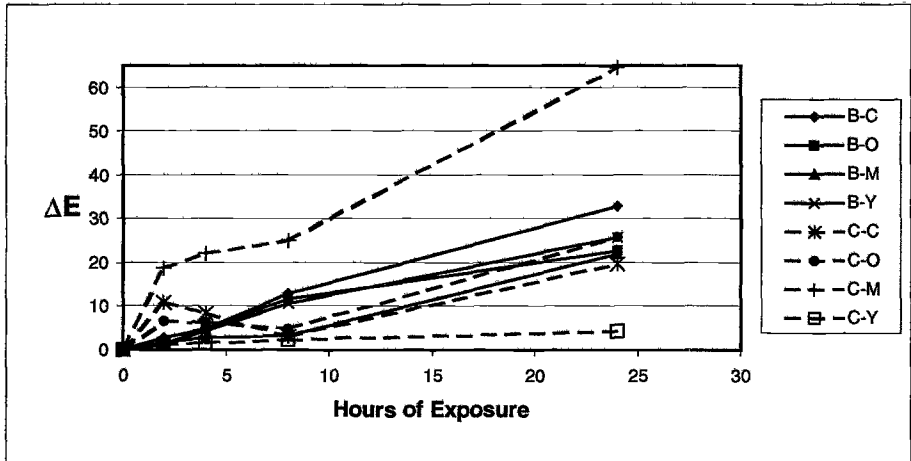


Figure 8 - Total Colorshift Results from the Xenon Arc Through Window Glass Exposure For B and C Inkjet Printer Specimens.

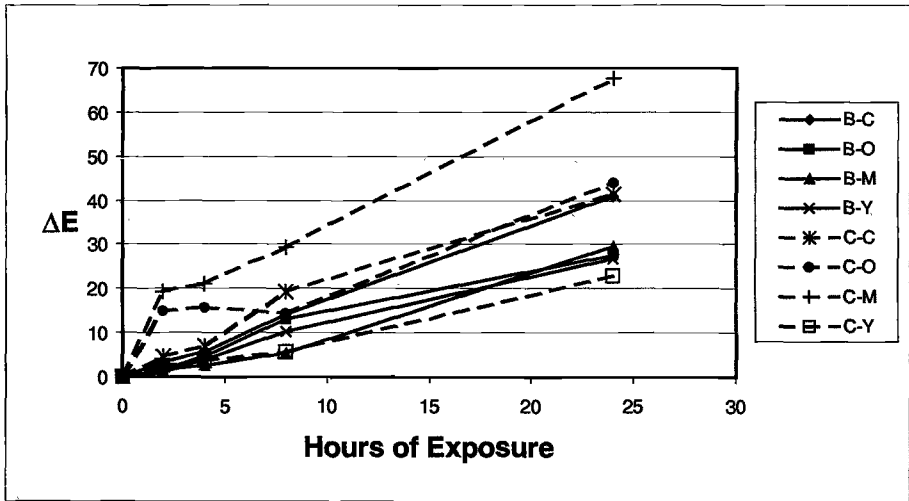


Figure 9 - Total Colorshift Results from the Xenon Arc Through Quartz Exposure for B and C Inkjet Printer Specimens.

The total colorshift in the xenon arc under window glass and quartz is very rapid compared to the previously discussed tests. The relative performance ordering during xenon arc under window glass exposure (Fig. 8) approximates the accelerated display and fluorescent 150 hour plus results in roughly eight hours. The rapid colorshift observed between 8 and 24 hours reflects loss of ink that permits the appearance of the white paper substrate to begin contributing to ΔE. This result demonstrates that ink types B and C should not be placed in direct sunlight through window glass environments for even brief time periods.

Total colorshift during xenon arc through quartz exposure (direct sunlight simulation) is similar in rate to those observed under window glass (Fig. 9). The filtering of light between 280 and 330 nm that occurs through window glass does afford some slight protection to the cyan, orange and yellow type C inks compared to direct xenon arc exposure.

Correlation – Picking the Most Durable Ink(s)

Selecting the “best” accelerated test depends on the real environment to which the ink will be exposed. In this particular study, the real environment was defined as the 142 cm real display. As primarily an academic exercise, the accelerated tests can be evaluated for their predictive ability using non-parametric statistics. Spearman rank correlation is commonly used to access accelerated test performance compared to the real world (2, 3). The most that should be expected from a single accelerated test is to rank the durability performance in the same order as the service environment. This implies that a Spearman rank correlation coefficient (r_s) of 1 describes the perfect test. By

inspecting Figure 10, all of the exposure tests do a reasonable job of ranking the total colorshift stability of the inks with r_s values between 0.8 and 0.9. The accelerated display (46 cm) is the best at predicting the 346 hour exposure rankings for the real display by approaching an r_s of one at 50 hours.

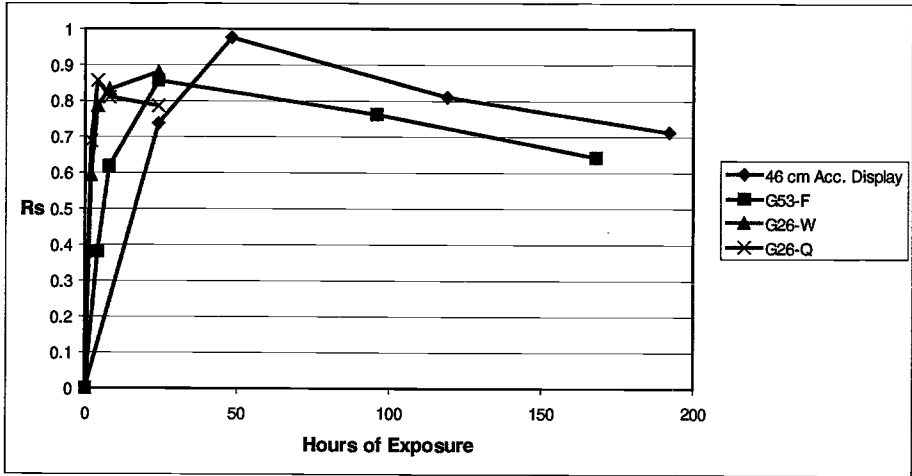


Figure 10 – Spearman Rank Correlation for the Various Accelerated Exposures Compared to the 142 cm “Real” Tru-Aim Exposure Results at 346 Hours.

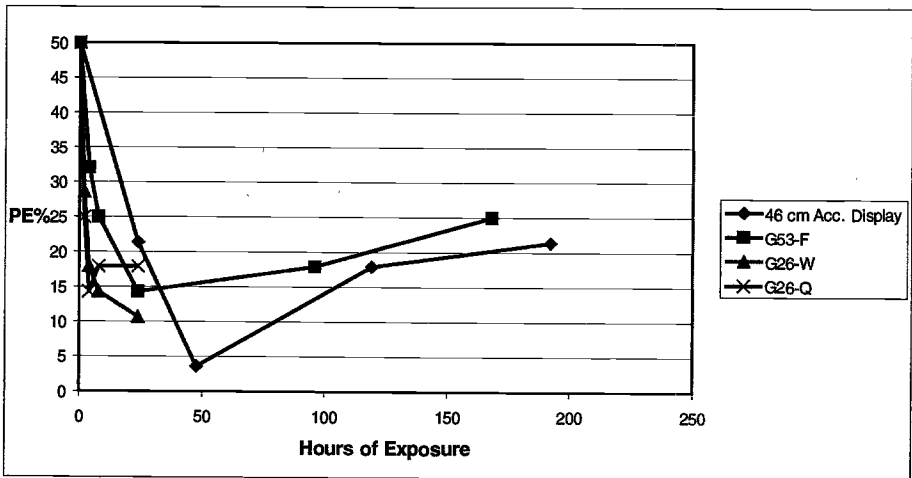


Figure 11 – Percent Pair Error for the Various Accelerated Exposures Compared to the 142 cm Real Display Exposure Results at 346 hours.

The value of having an accelerated test that reaches an r_s value of 1 compared to 0.9 is difficult to assess. Percent pair error (PE%) provides a more quantitative measure of test goodness (2) and is plotted for these same exposures in Figure 11. The PE% statistic is a measure of the probability of selecting a random pair of specimens from the accelerated test that exhibit “reversed” performance compared to the same specimen pair in the service environment. By comparing PE% maxima, the accelerated display exposure is almost three times less likely to reverse a specimen pair result from the real display exposure (compared to the other accelerated tests). This is not surprising since both the accelerated and real display exposures used the same light source. The other accelerated tests probably would have displayed superior correlation if the service environment had been direct sunlight, sunlight through window glass, or fluorescent office lighting. It is important to use an accelerated test light source that is as similar as possible to the light source in the service environment.

Acceleration Factors

An antiquated but often used approach to predicting service life of materials in the weathering industry is to use “acceleration factors” (AF) for estimating the life of products in real world environments. Table 3 points out the futility of this approach. The first difficulty encountered is what criteria and time period should be used to determine acceleration. This is especially problematic with non-linear failure profiles. The criterion used for developing Table 3 is comparing rates during the initial stages of total colorshift (four to six ΔE units). The average acceleration factors (for eight B and C inks in each environment) correspond relatively well with the irradiance levels shown for the applicable light sources between 400 and 700 nm (Figure 12). There is roughly a one decade irradiance difference between the real display (142 cm) and the accelerated fluorescent and accelerated display exposures (between 400 and 700 nm), which matches the AF values of 8 to 9X for these two accelerated exposures. The two decade irradiance increase from the real display to the xenon arc exposures leads to a 130 to 150X ΔE rate increase. Since the exposure temperatures are also greater in the xenon arc, this acceleration level would also be appropriate.

Table 3 – Total Colorshift Acceleration Factors for B and C Ink Systems.

Exposure Test	Hours	Average ΔE	Average $\Delta E/hr$	Average AF	Range AF
142 cm Real Display	192	4	0.021	1	1---->1
46 cm Acc. Display	24	4.03	0.168	8.05	2.4---->29.1
G53-Fluorescent	24	4.42	0.184	8.84	5---->44.9
G26-Window Glass	2	5.53	2.765	132.7	43---->286
G26-Quartz	2	6.11	3.055	146.7	43---->217

[AF – acceleration factor]

The “Range AF” column demonstrates the fallacy associated with using acceleration factors to predict service life for future ink testing. The AF values are material dependent and vary up to a factor of ten in accelerated display and fluorescent exposure tests. This

makes the use of an average or single AF value extremely risky in estimating service life for a new material. Similar results for other material systems have been reported by

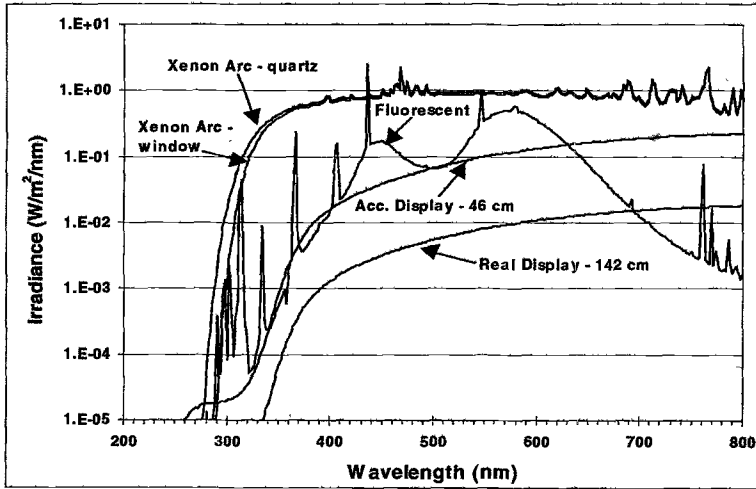


Figure 12 – Spectral Power Distributions for Exposure Light Sources.

Fedor who found acceleration factors ranging from 2 times to 35 times faster than outdoor exposure (depending primarily on polymer type) for a study recently conducted with fluorescent UV condensation devices (4). The misuse of these types of acceleration factors has led to numerous field failures and has been the primary contributor to the general distrust of results from accelerated weathering that has developed over the years.

UV/Visible Absorption Spectral Results

When the inks were printed on PET transparency films, the UV/Visible spectra of the inks can be easily collected both before and during exposure. An example of the initial UV/Visible absorption spectra for the cyan, magenta, and yellow primaries for printer A are shown in Figure 13. To function adequately as transparency graphics for overhead projectors, the inks range from an absorbance of 1 to 2 at λ_{\max} for the primaries, i.e., 0.1% to 10% transmission. [note - λ_{\max} is the wavelength of maximum absorbance for a light absorbing species.] The appropriate mixing of these inks provides the palette of colors available in inkjet printing. For example, the combination of magenta and yellow provides the orange color for printer B (Fig. 14). Ink families A, B, and C have similar primaries with slightly varying absorption spectra indicating some compositional differences in the inks. This is not surprising based on the varying exposure results observed for the three ink families.

The total colorshift for the C magenta (and orange) was extremely rapid in all of the exposure tests. This primary had the surprising result of an increase in absorbance at λ_{\max} during the initial exposure periods (Fig. 15). We suspect that this absorbance

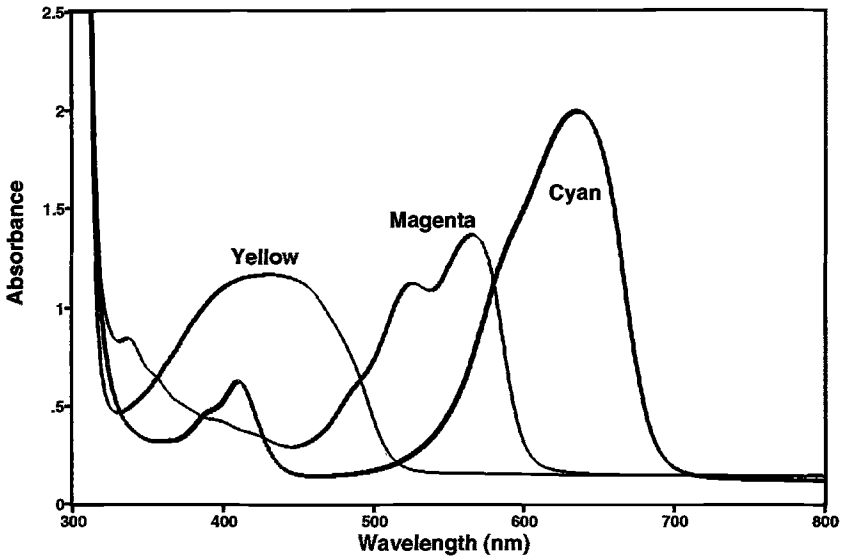


Figure 13 – UV Absorbance Spectra of B Inkjet Primaries (on PET film).

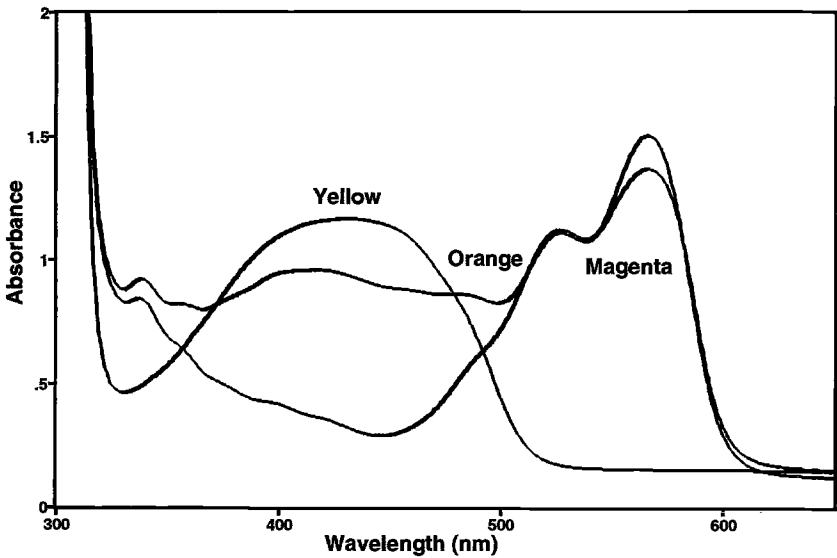


Figure 14 – UV Absorption Spectra of Ink B – Yellow and Magenta Primaries combined to give Orange (on PET film).

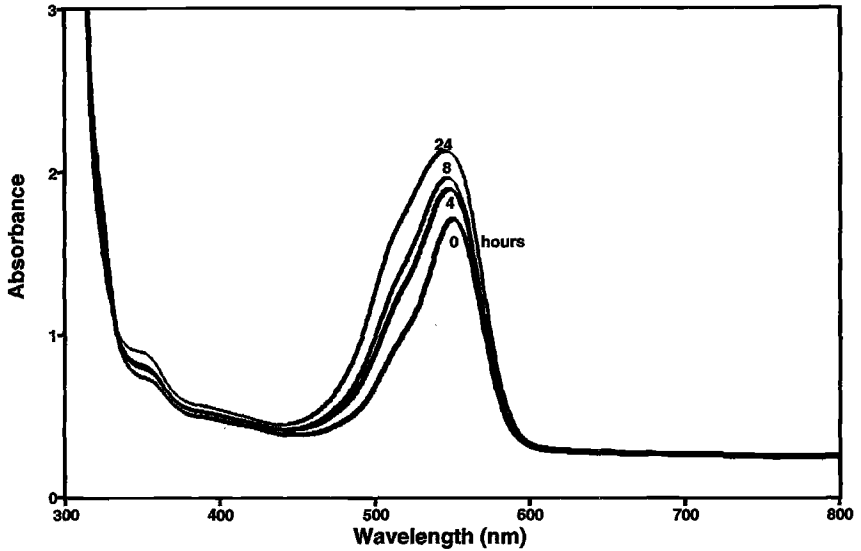


Figure 15 – UV Absorbance increase during Accelerated Display Exposure of Ink C Magenta.

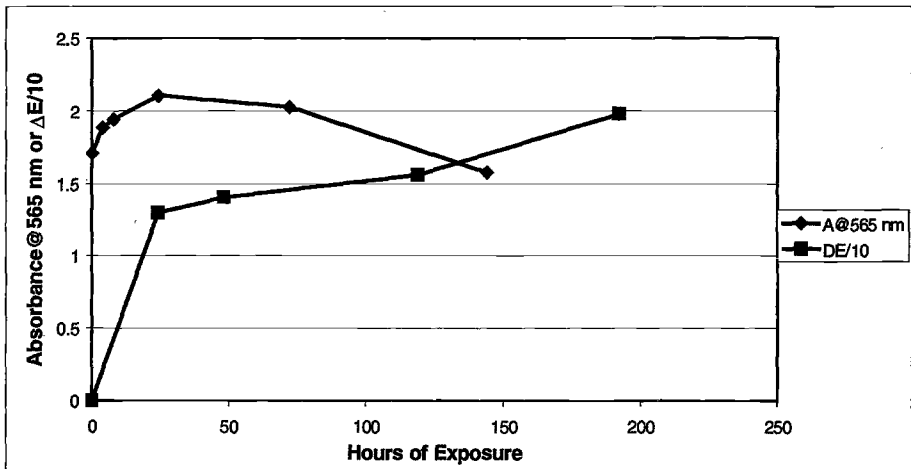


Figure 16 – Comparison of Colorshift and Absorbance Change for Ink C – Magenta During Exposure in 46 cm Accelerated Display Light Source.

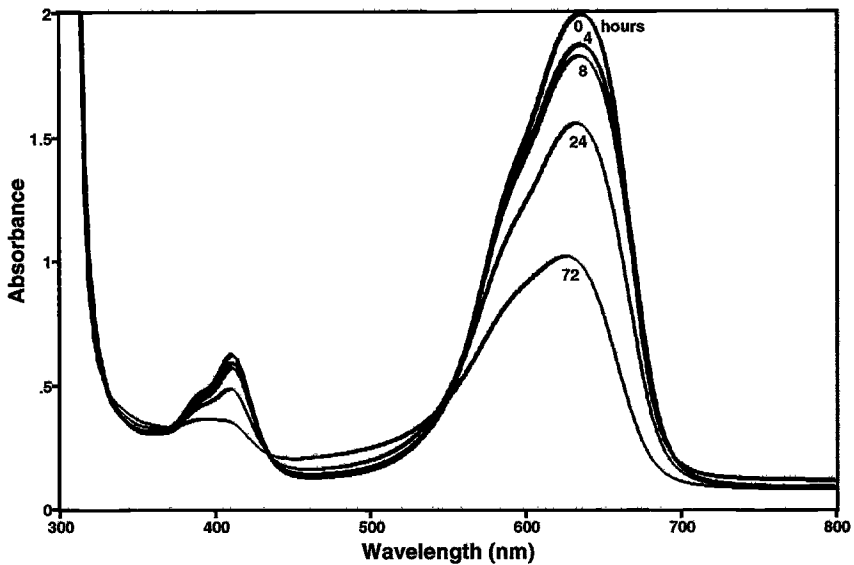


Figure 17 – UV Absorbance decrease during Accelerated Display Exposure of Ink B Cyan.

increase is caused by additional solubilization of colorant particles suspended in the thermal wax medium used in the C inks. None of the other C primaries exhibited this behavior. This increased absorbance led to more intense color for C print, but may well not be a failure even though there was extensive total colorshift. After 24 hours the absorbance of C magenta stabilized and started to decrease after 72 hours (Fig 16). During this time, the ΔE begin increasing again but at a slower rate.

The absorbance for B cyan decreased rapidly during exposure to the accelerated display light source (Fig. 17). The decrease in absorbance indicates a physical or, more likely, a chemical loss of colorant. This loss along with the slight absorbance increase between 400 and 550 nm gave the B cyan a gray-muddy appearance. This change became visually objectionable as absorbance dropped below 1 at λ_{max} .

Zero-Order Ink Service Life Predictions

Pickett and Moore have thoroughly described the photochemical loss of UV absorbers in polymer matrices (5, 6). In general, the loss rate is dependent on the UV absorber type and the polymer matrix. The rate follows simple zero order kinetics at “infinite” or high absorbance levels ($A > 2$) and first order kinetics at low concentrations. The loss is primarily photochemical for “functional” UV absorbers, i.e., UV absorbers that do not have poor compatibility or low volatility. Inkjet inks appear to follow this same behavior. Although this has not been confirmed, light primarily in the visible absorption maxima for these inks is probably causing the degradation. The loss of ink absorbance is linear with exposure time down to absorbance equals one. Below $A=1$, the

loss rate starts to diminish (becoming concentration dependent) as has been observed with UV absorbers in polymer matrices (5). This is evident in the limited absorbance data collected for B cyan in the accelerated display exposure in Figure 18. If the ink absorbance in the real display exposure is also following zero-order loss kinetics, a linear extrapolation should reasonably predict the loss profile. The appearance of this particular ink became “muddy” at A=1. This same appearance may be expected in approximately 750 hours of Real Display exposure. This exercise is trivial for such short-lived materials, but could be useful as durability for inkjet materials increase and their use expands to more stringent environments.

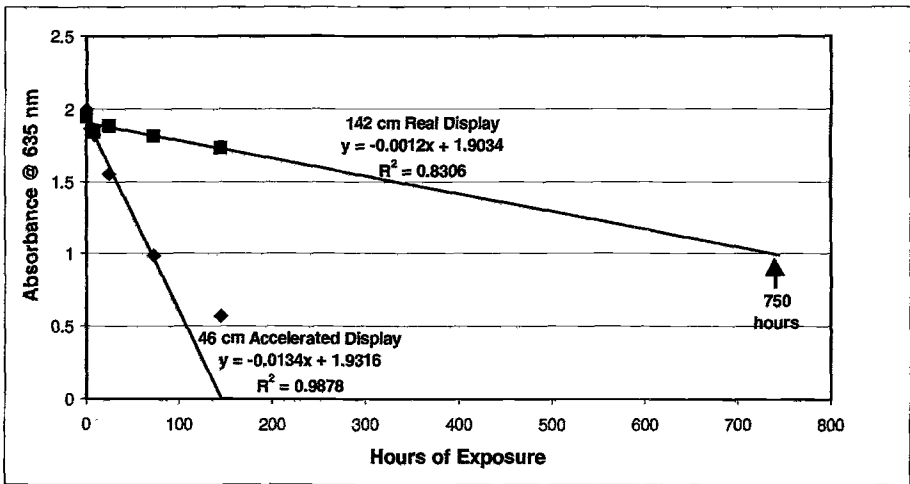


Figure 18 – Zero Order Projection to Absorbance = 1 for 142 cm Real Display Exposure and for 42 cm Accelerated Display Exposure of Inkjet B Cyan.

Summary

Although the inkjet inks are relatively light sensitive, the battery of exposure tests were able to determine significant durability differences. Certainly, Printer A inks were less susceptible to total colorshift and were the only inks somewhat resistant to a sunlight through window glass simulation. Generally there were two stages of colorshift (changes in CIE Lab values) observed with the inks. In the “milder” exposures (real and accelerated display and fluorescent), L* values were relatively stable. Most of the contribution to ΔE came from changes in a* and b*. The same trends were observed in the initial stages of the more severe simulated sunlight exposures. During longer exposure periods (> 8 hrs) these more subtle colorshifts were dominated by an increase in L* as the inkjet colorant began to fade and the paper substrate began to contribute to ΔE.

A light source that closely simulates the spectral power distribution of the service environment often provides the best rank correlation. Ideally, the accelerated and service

light sources should have an identical short wavelength cut-on and, proportionally, the same intensity distribution throughout the effective spectral region.

An equivalent change in a physical property, especially total colorshift, does not mean subjective failure. The rapid ΔE change of printer C's magenta was an increase in color saturation, which is not nearly as objectionable as fade followed by appearance of the substrate. Failure in this instance would be when the user was offended by the appearance, which probably occurs with fade. The user determines failure, not a physical property measurement.

Although more work is needed, the inks appear to exhibit photochemical loss that is similar to that observed with UV absorbers. Using the same loss models may be useful in estimating service life, but is not of significant utility unless the durability of these ink types is greatly improved.

Absolute color and colorshift values will be dependent on a number of factors; paper type, ink lot and age, operating condition and maintenance level for the various printers, and the variability inherent in the accelerated tests. Obtaining highly repeatable and reproducible data on an absolute basis is extremely difficult in comparative weathering studies. Coping with this variability is the primary strength of rank correlation approaches for determining accelerated test goodness [2].

References

1. Ketola, W.D., Fischer, R.M., Thomas, L.J., "Stress Analysis and Accelerated Test Design for Interior Light Environments", *Durability 2000: Accelerated and Outdoor Weathering Testing, ASTM STP 1385*, Warren D. Ketola and John D. Evans, Eds., American Society for Testing and Materials, West Conshohocken, PA, 2000.
2. Fischer, R. M. and Ketola, W. D., "Accelerated Weathering Test Design and Data Analysis", Chapter 17, *Handbook of Polymer Degradation*, 2nd Edition, S. H. Hamid, Editor, Marcel Dekker, New York, 2000.
3. Fischer, R. M., "Accelerated and Weathering Test Development with Fluorescent UV-Condensation Devices", SAE Technical Paper Series 841022, 1984.
4. Fedor, G. and Brennan, P., "Correlation between Natural Weathering and Fluorescent UV Exposures", *Durability Testing of Non-Metallic Materials, ASTM STP 1294*, Robert J. Herling, Ed., American Society for Testing and Materials, Philadelphia, 1996, pp. 91-105.
5. Pickett, J. and Moore, J., *Polymer Degradation and Stability*, Vol. 42, 1993, pp. 231-244.
6. Pickett, J and Moore, J., *Die Angewandte Makromolekulare Chemie*, Vol. 232, 1995, pp. 229-238.

Bhakti Patel,¹ Jacob Tikhtman,¹ Fred Lee,² and Kurt Scott³

Advances in Accelerated Weathering Instrumentation Technology Using Advanced Control Systems

Reference: Patel, B., Tikhtman, J., Lee, F., and Scott, K., “Advances in Accelerated Weathering Instrumentation Technology Using Advanced Control Systems,” *Durability 2000: Accelerated and Outdoor Weathering Testing*, ASTM STP 1385, J. D. Evans and W. D. Ketola, Eds., American Society for Testing and Materials, West Conshohocken, PA, 2000.

Abstract: For laboratory weathering instruments to be most useful, they must have, among other qualities, the ability to conduct tests repeatably and reproducibility. Repeatability is the measure of a specific instrument’s ability to duplicate results from one test to another. Reproducibility is the measure of the ability of instruments of the same model to duplicate test results. As users become more sophisticated, the demand for instruments capable of very good reproducibility and repeatability increases. Thus, instrument manufacturers are constantly challenged to deliver suitable instruments to the testing community. For those tests that are influenced by multiple parameters, some of which are synergistic, while others are offsetting, the challenge is even more pronounced.

This paper discusses the concepts and features incorporated in a particular type of xenon weathering instrument to control critical test parameters, whether they are mutually compatible or not.

Keywords: xenon, reproducibility, repeatability, control, accelerated weathering, weathering conditions, simulation, instrumentation.

¹Research Program Manager, ²Standards Program Manager, Weathering Instrumentation Products, Atlas Electric Devices Company, 4114 N. Ravenswood Ave, Chicago IL.

³General Manager, Laboratories and Calibration Services, Atlas Electric Devices Company, 4114 N. Ravenswood Ave Chicago IL.

Introduction

Meaningful accelerated weathering tests require a good technical understanding of the outdoor environment and simulation of outdoor conditions in laboratory weathering devices. Since the first generation of laboratory weathering devices based on mercury arc and carbon arc UV light sources was introduced in the 1920s, continuous efforts have been made to improve their quality to better simulate the service environment. To date, one of the primary advances has been the utilization of appropriately filtered xenon arc light sources because of the close approximation of its spectrum to that of terrestrial solar radiation.

As outdoor monitoring technology and the understanding of material degradation progress, the need, not only to simulate the environment but also for precise and repeatable control of the test conditions in laboratory devices arises. However, synergistic effects of multi-parametric conditions, such as chamber temperature, humidity, irradiance, black panel temperature and ambient laboratory atmosphere, impair the instrument's ability to monitor and control these parameters simultaneously when only simple on-off controls are used.

Another driving force for accurate parameter control comes from industries that have developed more stringent performance requirements. As researchers discover more about the science of weathering, the need for better and more accurate simulation of outdoor weathering conditions increases. Often, new research findings are incorporated in updated and more rigorous testing specifications. For example, the automotive industry now requires independent control of chamber air temperature (dry bulb) along with black panel temperature (BPT)[1], as well as improvements in steady state error (SSE) i.e. tolerance of the BPT control. At the same time, high accuracy of controls has been demanded. Tolerance requirements have been tightened from 10% to below 5% and in some cases, to as little as 2%.

Existing industry requirements often mean that new instruments that are developed to meet anticipated future demands also must meet specifications that currently exist. This constraint means that even as more precise controls and modern measurement techniques are used to yield better performance and tighter controls in order to conform to stricter new standards, the instruments in which they are deployed will often be measured by the standards developed for older, cruder instruments. This is problematic particularly when performance of a device is measured by performance of standard reference materials (SRM). In many cases, newer technology and tighter controls will actually mean a difference in a parameter's effective control point, which will impact the performance of SRMs. This dilemma presents another challenge to the instruments' manufacturer since it is necessary to demonstrate reproducibility between older and emerging instruments during the transitional period when both are being used.

Modern instruments require more advanced logical controls to satisfy the following requirements: 1. *Proper* controls to minimize any synergistic and cumulative effects of controlling parameters. 2. *Precise* controls to conform to more stringent industry requirements, 3. *More* controls to meet increasingly complex requirements, 4. *Compliant* controls for materials conformity. In this paper, several

examples of advanced control implemented in new designs of a particular manufacturer's accelerated weathering devices.

Overview of Process Control and the Reaction (Response) Curve

The main advantage of advanced controls is to improve in-process characteristics. Improved process characteristics are often depicted by more rapid and precise process reaction curves. In a simple control system, one can examine both the maximum rate of change (process gain) and the time to reach this maximum rate of change (delay time). Similarly, in a dynamic system one can characterize the response performance using the following measures [2]: 1. Speed of the response, 2. Accuracy, 3. Relative stability and 4. Sensitivity. The speed of the response is a measure of how quickly the system reaches its final value. Accuracy is a measure of the proximity of the final, and the desired response. Relative stability is a measure of system stability. Sensitivity is indicated by the overall impact on the system response, as at least one of its control parameters is changed. The speed of response (1) and accuracy (2) are used in time domain measurements as discussed in this paper. The time domain measurement analyzes a dynamic response by partitioning the total response into its steady-state and transient components. The steady-state portion is that part of the response that remains as time approaches infinity whereas the transient response is the part that vanishes as time approaches infinity. Figure 1 identifies the measurement parameters used for both the steady-state component and the transient component analyses.

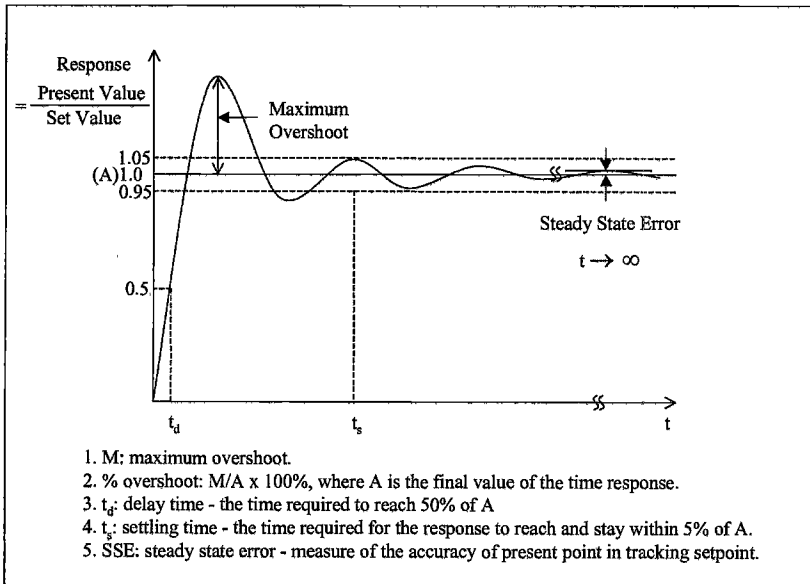


Figure 1. *Dynamic System Response*

Advances in Process Controls

There are four basic control modes [3]: 1. On-Off, 2. Proportional, 3. Rate (Derivative) and 4. Reset (Integral). The development trend in these control modes follows the increasing sophistication of microprocessors. The trend has been from On-Off control mode to Proportional Control and to Proportional plus Rate and Reset mode. These advances in process control have been incorporated into equipment introduced over the last twenty to thirty years. Table 1 provides a listing of process control advances for various parameters that have been introduced since the 1970's. The particular combinations of process controls are assigned a letter designation, which is used for comparison of dynamic responses later in the paper.

In On-Off Control, the output has only two states, completely on, or completely off. One state is used when the response is anywhere above the desired value (setpoint) and other state is used when the response is anywhere below the setpoint. Since the controlled variable must deviate from the setpoint to cause control action, the process response is usually cyclic.

Compared to the full-on or full-off functionality of the On-Off Control, the Proportional controller adjusts its output to be proportional to the "demand," which is the deviation of the controlled variable from the desired setpoint value. This action returns the controlled variable to the desired setpoint value without the rapid cycling and overshooting characteristics of On-Off Control. Proportional Control reduces the inherent cycling around a set point that is characteristic of On-Off Control, but introduces a different type of inherent problem, called offset.

Offset is a deviation from a set point caused by a change in load ("demand"). The load is determined by factors such as capacity, heat loss and operating point. If the load changes, the controller has no way of "knowing" that the control system itself has changed. It still adds the given deviation from the setpoint. In other words, the proportional controller returns the system to a new value that is the "offset" from the setpoint. To overcome this inherent offset, the control mode known as Reset or Integral Control has been developed.

The Integral Control can be described as "offset-based" control. It is slow to act, and based only on the steady state error signal. As long as there is a difference between the setpoint and the actual value of the controlled parameter, a small corrective control action occurs. This corrective action is obtained by integration to determine the area between the actual signal and setpoint. Generally, Proportional plus Reset (integral) controls are used in process applications.

Offset can be reduced by Integral Control, and accuracy of control can be improved by increasing the Proportional Control gain, effectively narrowing the band. However, a narrow band, even with its advantages of fast speed and reduced offset, also has disadvantages and dangers of instability especially during transitional periods of a cycle. It is common for a PI (Proportional plus Integral) controller to overshoot the setpoint on start-up. Therefore, Derivative Control was developed to compensate for the overshoot.

A "Derivative" or "Rate of Change" controller is one that has output which is proportional to the rate of change of the error signal. The rationale for rate action is

that a larger deviation from setpoint will start out at a faster rate. Thus the rate signal anticipates the magnitude of future errors.

A three-mode controller combining Proportional, Integral and Derivative (PID) actions is usually required to control difficult processes. A PID Control results in two advantages: 1. With the rate action being derived before the desired value is reached, set-point changes do not produce large system upsets because of derivative action. 2. In a properly tuned controller, the process response will approach the setpoint smoothly without overshoot. This is accomplished as the signal provided by the Derivative plus deviation becomes sufficient to create the proper reset value as the controlled parameter approaches its setpoint.

Table 1. *Advances in Parameter Control in Laboratory Accelerated Weathering Equipment.*

Year	Type	Air Heater	Damper	Blower	Humidity	Irradiance
70 – 80s	D	On/Off	On/Off	Fixed	On/Off	PI
80s	C	On/Off	On/Off	PID or Fixed	On/Off	PI
Early - Mid 80s	B	PI	PID	PID	PI	PI
Mid 90s	A	PI	APID*	PID	PI	PI

*Advanced Double PID Control With Time Dependent Algorithms.

Advanced Double PID Control With Time Dependent Algorithms (APID)¹.

APID is an innovative control system that utilizes double PID controls and time-dependent algorithms to enhance multivariable parameters of Type A instruments, particularly for temperature and humidity control [4]. In earlier weathering instruments, both the damper and the heater were controlled by a single loop system, in which the damper opens and the heater reduces its output as the temperature rises. Conversely, as temperature falls, the damper closes and the heater output is increased. As briefly mentioned in the previous section, instruments employing these types of control systems tend to have variables that oscillate. In weathering chambers, temperature oscillates as the damper and the heater work in conjunction with the temperature-monitoring sensor in a continuous attempt to stabilize the temperature of the system at the desired level. Similarly, humidity can be significantly affected by the operation of this type of damper and heater control action.

In the APID system, main control is comprised of two PIDs that are specifically programmed to minimize the oscillation and ultimately stabilize the

¹ This type of control system described is used in the SmartDamper[®] system supplied in some equipment made by Atlas Electric Devices Co.

variables to approach a constant value. In this control system, the first eight minutes of the control process is designed to identify the correct position of the damper to best accommodate the chosen parameters (set points). Normally, the impact of incoming moist, laboratory air can be a significant factor in this determination. But because the quality of ambient air is so variable from laboratory to laboratory, at the first stage of control, it is necessary to precondition or standardize the incoming air so that the controlling program is presented with a known starting point. During the next two minutes, another process takes place to find the average position of the oscillating damper determined by the previous PID loop. Once its average angular position is found, the damper is fixed at a slightly greater aperture for the remainder of the test cycle. From that point, the second PID control that operates the air heater assumes management of the process. The net effect of this time specific control process is to have the damper optimally fixed to avoid unnecessary losses by eliminating excessive and compounding swings in by both damper and heater controls. A simplified process control flow diagram is shown in Figure 2.

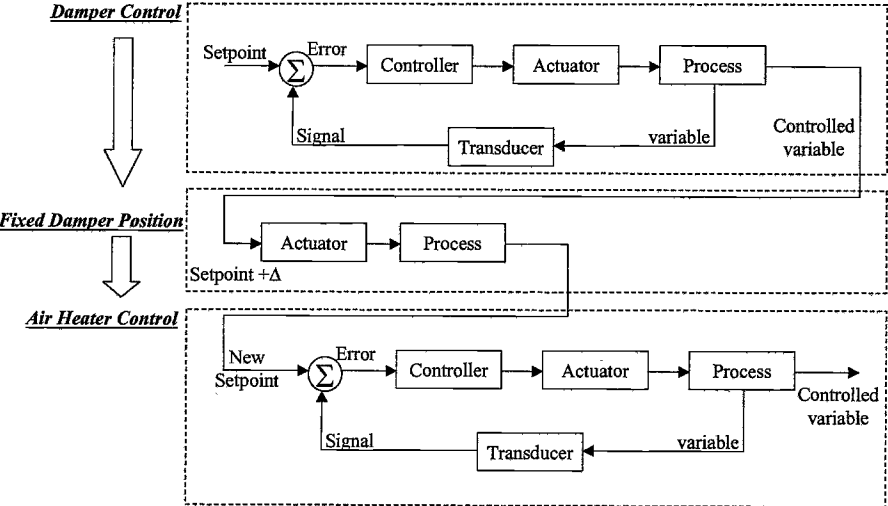


Figure 2. APID Process Control Flow Diagram

Experimental - Data Acquisition

An experiment to compare control features of different vintage instruments was conducted. Four controlled variables, black panel temperature, chamber temperature, humidity and irradiance were recorded from instruments representing three generations. The data were collected as the instruments ran the Society of Automotive Engineers (SAE) J1885^[1] standard test method. Types A, C and D instruments were used. Type C instruments are equipped with on/off type control for three moist air related variables; black panel temperature, chamber temperature and relative humidity. Irradiance is controlled by a PI control system. In Type C and D instruments, relative humidity is determined by psychrometric calculation, using the dry bulb temperature and wet bulb depression (difference between wet and dry bulb temperature) readings. By contrast, relative humidity is measured directly in the Type A instruments.

The C instruments control system is distinguished from that of the D, by the PI blower control. The PI blower control replaced the fixed speed blower control, in order to minimize oscillations of the controlled temperatures. Subsequent to its introduction, the PI blower was retrofitted to most of the Type D instruments installed in the field. All Type A instruments are equipped exclusively with PI, PID and APID for all controlled variables. Type B instruments are equipped with PI and PID controls, but not the APID control which was developed after its introduction.

The set points for the controlled variables as stipulated by SAE J1885, are 0.55W/m^2 irradiance at 340nm, 89°C Black Panel Temperature (BPT), 62°C Chamber Dry Bulb Temperature (DB) and 50% relative humidity (RH). The test was started with equalized moist air condition in the chambers, i.e. BPT and DB were showing no offsets from each other, indicating that the chambers were adequately equalized. To show the ramping effect (dynamic system response), the test parameters were recorded before the instruments were turned on. After ramping, during the transient response of the controlled variables, the tests were continued for approximately 45 minutes to observe the characteristics of steady state response. The data presented in this study was acquired by the installed data acquisition system for each respective instrument.

Data Presentation and Discussion

There are four components of interest that characterize both transient and steady-state response portions of a cycle. Data shown in subsequent charts and tables are measured at the control points and are representative of the dynamic responses observed in each instrument. In our evaluations, these were recorded from the dynamic response curve during the SAE J1885 initial light cycle. There is maximum overshoot (M), % overshoot, settling time (t_s), and steady-state error (SSE). The data are shown in Table 2. In general, the Type D control as illustrated in Figure 3 was improved upon in the Type C model shown in Figure 4. Especially, M, % overshoot and SSE were considerably decreased. Settling time remained the same.

Table 2. *Dynamic Response of Three Different Control Systems*

	Parameter	Type D ²	Type C ²	Type A ²
BPT	M	0.9	0.3	-0.1
	% Overshoot	1.0	0.3	-0.3
	t _s (min)	6	7	6.1
	SSE (°C or %)	1.09	0.39	0.18
Chamber Temp	M	9.7	2.3	8.4
	% Overshoot	15.3	3.8	4.2
	t _s (min)	4.4	4.6	5.6
	SSE (°C or %)	3.25	0.96	0.18
Relative Humidity	M	10.2	2.2	12
	% Overshoot	20.7	8.3	26.3
	t _s (min)	3.8	4.2	2.8
	SSE (%)	4.11	1.85	0.25

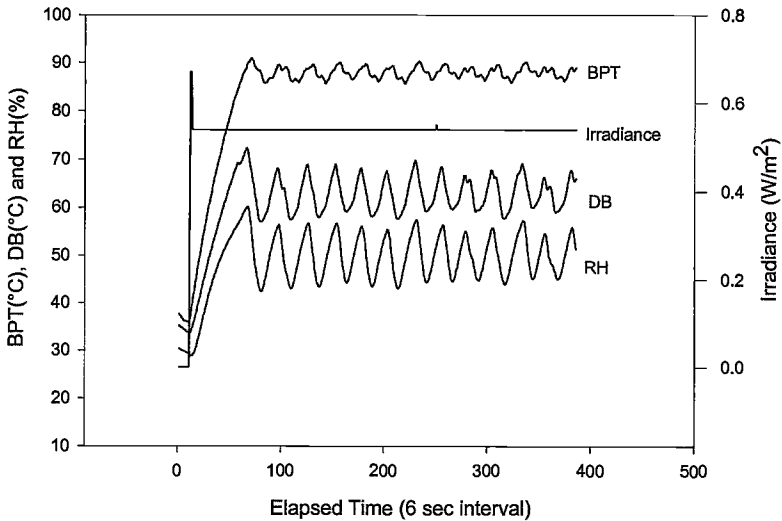


Figure 3. *Type D Process Response Curve*

² Type D, C and A measurements were made in Ci65, Ci65A and Ci4000 instruments manufactured by Atlas Electric Devices Co. respectively.

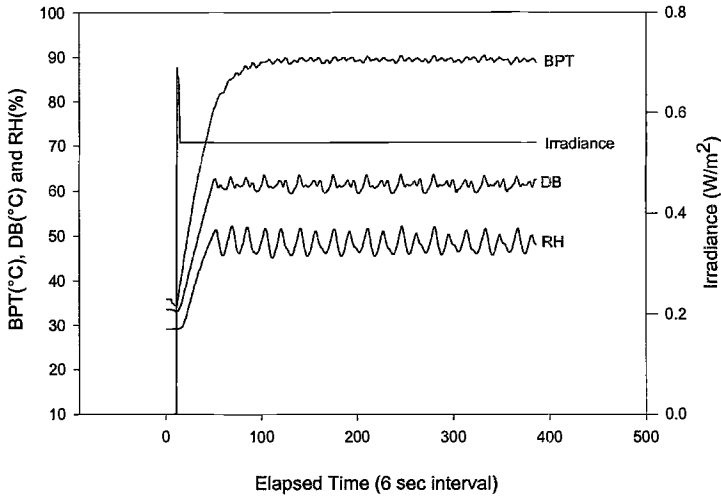


Figure 4. Type C Process Response Curve

By examining the oscillating response curves, one can deduce that the Type C2 and D3 instruments were controlled mainly by an on/off control system. However, the C2 response curve showed more than ordinary function oscillations, indicating that there were modifications to its basic on/off control system. This is more obvious when compared to the D3 system, it is also obvious that these three moist air-related parameters were indeed synergistically affecting each other. However, more importantly, the reduction in BPT fluctuation shows that the varying rate of convective heat loss due to changeable air mass velocity, can be very effective in controlling BPT. In this case, the difference in convective heat loss was due to the differences in mass velocity created by the variable speed blower motor. This relationship is described below [5, 6]. This mass flow change also affects the chamber dry bulb temperature since that measurement device also derives heat (temperature), using the same convective heat transfer.

$$q = hA\Delta T, \quad h \propto \text{Re}, \quad \text{where } \text{Re} = \frac{Gd}{\mu} = \frac{\dot{m}d}{\mu A} \quad (1)$$

- where
- q = heat loss or gain
 - h = convection heat transfer coefficient
 - Re = Reynold's number
 - A = area
 - T = temperature
 - G = mass velocity
 - \dot{m} = mass flow rate
 - d = distance from edge of plate
 - μ = dynamic viscosity

Improvement in humidity fluctuation is a secondary effect, resulting from a more stable moist air condition achieved in the chamber. Nevertheless, it is postulated that the more effective heat transfer that favorably impacts the wet bulb temperature sensor also causes this improvement. However, it is reasonable to assume that the net effect of reducing the fluctuation in humidity was partially impaired by an additional heat transfer resulting from a mass transfer of water evaporation at the wet bulb sensor. When a wet bulb temperature reading is made, there is no net energy transfer at the steady state condition. Consequently, the heat required to evaporate the water surrounding the wet wick must be drawn from the chamber air. Hence, the energy balance at that instance would be as described below. Here, it can be seen that both the heat transfer coefficient and the mass transfer coefficient are affected by mass velocity.

$$hA(T_{\infty} - T_w) = \dot{m}_w h_{fg}$$

$$\dot{m}_w \approx h_D A \Delta C \quad (2)$$

where

$$h = f(\text{Re}) \text{ and } h_D = f(\text{Re})$$

and

- T_{∞} = surrounding (ambient) air temperature
- T_w = saturation temperature
- \dot{m}_w = mass flow rate due to water evaporation
- h_{fg} = evaporation enthalpy
- h_D = mass transfer coefficient
- C = concentration through which diffusion occurs

The dynamic response curve for the A2 instrument (Figure 5) shows tremendous improvement and accuracy in all control parameters. All four measures of dynamic response (M , % Overshoot, t_s and SSE) show good stability. The steady-state error for each of the three measured parameters (BPT, DB and RH) is much less than one measurement unit, signifying the excellent stability of the system. Figure 5 clearly demonstrates the improved characteristics of PID and APID controls. When compared to the C2 and D3 instruments where no PID control is employed, the Type A2 response has no noticeable oscillation during steady state operation (Figure 6). Two minor flaws of the PID control were observed in the A2 response. The first is the one extra minute delay of t_s ; the second is the initial overshoot of the relative humidity control. However, relative humidity reached its 5% deviation of set point within three minutes. This is also an improvement over Type C2's four-minute settling time. The most remarkable improvement was the relative humidity control. The A2's response shows less than ¼% fluctuation in relative humidity control throughout its steady state operation (Figure 7).

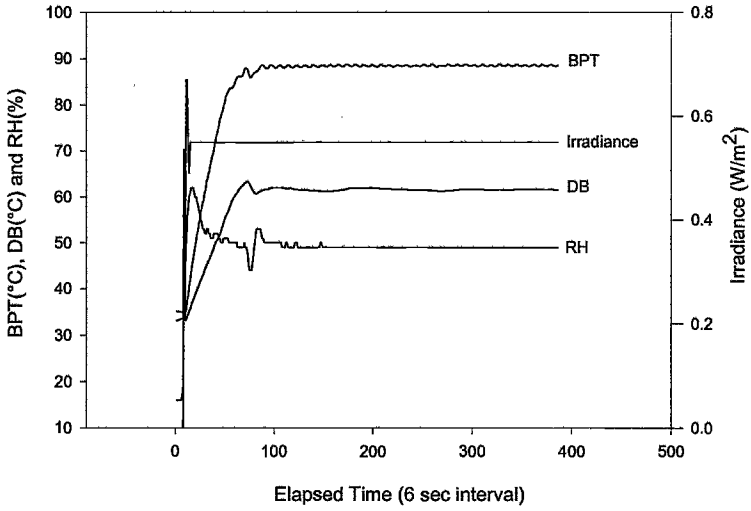


Figure 5. Type A Process Response Curve

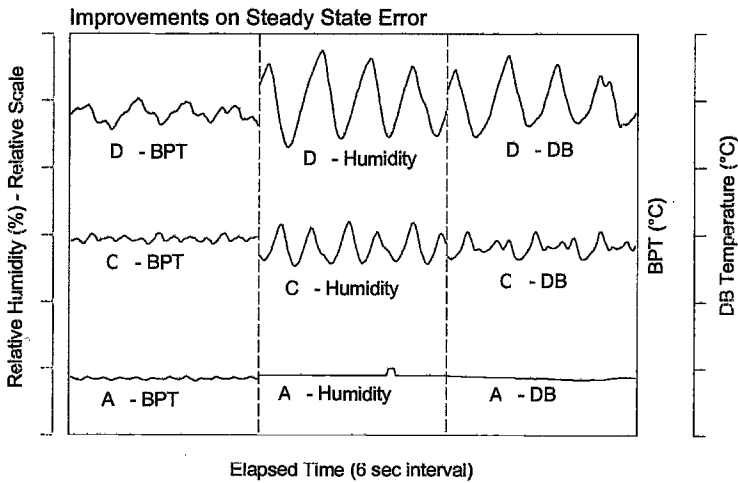


Figure 6. Improvements in Process Control

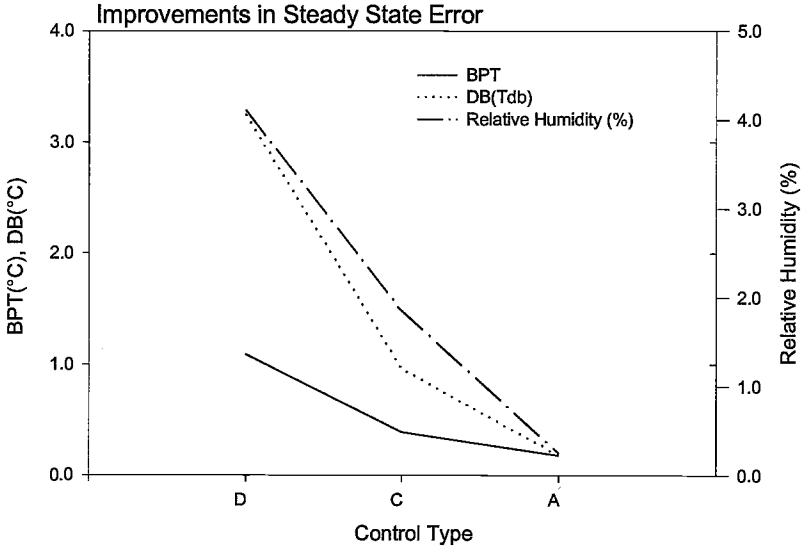


Figure 7. *Improvements in Steady State Error*

Summary

The innovative application of state-of-the-art process control technology has resulted in the unprecedented ability to effectively eliminate in-test fluctuations of the critical weathering parameters. It is generally accepted that fluctuations in the control of light, humidity and temperature are the primary causes of the variability that have historically plagued weathering tests. It therefore stands to reason that their elimination represents a major step in addressing the issues of repeatability and reproducibility. Limited, preliminary studies employing the latest test instruments described in this paper have shown promising results. Now that these instruments are being used more widely, we believe it is in the interest of the weatherability testing community to conduct round-robin tests to establish a benchmark of current, best test capability.

References

[1] SAE J1960 – “Accelerated Exposure of Automotive Exterior Materials Using a Controlled Irradiance Water Cooled Xenon Arc Apparatus”, SAE, 400 Commonwealth Drive, Warrendale, PA 15096.

[2] Silva, C. W. and Aronson, M. H., “Process Control,” Professional Course Material, Measurement and Data Corporation, Pittsburgh, PA, 1990.

- [3] Lee, G. K. H., "Dynamic Response," The Electrical Engineering Handbook, CRC Press, Boca Raton, FL, 1985, pp. 2106-2113.
- [4] Tikhtman, J., et al., U.S. Patent 5,503,032, Apr. 2, 1996.
- [5] Hollman, J. P., "Heat Transfer," 7th Ed. McGraw-Hill, New York, NY, 1990, pp. 217-221.
- [6] McQuiston, F. C. and Parker, J. D., "Heating Ventilating and Air Conditioning – Analysis and Design," John Wiley & Sons, New York, NY, 1988, pp.52-54.

Predicting the Durability of Building Stone Using Accelerated Weathering

Reference: Bortz, S. A., and Wonneberger, B., “Weathering & Durability Testing of Dimension Stone,” *Durability 2000: Accelerated and Outdoor Weathering Testing, ASTM STP 1385*, J. D. Evans and W. D. Ketola, Eds., American Society for Testing and Materials, West Conshohocken, PA, 2000.

Abstract: The importance of weathering of building stone is becoming widely recognized, and there is a need in modern thin stone design (less than 2 inches) to be able to estimate their durability. Stone deterioration processes include a number of agents, including salts, air pollution, freeze-thaw and biodeterioration. While the weathering properties of dimension stone can be judged by the examination of buildings in which it has been used, this method cannot estimate the durability of a different stone, a stone from a different part of the same quarry, a stone from a new quarry, or if the stone is to be used under different environmental conditions. Data is presented in this paper to show a correlation can be determined between natural and accelerated weathering of building stones. Real timeline information has been obtained by comparing accelerated weathering test data with data that is obtained from naturally weathered stone specimens. An estimate can be made to assess the life expectancy of a building stone subjected to natural weathering by using the accelerated weathering test procedure described in this paper. Based on our studies, 12 to 16 freeze-thaw cycles of the test procedure can be considered approximately equal to one year of natural weathering in the Chicago area.

Keywords: laboratory testing, field testing, building stone, freeze-thaw, comparison studies, natural weathering, and accelerated weathering

Introduction

Natural building stones are subjected to a variety of weathering conditions, both natural and non-natural. Under these conditions, durability depends upon the stone’s physical and chemical nature. Weathering of natural building stone consists of the reaction to environmental conditions at the exposed surfaces that are subjected to water and atmosphere. Reactions caused by weathering are controlled by water and the natural chemicals and gases dissolved in the water. The water may penetrate the stone under various conditions.^[1] Temperature, moisture, organic acids, and dissolved carbon

¹Senior Consultant, Wiss, Janney, Elstner Associates, Inc., 330 Pfingsten Road., Northbrook, IL 60062-2095

²Senior Architect, Wiss, Janney, Elstner Associates, Inc., 330 Pfingsten Road., Northbrook, IL 60062-2095

dioxide influence weathering rates. The average rainfall is a major controlling factor of the weathering rate.^[2] This factor, and our contemporary industrial society, can accelerate the natural weathering processes due to elevated pollutant concentrations on the stone surface. Acid pollutants from air and rainfall are serious hazards to carbonate rocks such as limestone and marble.^[3] These acid pollutants can also affect some silicate rocks and granite; but often to a much lesser degree.

Another factor that can affect the natural weathering of stone is temperature cycling. Not necessarily does cyclic freezing need to occur to cause the natural weathering of building stone. Warm temperature cycling can cause differential volume changes of mineral grains that can lead to stone deterioration. Elevated temperatures can accelerate the dissolving of the carbonate minerals, while frost can cause damage to both carbonate and silicate stones.^[4]

Weathering

The terms “weathering” and “decay” are frequently used in somewhat different senses. Weathering may be used to describe those changes developed by the action of the weather that add to the aesthetics of a building and give character to its materials. “Decay” on the other hand, usually refers to undesirable changes caused by the weather that can possibly lead to dangerous conditions. Although “weathering” and “decay” are accurate descriptions for the behavior of building stone that is exposed to exterior environmental conditions, it is preferable that the term “weathering” include all those changes, desirable and undesirable.

Durability

Durability is an important issue when specifying stone used on the exterior of a building. When existing design parameters do not cover changes caused by weathering, the stone can fail and possibly fall from the building. Therefore, it is important the durability of building stone is considered early in the planning stages. In the past, evaluation of the durability of a particular stone type was based only through experience from long term use. Although experience is still a valuable tool, it is now possible to use a laboratory accelerated weathering test to determine and specify the durability of a particular building stone.

Weathering varies with climate and with the characteristics of the stone used and the degree and angle of exposure to the weather. From these differences we can extract useful information about the rates of natural alteration of the kinds of rock from which the building stone was cut. Fast or slow, chemical and mechanical alterations occur everywhere at the earth’s surface. Mechanical weathering is distinct from chemical weathering, although the two processes work in close coordination. Disintegration, which is the mechanical breakup of rocks, exposes additional surfaces to air and water. Therefore, disintegration can accelerate decomposition.

Chemically active rainwater and water vapor are the means for accelerated decomposition of building stone. Rainwater brings to the ground carbon dioxide that is present in the air. This combination of the water and carbon dioxide forms carbonic acid.

Sulfurous acid is also developed as a residual compound in the atmosphere from the burning of high sulfur fossil fuels. Nitric acid also forms when nitric oxide from burning gasoline mixes with water. These chemicals, in the form of air pollution and acid rain, will dissolve the surface of building stone. However, this is often a slow process. Table 1 provides measurements of the amount of surface loss that occurred for marble and limestone after one-year of exterior exposure.

Table 1 – *Stone Surface Recession and Roughness after One Year of Natural Weathering Exposure* ^[5]

Stone	Specimen	Recession – Avg. μm (in.)	
Marble	Sample 1	10.5	(0.00041)
	Sample 2	13.7	(0.00054)
Limestone	Sample 1	13.2	(0.00052)
	Sample 2	16.6	(0.00065)

Based on the information provided in Table 1, the amount of surface erosion that can be expected over a 100-year period can be estimated as shown in Table 2. Because the flexural strength of a panel is proportional to the square of the thickness of the stone, and a 1.5 mm (1/16 in.) reduction in thickness is indicated for limestone after 100 years of exterior exposure, the potential strength loss due to reduction of cross-section alone can be approximately 10 percent for 3 cm (1 3/16 inch) thick limestone panels.^[6] These tables provide good information regarding surface loss due to weathering of particular stone specimens, however, our experience has shown that the rates of surface erosion can vary greatly in stones having similar mineral compositions; sometimes much greater than shown here.

Table 2 - *Stone Surface Recession Over a 100-Year Period Based on Data from Table 1*

time (yr.)	Marble		Limestone	
	μm	Inches	μm	Inches
10	121	0.005	149	0.006
20	242	0.010	298	0.012
50	605	0.024	745	0.029
100	1,210	0.048	1,490	0.059

Mechanical weathering is the result of changes in internal dimensions. The dimensional changes are due to the heating and cooling of the minerals that comprise the stone. The various minerals often have quite different coefficients of thermal expansion within the body of a single stone type.

Another mechanical weathering mechanism is exfoliation. This consists of the separation of successive layers at the bedding planes or rift of building stone during weathering. A close look at exfoliated stone will often reveal evidence of chemical

weathering, as well as granular disintegration and the development of expansion cracks.

Weathering that occurs by mechanical means proceeds at the same time and often in the same places as the more widespread chemical weathering. Although the two groups of processes act together, the action of one promotes the action of the other. A 10 percent increase in volume occurs when water freezes. If this occurs in a confined space, very high tensile stresses will result in the stone. The constant freezing and thawing of entrapped water will cause the eventual disintegration of the stone. The freezing water will pry the stone material apart. Depending on the geographical location as well as solar orientation of the stone panel, freezing and thawing can occur several times in a single day.

In summary, it is the kind of stone and climate that influences mechanical weathering. We have observed exfoliation and strength changes in our accelerated weathering studies. These observations are discussed further in the following sections of this paper.

Role of Chemical Weathering

Rainfall that enters the stone's pores is a controlling factor of the weathering rate. Certain stone minerals can be dissolved by percolating water solutions or by the chemical reaction. The amount of CO₂ in the water determines the aggressiveness of the water that dissolves the stone. Weathering reactions also depend on temperature. Higher temperatures will increase the rate of chemical reactions. Hence, such reactions are magnified more in the tropical areas than in colder temperature zones.

Rates of silicate weathering are more difficult to evaluate because many factors are involved that may influence the process. Stone exposed to air pollution may undergo undesirable discoloring and loss of polish and hardness. We have observed this in our practice. There are estimates that a 1-1/2 to 2 times increase of the weathering rate occurs by solubilization and hydrolysis with each temperature increase of 10°C (18°F). In addition, it is estimated that the weathering rate can increase nearly 20 to 40 times in tropical moist areas.^[7]

There have been observations that 10 mm (13/32 in.) of a limestone surface has been lost over a 300-year period of natural weathering, with about the same loss of a marble surface over a 150-year period.^[8] Sandstone with feldspar and mica as impurities will lose about 2.5 mm (5/64 in.) over 200 years, while almost pure quartz sandstone will remain sharp and clear over the same period. However, experience has shown that the rates of surface erosion can vary greatly in stones having similar mineral compositions. Figure 1 is sandstone that has been on a Chicago building for 100 years and shows much greater erosion than the 1.4 mm loss for the 100-year old sandstone previously noted.



Figure 1 – Sandstone on 100-year old building

Temperature Effects on Weathering

As previously discussed, a mechanical form of weathering is from differential thermal expansion of the minerals that constitute the various stones. Volumetric or linear expansion of the different mineral materials that comprise the same stone mass can cause disintegration of the stone when heated such as through solar heating. Temperatures as high as 82°C to 88°C (180°F to 190°F) have been measured on dark stone surfaces on building facades. Stone minerals expand with increasing temperature; however, they expand to different degrees. Quartz expands about four times more than feldspars and twice as much as hornblende. Quartz is considered the most critical mineral under conditions of heating of granites and quartzitic sandstones.^[9] When quartz expands during heating, it exerts pressure against the surrounding crystals. These stresses can cause microcracking within and between adjacent crystals in the granite, lowering the strength and allowing other weathering phenomena, both chemical and freezing, to accelerate the disintegration processes.

The thermal expansion data shown in Figure 2 indicates that individual stone crystals that comprise a single stone will have different expansion properties. The forces exerted against one another within a single section of stone can eventually cause the mineral structure to crumble. Stone that is low in quartz and carbonate minerals will expand very little with increases in temperature.

Differing expansion characteristics can also exist in individual crystals of a stone. For instance, even though the expansion of calcite is shown to be minimal in Figure 2, calcite exhibits linear thermal expansion parallel to the long axis of about 0.2 percent, but contracts about 0.1 percent perpendicular to the long axis. The differing expansive rates of calcite in crystallographically-oriented marble disrupt the structure of the stone. Permanent increased volume results because the crystalline structure of the stone crumbles as it disintegrates. Figure 3 shows microscopic images at both sides of a single marble panel where only one face of the panel has been exposed to cyclic heating and cooling. A splitting of the crystalline structure of the marble is apparent in the image taken at the heated section of the stone panel. The slipping of the split crystals do not

allow the stone to return to its original dimensions as it cools and dries because the split crystals bind against one another. This phenomenon is known as hysteresis. The distortion often occurs more greatly on one side of a thin marble panel than on the other side. The increased dimension of the one side on a single thin stone panel is permanent and leads to a bowing of the panel.

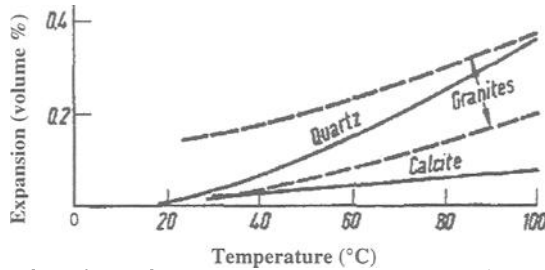


Figure 2 – Thermal expansion of calcite, quartz and granite.^[10]

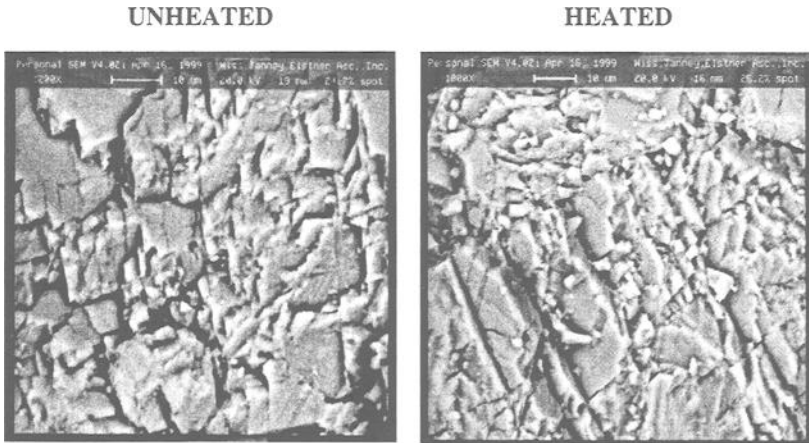


Figure 3 – Scanning electron microscope images of hysteresis tests of Vermont Danby Marble.

Effect of Freezing on Stone

As discussed previously, a mechanical weathering process results from freezing water. Damage to stone results when temperatures are below freezing and any absorbed water forms ice crystals. The expansive crystallization pressure is very important as it produces tensile forces on the stone structure.

The structure of stone contains capillaries that can transfer water. These capillaries may also contain clays, some of which may expand when wet. The water-filled capillaries exert forces against the capillary walls either by expanding water from

ice crystallization during freezing, or by the swelling of expansive clay minerals when wet or by osmotic forces due to differential concentrations of dissolved material. The outward forces of the expansion produce tensile stresses in the stone structure. Therefore, the tensile strength of the stone is of greater importance than the compressive strength with regard to freeze-thaw durability. For a brittle material such as stone, the compressive strength is generally 10 to 15 times greater than the tensile strength.

Water itself expands just before it reaches a solid state. The ice volume is at a maximum and the density at a minimum near 0°C (32°F) (from 1,000 kg/m³ (62.4 lb/ft³) in an unfrozen state to 916 kg/m³ (57.2 lb/ft³) in a frozen state).

Accelerated Weathering Test

A good laboratory test for the durability of building stone must consider environmental factors, such as temperature, air pollution and rain. In addition, the designer must consider not only wind loads, but also the fact that the stone can vary from quarry to quarry, from one area within a single quarry to another, and possibly within a single quarry block. Therefore, it is important to test the specific supply of stone for a large building project. Stone used successfully on a similar project in the past may not have the same physical or mechanical properties for the current project.

Based on the previously discussed environmental effects on the properties of stone, a procedure was developed at the Illinois Institute of Technology (IIT) Research Institute, and later refined at Wiss, Janney, Elstner Associates, Inc. (WJE), that considers the environmental factors. The test procedure consists of placing a stone specimen with minimum dimensions of 30 mm (1 1/4 in.) thick, 100 mm (4 in.) wide and 380 mm (15 in.) long in a 4 pH sulfurous acid solution to simulate acid rain. The specimens are immersed 6 mm (1/4 in.) to 10 mm (3/8 in.) deep in the solution in a stainless steel pan. Each specimen is also set on 6 mm (1/4 in.) diameter rollers to assure the 100 mm (4 in.) wide face is subjected to the action of the bath solution. The specimens are then subjected to 100 cycles between -23°C to +77°C (-10°F to +170°F) to simulate heating and cooling as well as freezing and thawing.

Early experiments performed at IIT were limited to 30 cycles because of the laborious manual operation that was required, even though it was apparent that this was not a long enough duration to produce adequate information regarding the long-term durability of the stones that were tested.^[11] The initial test procedure was a 9-step process using various chemicals and temperature cycling that required a 24-hour duration for each cycle. Later experimentation showed that freezing and thawing (heating and cooling) were the primary sources of change; therefore, the procedure was simplified to an automated system and the number of freeze-thaw cycles was increased to 100 at four cycles per day.

Before the test procedure is started, the test specimens are evaluated for dynamic Young's Modulus of Elasticity (sonic modulus) using ASTM Procedure C 215, 'Test Method for Fundamental Transverse, Longitudinal and Torsional Frequencies of

Concrete Specimens.” The sonic modulus test is repeated after every 25 freeze-thaw cycles. This testing is a non-destructive means to evaluate changes in physical and mechanical properties of the stone specimens during the accelerated weathering test. The sonic modulus test provides information regarding the stiffness of the stone specimens. As the internal structure of the stone specimens deteriorate during the accelerated weathering test, the stiffness will become reduced and the flexibility increased. A curve can be charted over the duration of the testing by comparing the changes in sonic modulus. This information can then be further evaluated as an indirect means of determining the loss of strength during the accelerated weathering test by comparing the data to flexural strength test results that are obtained before and after the accelerated weathering test. Figure 4 shows the relationship of sonic modulus to actual flexural strength developed from marble specimens. There is a good correlation at each measured cycle between actual strength of tested specimens and sonic modulus.

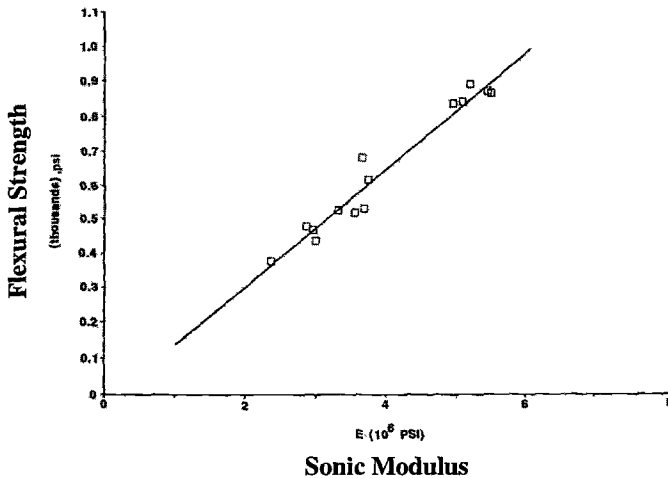


Figure 4 – Modulus of elasticity (E) vs. flexural strength.

Natural Weathering Studies

The accelerated weathering test allows comparisons to be made between stones. However, there has been criticism that this test procedure has no relationship to natural weathering. Arguments have also been made that the test has no meaning for building projects that are in warmer climates. To counteract these comments, we have compared sonic modulus and strength test results from stone subjected to natural weathering to similar test results determined from stone subjected to the accelerated weathering test procedure. Previously, it was discussed how just heating and cooling, acid rain, and other pollutants can affect the properties of building stone. For warmer climates, the test procedure can be modified to cycle between +5°C and +77°C (+40°F and +170°F).

Several years ago, twelve domestic marbles were placed on the roof of a building located immediately south of the main business district in Chicago. The marbles were

monitored quarterly using sonic modulus testing. Figure 5 shows the results of this work, including the results for Vermont Danby marble. In addition, we are currently exposing granite, marble and limestone specimens to natural weathering on the roof of a WJE building in Northbrook, Illinois. As shown in Figure 6, the specimens are strapped to a plywood rack that is tilted 45° toward the south. Figures 7 through 9 show the sonic modulus curves that have so far been determined after 4 years of exposure. These tests will be extended over a 10-year period.

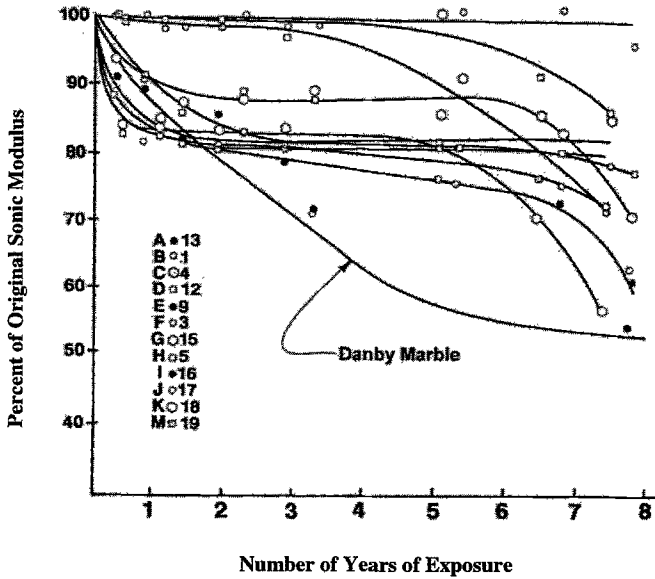


Figure 5 – Natural weathering test results for 12 different domestic marbles.

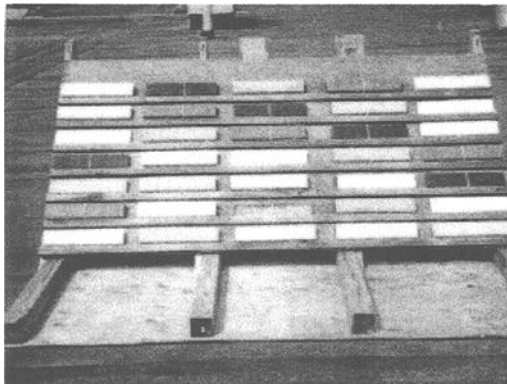


Figure 6 - Stone test specimens exposed to natural weathering on roof.

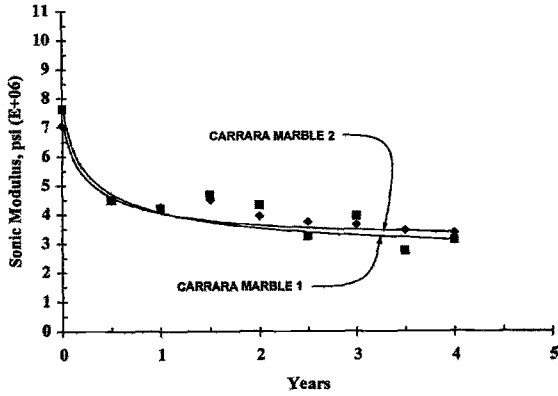


Figure 7 - Natural weathering studies with Marble.

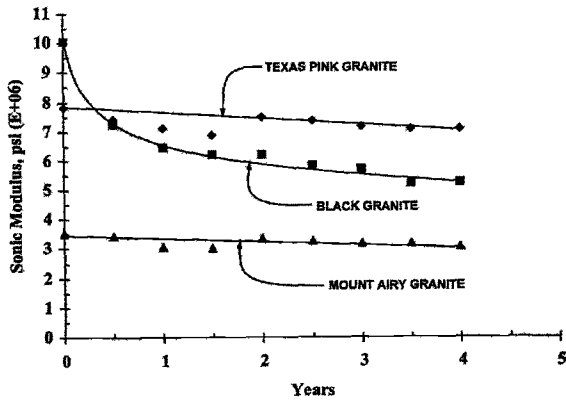


Figure 8 - Natural weathering studies with Granites.

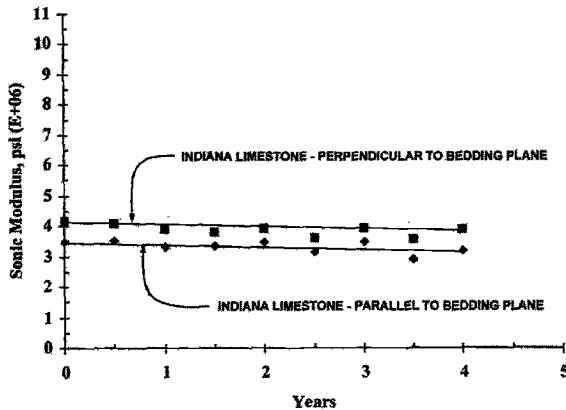


Figure 9 - Natural weathering studies with Limestones.

Laboratory Data and Correlation with Natural Weathering

Figure 10 shows the change in sonic modulus that occurred when granite was subjected to the 4 pH sulfurous acid bath solution previously discussed. The parallel and perpendicular indications shown in the chart are noted for specimens that were load tested in flexure in the parallel and perpendicular to rift orientations. Acid exposure apparently has little or no effect on the granite. However, as previously shown in Figure 8, the hot and cold temperature environment in northern Illinois does appear to cause differential expansion of the individual minerals that comprise the current rooftop granite specimens and lead to breaking of the bond between the mineral crystals.

Figure 11 is a similar sonic modulus curve for marble under actual weathering conditions. The change in property is due to differential expansion and contraction of the individual calcite crystals, and some dissolving of the calcite. Although some calcite dissolves in the acid solution, this essentially neutralizes the acid. Figure 12 consists of sonic modulus curves for different limestones. The Massangi and Valders dolomitic limestones show no basic effect while the Indiana Limestone has a slight downturn at the end of 100 cycles.

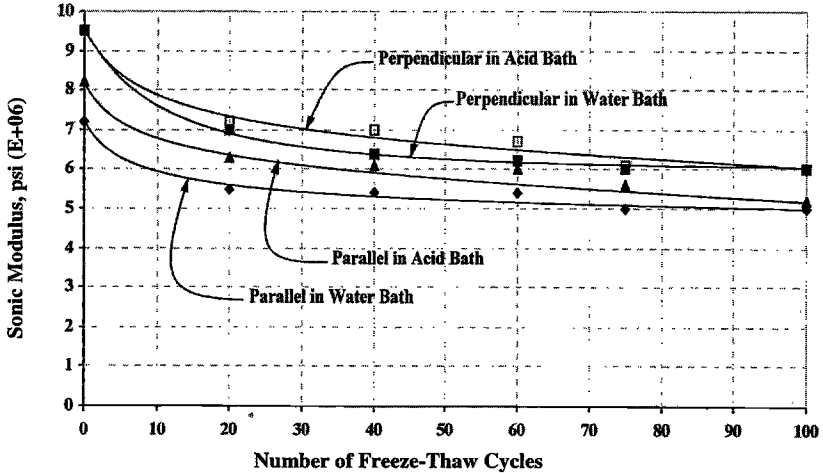


Figure 10 – Accelerated weathering test results for Rockville Beige Granite

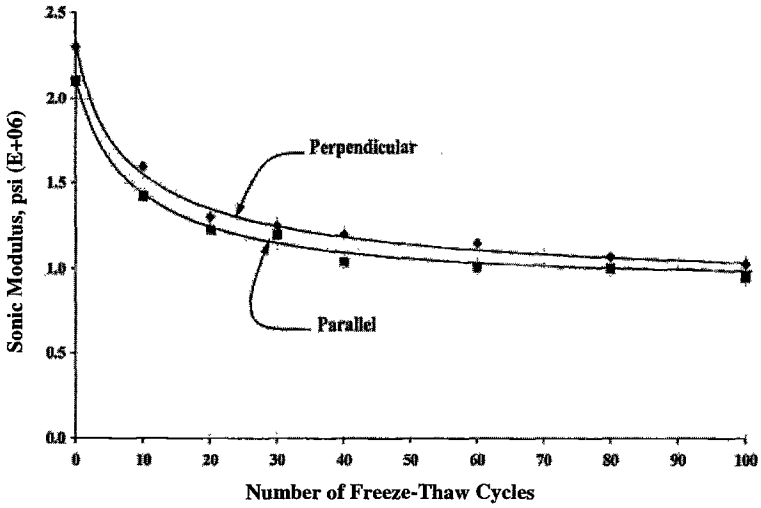


Figure 11 – Accelerated weathering test results for Danby Marble

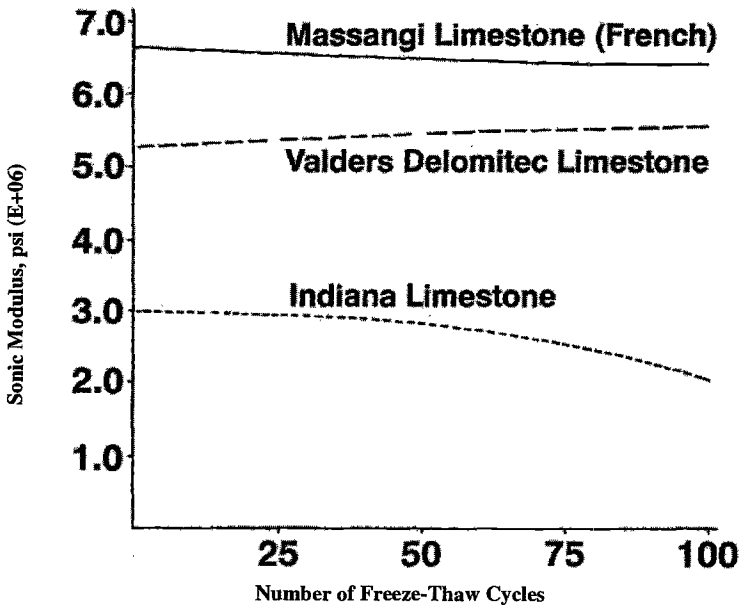


Figure 12 – Accelerated weathering test results for three different types of limestone.

Recently, we had an opportunity to perform tests on a second set of Danby marble. The previously shown Fig. 11 presents the change in sonic modulus determined during these tests. Figure 13 presents the natural weathering and accelerated test curves shown in Figs. 5 and 11. These curves show 100 freeze-thaw cycles of durability testing can be considered equivalent to 6 or 8 years of natural weathering. Therefore, 12 to 16 freeze-thaw cycles would be equivalent to one year of natural weathering in a northern temperature environment. Our data from this work and similar additional work using naturally weathered stone from buildings was compared with data obtained from durability testing of attic stock stone, (stone kept in reserve, but not exposed to weathering). This work indicated that real-time effects could be estimated from laboratory tests.

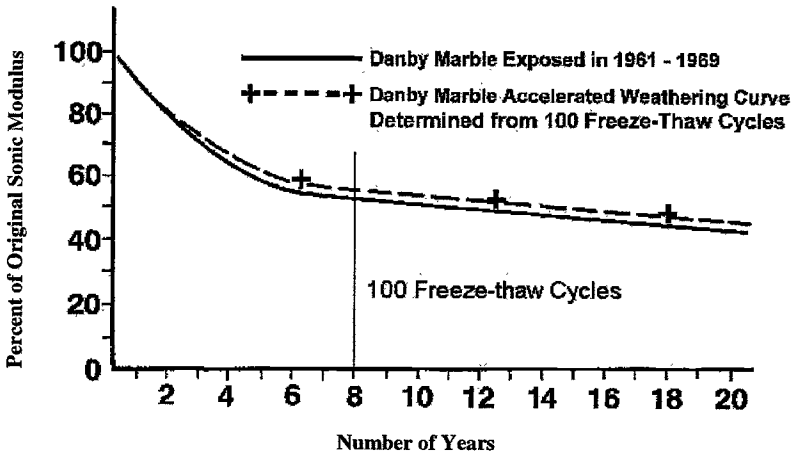


Figure 13 – Superimposed natural and accelerated weathering results from data previously shown in Figures 5 and 11 for Danby Marble.

Evaluation of a 10-year-old marble-clad high rise office building in Rochester, New York, permitted evaluation of actual strength degradation from natural weathering. Many panels from the building facade, and panels that had not been exposed to natural weathering, were provided for durability tests. This provided a large statistical population for data analysis. A weathering chart was plotted using the modulus of elasticity and flexural strength data, Fig. 14. In this figure, the flexural strength chart has been superimposed over the elastic modulus chart.

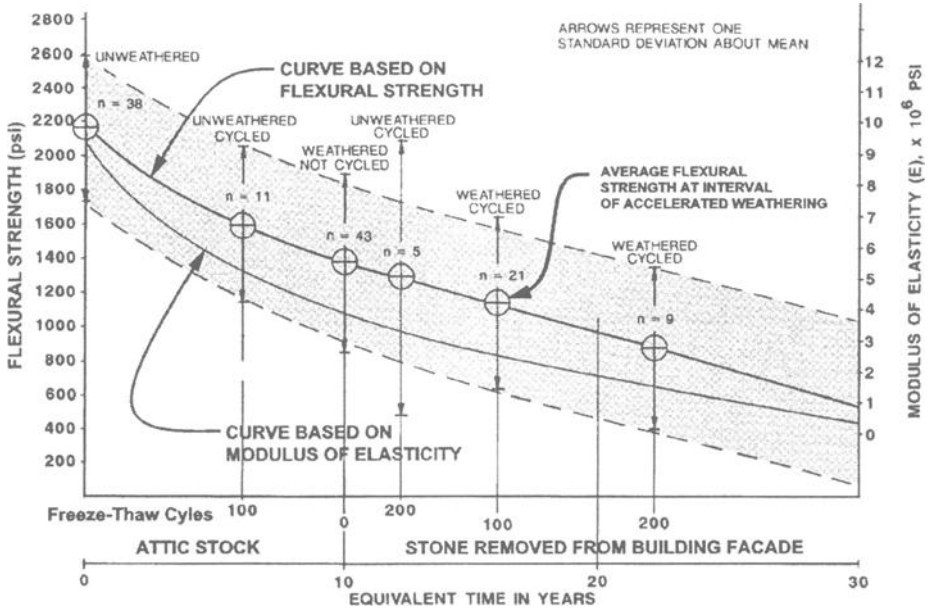


Figure 14 – Relation of number of cycles to years, Building 1.
Plot based on flexure data in equal number of samples.

Two other marble-clad buildings were also studied. Composite curves for weathered and unweathered stone were developed, Figs. 15 and 16. For the marble in Fig. 15, 12 to 13 cycles of accelerated weathering were found equivalent to one year of natural weathering on a building in Rochester, New York. For the marble in Fig. 16, 16 cycles of accelerated weathering were seen to be equivalent to one year of natural weathering on a building facade in Chicago. The plot in Fig. 16 is based on actual flexural strength of the stone, not sonic modulus. Note the curves for sonic moduli are similar to the curves for flexural strength.

The process of obtaining the curves shown is empirical. To provide guidance regarding the meaning of accelerated weathering, the data from weathered and unweathered stone had to be related in some manner. Data was plotted for elastic modulus vs. accelerated aging cycles for both the unweathered and weathered stone. They were analyzed such that the original sonic modulus and strength for the weathered stone are close to being a tangent to the curve for sonic modulus and strength of unexposed stone subjected to the durability test. This occurred at approximately 160 cycles. Using these relationships, the conclusion was drawn that 160 cycles of accelerated weathering appeared to be equivalent to 10 years of natural weathering on the building. Thus, 16 cycles were determined to be equivalent to one year of service life in upper state New York. While this cannot be considered a rigorous proof of the time relation of natural aging to accelerated aging, the empirical data from the laboratory and

field observations indicate this is a reasonable approximation of what the designer can expect regarding changes in strength properties from natural weathering.

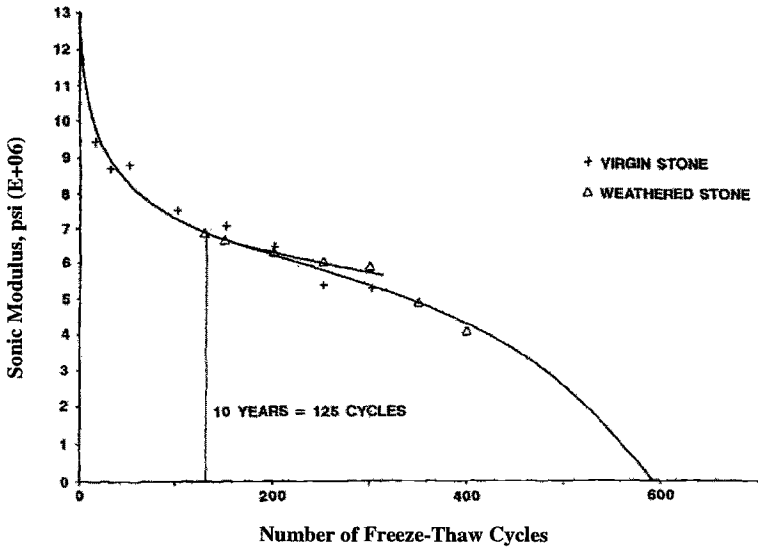


Figure 15 - Number of accelerated weathering test cycles vs. sonic modulus determined from Georgia Golden Vein marble specimens.

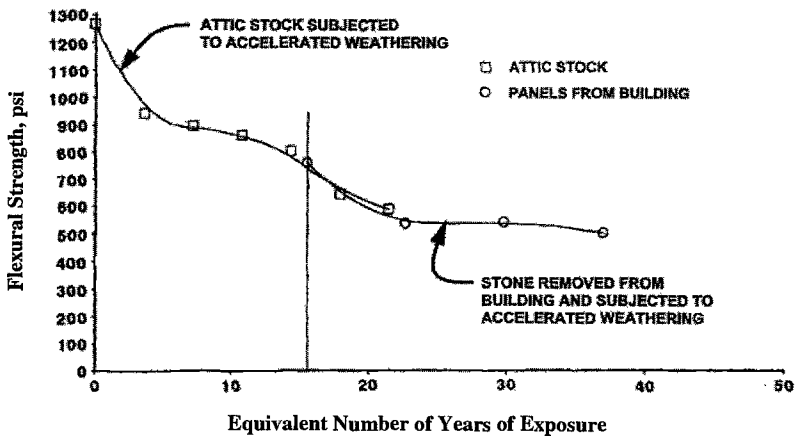


Figure 16 - Comparison of durability test cycles to years of natural weathering determined from White Carrara marble specimens.^[12]

The three marbles tested indicate approximately 15 cycles of accelerated weathering is equal to one year of natural weathering on the buildings. All of these data correlates with the rooftop test and laboratory accelerated weathering of the Danby marble previously discussed.

Limited data has also been obtained for granite and limestone. The results of these tests have been similar to those obtained from the more extensive marble data. Based on this data, approximately 13 cycles represent one year of natural weathering for granite, 12 to 13 cycles represent one year for marble, and 12 cycles represent one year for limestone in the Chicago environment. Chicago is a good average freeze-thaw environment for evaluation of an accelerated weathering test procedure such as presented in this paper and comparing it to actual natural weathering.

Conclusions

The efforts described in this paper include the results from several years of durability (accelerated weathering) testing. These tests were performed in an effort to predict the long-term durability of thin stone when exposed to natural weathering. The accelerated weathering test procedure described in this paper will distinguish between a durable and less durable stone under natural weathering conditions. The procedure will also provide an indication of strength loss due to weathering. This data can affect the structural design for long-term reliability of thin stone panels on high-rise buildings.

The data obtained shows useful information can be obtained from thin stone specimens less than 50 mm (2 in.) subjected to the described accelerated aging test for at least 100 cycles. As discussed previously in the test procedure description, 100 freeze-thaw cycles was deemed adequate to assess the durability of stone specimens. If comparison tests can be made using naturally weathered stone and unweathered stone, a relationship can be determined between number of cycles and time. The design can then be optimized by either increasing the thickness of the panel or reducing the unsupported span. These options will reduce load stresses and increase the service life of the stone.

The weathering curves provided can be used for design by determining where the allowable working stress crosses the strength loss curve for the stone. When data for naturally weathered stone is not available, an estimated cycle per year can be used from the data in this paper, assuming 12 to 16 freeze-thaw cycles of the durability test procedure is equivalent to one year of natural weathering in a temperate climate.

References

- [1] Schaffer, R. J., *The Weathering of Natural Stone*, Department of Scientific and Industrial Research, Building Research, Special Report No. 18, Published by His Majesty's Stationary Office, 1932, pages 98-105.
- [2] Nahon, D. B., *Introduction to the Petrology of Soils and Chemical Weathering*, John Wiley & Sons, 1991, pages 4-8.
- [3] Ibid 1.

- [4] Ibid 2.
- [5] Laboratory studies performed at the Argonne National Laboratories, 1975.
- [6] Polakowski, N. H., Ripling, E. J., *Strength and Structure of Engineering Materials*, Prentice-Hall, Inc., 1966, pages 336-376.
- [7] Ibid 2, pages 4-7.
- [8] Winkler, E.M. "Important Agents of Weathering for Building and Monumental Stone," *Engineering Geology I*, 1966, pages 381-400.
- [9] Winkler, E. M., *Stone: Properties, Durability in Man's Environment*, 2nd Ed., Springer-Verlag, 1975, page 171.
- [10] Ibid 9, page 125.
- [11] *Marble Engineering Handbook*, Marble Institute of America, 1960.
- [12] The Chicago Committee on High Rise Buildings, *Exterior Claddings on High Rise Buildings*, Report No. 12, 1990, pp. 123-161.

Lightfastness of Artists' Pencils: Natural & Accelerated Exposure Results

Reference: Brennan, P. J. and Everett, E. T., “**Lightfastness of Artists’ Pencils: Natural & Accelerated Exposure Results,**” *Durability 2000: Accelerated and Outdoor Weathering Testing, ASTM STP 1385*, J. D. Evans and W. D. Ketola, Eds., American Society for Testing and Materials, West Conshohocken, PA, 2000.

Abstract: Colored pencils are the medium of choice for many artists, however, there is currently no standard methodology to help artists choose between pencils with good, bad, or indifferent lightfastness. A research project to correlate the performance of artists’ pencils was initiated by the ASTM D01.51.14 Colored Pencil Task Group. Three artist pencil manufacturers participated in the study. Replicate pencil specimens were exposed in Florida and Arizona benchmark locations under glass and in three different models of Xenon Arc lightfastness test apparatus. Two of the models were small, less expensive “tabletop” units, while the third xenon-arc was a full-size, free-standing tester. The resulting data was analyzed using both rank order and ASTM D4303 lightfastness categories. There was excellent rank order correlation between natural and accelerated exposures.

Keywords: Accelerated weathering, exposure testing, under-glass outdoor exposures, rank order correlation, xenon-arc

¹Senior Vice-President, Q-Panel Lab Products, 26200 First Street, Cleveland OH 44145.

²Technical Specialist, Q-Panel Lab Products, 26200 First Street, Cleveland OH 44145.

Lightfastness of Artists Pencils

I Introduction

Colored pencils are the medium of choice for many artists. However, there is no current, effective way for artists to properly distinguish between pencils with varying levels of lightfastness. Since many artists want their work to last for a very long time, this uncertainty can be a significant issue.

At the January 1999 meeting of ASTM D01.57.14 Colored Pencil Task Group¹ meeting, it was agreed to develop a standard addressing lightfastness testing of artists' colored pencils. The following study was designed to supply the data necessary to develop a standard test method to distinguish between various quality levels of colored pencils.

II Test Objectives

The objectives of this lightfastness study were to:

1. Determine if natural, under glass exposure tests are useful for colored pencil specimens. That is, are they an appropriate benchmark test to simulate actual end-use environments.
 - Determine if Florida Under Glass exposures need mechanical ventilation to avoid water droplet spotting. Previous Florida Under Glass tests in non-mechanically ventilated enclosures exhibited water spotting on test specimens.
 - Determine if Arizona is a useful exposure site for under glass exposures of colored pencils. ASTM D4303, Test Method for Lightfastness of Pigments Used in Artists' Paints, does not specify Arizona as an outdoor exposure location. Arizona typically produces higher UV dosage and higher temperatures than Florida, with lower humidity levels.
 - Determine from the three outdoor exposure tests (i.e. Florida Under Glass, Florida Under Glass-Ventilated and Arizona Under Glass) which test(s) are useful and provide meaningful test results.
2. Determine correlation (if any) between natural and accelerated exposures.
3. Determine correlation (if any) between various models of xenon arc exposure devices (all conform to ASTM G151, Practice for Exposing Nonmetallic Materials in Accelerated Test Devices that Use Laboratory Light Sources and ASTM G155, Practice for Using Xenon Arc Light Apparatus for Exposure of Nonmetallic Materials).

¹

D01 is the Committee on Paint and Coatings. D01.57 is the subcommittee on Artists' Materials.

- Three models of xenon-arc testers were used in the study. Two were small, less expensive "tabletop" units, while the third xenon-arc was a full size, free-standing tester. One of the tabletop testers employed a wide-band irradiance measurement system which differed from the narrow-band irradiance measurement system utilized in the other testers. In addition, each of the three xenon-arc testers utilized somewhat different filters to achieve the "Sunlight through Window Glass" spectra specified in ASTM G155. These factors, as well as machine-to-machine variability, could be expected to have an effect on test results.
4. Determine whether less expensive, "tabletop" xenon-arc tester provide the same results as more expensive, full-sized xenon-arc testers.
 5. Determine an appropriate control (e.g., colored pencil with a known durability) for use in future tests.

III Test Specimens

Colored Pencil Test Specimens. Three colored pencil manufacturers participated in the study. Each prepared two replicate specimens of five colored pencil types. Each pencil type was applied to a paper substrate by rubbing. The paper substrate used was bright white in color, acid-free, and of a type which, historically, had been shown not to change color during or after exposure.

The five pencil types provided by each manufacturer were of various colors and durability levels, ranging from very good to very poor. This was to provide a representative spread in the data. For a test of this type, it is essential that specimens of various durability levels are tested together. This is the only real way to determine what is really happening to the specimens in the tests. Also, using both "good" and "bad" quality specimens in a test assures a more meaningful ranking of the specimens.

Other Test Specimens. The Society of Dyers & Colourists (SDC) supplied specimens of blue pigmented papers of varying lightfastness (Lightfastness Standards 1-8) for use in the study. These pigmented papers are experimental and are intended to replace the ISO Blue Wool series as a reference material. SDC Lightfastness Standards 1-8 range in pigment formulations and in sensitivity to UV light. The purpose of including these paper substrates was to determine an appropriate SDC Lightfastness Standard for use as a reference material.

In addition, the Colored Pencil Society of America (CPSA) supplied two replicate test specimens of four commonly used artists' papers, or boards, to be included in the six lightfastness tests. These paper substrates were included in the study to determine whether substrate yellowing would occur and, if so, how the test methodology should address the issue of substrate yellowing.

IV Test Protocol

Six lightfastness exposures were conducted as follows:

Natural Sunlight Exposure Tests. Specimens were exposed to natural sunlight using three under glass techniques. Temperature, humidity, and condensation (if present) are not typically monitored or recorded in these types of exposure devices and were not recorded for this test. Specific test conditions for each of the natural exposures are noted below:

1. Arizona Under Glass - Natural Exposure

- ASTM G24, Practice for Conducting Natural Light Exposures Under Glass
- Location: Q-Lab Weathering Research Service, Phoenix, Arizona
- Test Enclosure: per G24, Type A
- Exposure Angle: 45°S under glass
- Exposure Duration: 1262 MJ/m² at 300-3000 nm, per G 24

2. Florida Under Glass - Natural Exposure

- ASTM D4303, Method A
- Location: Q-Lab Weathering Research Service, Miami, Florida
- Test Enclosure: per G24, Type A
- Exposure Angle: 45°S under glass
- Exposure Duration: 1350 MJ/m² at 300-3000 nm, per ASTM G 24²

3. Florida Under Glass-Vented - Natural Exposure

- Modified ASTM D4303, Method A
- Location: South Florida Test Service, Miami, Florida
- Test Enclosure: a modified under glass exposure box, ventilated with mechanically actuated blowers operating 24 h a day, seven days a week.
- Exposure Angle: 45°S under glass
- Exposure Duration: 1262 MJ/m² at 300-3000 nm, per ASTM G 24

Accelerated Laboratory Tests (Xenon-Arc). Specimens were also exposed in three different xenon-arc test chambers filtered to simulate exposure to sunlight through window glass. Figure 1 shows the Spectral Power Distribution of a xenon-arc test device utilizing Window-Glass Filters compared to C.I.E. Sunlight No. 85, *Recommendations for the Integrated Irradiance and the Spectral Distribution of Simulated Solar Radiation for Testing Purposes*, and sunlight through glass. Specific test conditions for each of the laboratory exposures is noted as follows:

²

The radiation dosage exceeded the target of 1260 MJ/m² by 90MJ. This overexposure was due to removing the test specimens in preparation for Hurricane Floyd and then inadvertently returning them to the exposure field for an additional week beyond the target dosage.

1. Q-SUN/1000 Xenon Arc (ASTM D4303, G151/G155)

- Location: Q-Lab Weathering Research Service, Florida
- Filters: Window Glass Filter
- Irradiance level: 0.35 W/m²/nm at 340 nm
- Radiant Exposure: 510 kJ/m² at 340 nm
- Exposure Cycle: Continuous Light at 63 +/- 2.5°C

2. Suntest CPS+, Xenon Arc (G151/G155)

- Location: South Florida Test Service
- Filters: Quartz Dish w/Selectively Reflectively Coating, plus Window Glass Filter
- Irradiance level: 490 W/m² at 300-800nm
- Radiant Exposure: 510 kJ/m² at 340 nm
- Exposure Cycle: Continuous Light at 63 +/- 3°C

3. Ci 35 Xenon Arc (ASTM D4303, G151/G155)

- Location: South Florida Test Service
- Filters: Window Glass Filter
- Irradiance level: 0.35 W/m²/nm at 340 nm
- Radiant Exposure: 510 kJ/m² at 340 nm
- Exposure Cycle: Continuous Light at 63 +/- 3°C, 55 +/- 5% RH

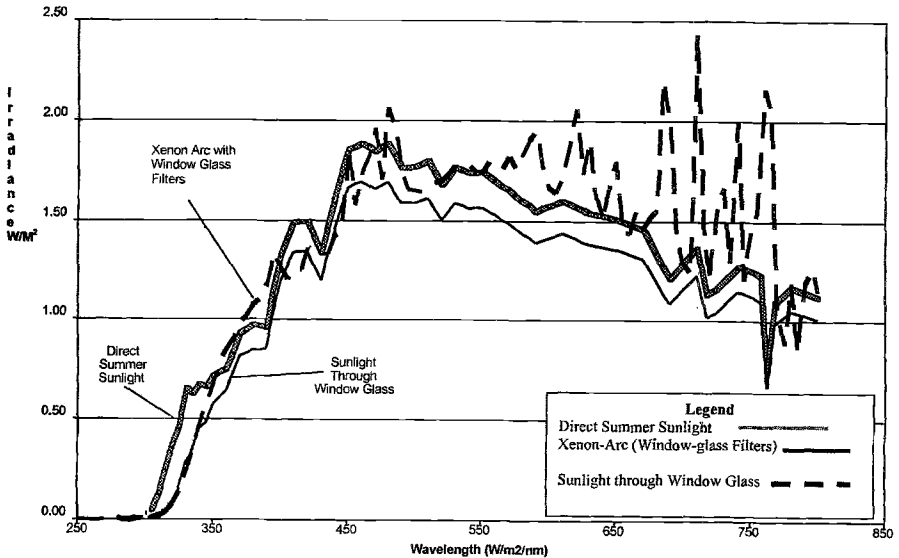


Figure 1: *Direct Sunlight, Sunlight Through Window Glass and Xenon Arc*

V Instrumental Color Measurements

Instrumental color measurements were performed on all test specimens both before and after exposure. Specimens were measured with a spectrophotometer in accordance with ASTM E 1349, Test Method for Reflectance Factor and Color by Spectrophotometry Using Bidirectional Geometry, using Illuminant C and the 1931 2° observer and excluding specular reflection. Measurements utilized the CIE 1976 L*A*B* color difference equation in accordance with ASTM D 2244, Test Method for Calculation of Color Differences from Instrumentally Measured Color Coordinates. The color change is reported in total color difference units (ΔE).

To minimize variability in color measurements, all measurements were performed at Q-Lab Weathering Research Service, Florida. The instrument used was a Hunterlab Colorquest 45°/0° Spectrocolorimeter.

VI Data

Results were analyzed using ΔE color change, D4303 Lightfastness Categories and rank order correlation.

Delta E Color Change. Instrumental color measurements were taken on all test specimens before and after exposure. The color change in ΔE units was recorded for each specimen. The color measurements were averaged for specimens of one exposure test and then were compared to color measurement averages obtained for the same specimens exposed in a different test. There were 14 cases where results from the different exposures were significant enough to place a pencil specimen in an entirely different lightfastness category. Table 1 shows the colored pencil ΔE color change for all six lightfastness exposures.

The average of all ΔE data in Table 1 confirms that the Arizona Under Glass exposure was 16% more severe than Florida (on average). It was also more severe than the xenon arc exposures.

Table 1 also shows ΔE discrepancies between specimen replicates. For example, Z Orange-1 and Z Orange-2 specimens showed nearly a 10 ΔE difference in the Arizona Under Glass exposure. A similar discrepancy for the same color occurred in the CPS+ Xenon exposure. In all, there were 6 instances where there was a ΔE difference between replicate specimens of 4 or more. The use of a third replicate would have helped to provide more useful results in these cases.

Table 1--*Pencil Color Data-delta E*

Specimen	Arizona/UG	Florida /UG	Florida/YUG	Q-SUN Xenon	Ci35 Xenon	CPS+ Xenon
Y RED-1	13.3	1.1	2.3	5.7	1.2	1.4
Y RED-2	8.5	1.4	1.6	5.7	2.3	3.8
Z RED-1	46.4	36.9	39.1	26.7	36.5	24.4
Z RED-2	45.1	36.3	39.2	28.5	35.4	24.2
X ORANGE-1	79.8	80.4	80.7	79.7	80.6	75.5
X ORANGE-2	79.9	80.3	80.0	79.3	79.3	77.4
Z ORANGE-1	39.5	38.6	39.8	37.3	37.3	28.7
Z ORANGE-2	31.9	37.1	43.5	34.8	37.8	22.4
Y FLESH-1	25.8	27.0	25.6	19.7	24.9	22.8
Y FLESH-2	25.3	25.9	24.4	19.7	25.0	22.2
Z YELLOW-1	44.7	43.0	43.6	45.6	45.0	44.5
Z YELLOW-2	41.9	38.1	45.7	45.9	45.3	44.5
X Y.GREEN-1	21.6	12.1	5.9	6.1	9.2	7.2
X Y.GREEN-2	24.1	10.9	7.3	7.0	13.7	11.5
Y GREEN-1	3.4	3.1	4.0	5.8	1.4	0.8
Y GREEN-2	5.3	3.0	3.6	7.9	3.1	2.9
Z GREEN-1	33.7	28.9	32.2	19.3	17.7	14.9
Z GREEN-2	30.4	29.3	33.9	19.9	17.9	20.1
Y AQUA-1	12.0	8.6	9.9	5.8	5.7	5.2
Y AQUA-2	11.9	8.2	7.7	5.7	4.4	5.5
X BLUE-1	17.1	14.0	13.8	10.9	11.5	9.2
X BLUE-2	17.8	13.9	14.3	11.2	11.1	9.1
Y BLUE-1	33.3	20.3	18.5	26.8	18.0	22.4
Y BLUE-2	32.9	22.1	21.0	28.2	16.6	24.1
X PURPLE-1	31.2	31.1	34.0	23.0	21.4	25.2
X PURPLE-2	32.7	31.1	33.3	22.3	22.6	25.9
Z PURPLE-1	25.9	20.3	24.1	23.1	23.8	20.8
Z PURPLE-2	28.8	20.3	23.6	22.9	23.6	21.6
X BLACK-1	2.4	2.5	3.1	2.7	3.2	2.0
X BLACK-2	2.3	3.1	2.3	2.1	3.2	2.2
Average:	28.3	24.3	25.3	22.6	22.6	20.7

Table 2--SDC Blue Papers-delta E

Specimen	Arizona/UG	Florida /UG	Florida/VUG	Q-SUN Xenon	Ci35 Xenon	CPS+ Xenon
SDC-1	74.1	69.7	71.7	68.3	72.8	69.4
SDC-1	74.0	69.8	73.2	72.4	73.7	69.3
SDC-2	72.8	70.7	73.5	71.6	70.8	71.5
SDC-2	73.8	70.4	72.0	73.7	72.2	73.5
SDC-3	79.5	77.9	80.3	80.8	79.0	79.9
SDC-3	79.3	78.1	81.0	79.6	79.2	80.5
SDC-4	10.9	13.1	10.3	9.6	11.0	7.8
SDC-4	11.3	12.9	10.7	9.3	9.9	7.7
SDC-5	14.1	-	12.8	10.4	12.4	8.5
SDC-5	12.0	-	13.4	9.5	12.8	8.8
SDC-6	10.4	-	9.0	7.2	10.3	5.5
SDC-6	9.2	-	9.0	7.2	10.2	4.6
SDC-7	10.0	-	8.5	6.1	9.4	4.9
SDC-7	9.0	-	8.4	5.9	9.1	4.8
SDC-8	7.1	10.1	6.0	3.6	5.9	2.2
SDC-8	6.4	10.6	6.4	3.3	6.3	2.2
Average:	34.6	48.3	34.1	32.4	34.1	31.3

Table 2 shows the SDC blue paper delta E color change for all six exposures. SDC 1-3 exhibit delta E values ranging from 68 to 81. These specimens were severely overexposed and therefore do not provide useful data. The SDC-4 through 8 test specimens were much more useful, with delta E's of 15 or less. These papers contain a higher pigment loading and are more lightfast than SDC 1-3. SDC 5-7 were damaged by pigment coming off the paper substrate due to handling during hurricane field clearing and remounting for Hurricane Floyd. Therefore, it was not possible to obtain color readings. With the exception of the overexposed specimens, there appears to be good correlation among the various SDC paper types for all six exposure tests. The average delta E change for all six exposures is between 31 and 34.

D4303 Lightfastness Categories. In accordance with ASTM D4303, test specimens were assigned a Lightfastness Category ranking based upon the delta E color change. Categories range from a Category I (Excellent - very little color change) to Category V (poor - great deal of color change). In D4303, only Lightfastness Categories I and II are considered acceptable. Table 3 shows the D4303 Lightfastness Categories I-V and their respective ranges.

Table 3--D4303 Lightfastness Categories

Lightfastness I:	0 to < 4.0 delta E units
Lightfastness II:	> 4.0 to < 8.0
Lightfastness III:	> 8.0 to < 16.0
Lightfastness IV:	> 16.0 to < 24.0
Lightfastness V:	> 24.0

Table 4 -- Pencil Lightfastness Category Ratings

Specimen	Arizona/UG	Florida/UG	Florida/VUG	O-SUN Xenon	Ci35 Xenon	CPS+ Xenon
Y RED-1	III	I	I	II	I	I
Y RED-2	III	I	I	II	I	I
Z RED-1	V	V	V	V	V	V
Z RED-2	V	V	V	V	V	V
X ORANGE-1	V	V	V	V	V	V
X ORANGE-2	V	V	V	V	V	V
Z ORANGE-1	V	V	V	V	V	V
Z ORANGE-2	V	V	V	V	V	IV
Y FLESH-1	V	V	V	IV	V	IV
Y FLESH-2	V	V	V	IV	V	IV
Z YELLOW-1	V	V	V	V	V	V
Z YELLOW-2	V	V	V	V	V	V
X Y.GREEN-1	IV	III	II	II	III	II
X Y.GREEN-2	V	III	II	II	III	III
Y GREEN-1	I	I	I	II	I	I
Y GREEN-2	II	I	I	II	I	I
Z GREEN-1	V	V	V	IV	IV	III
Z GREEN-2	V	V	V	IV	IV	IV
Y AQUA-1	III	III	III	II	II	II
Y AQUA-2	III	III	III	II	II	II
X BLUE-1	IV	III	III	III	III	III
X BLUE-2	IV	III	III	III	III	III
Y BLUE-1	V	IV	IV	V	IV	IV
Y BLUE-2	V	IV	IV	V	IV	V
X PURPLE-1	V	V	V	IV	IV	V
X PURPLE-2	V	V	V	IV	IV	V
Z PURPLE-1	V	IV	V	IV	IV	IV
Z PURPLE-2	V	IV	IV	IV	IV	IV
X BLACK-1	I	I	I	I	I	I
X BLACK-2	I	I	I	I	I	I

Tables 4 and 5 show the Lightfastness Categories assigned to the artists' pencils and to the SDC papers.

Table 4 shows seven specimens where one replicate received a different D4303 Lightfastness Category rating than the other replicate in the same exposure. For example, in the Arizona Under Glass exposure, one XY Green received a Category IV rating, while the second received a Category V rating. The actual delta E differences between the replicate specimens were small, but in borderline cases, even a small difference can cause one replicate to receive an entirely different rating than the other.

The variability between replicates may be the result of non-uniformity in the exposure or it could reside in the sample preparation. With specimens of this sort, where the application of the color consists of rubbing the pencil onto the test substrate, one replicate may easily have had more pigment applied than the other. Also, color measurement techniques may be a source of error unless they are optimized for this application.

Whatever the cause for the variability, the presence of a third replicate would have made the data more useful. Table 5 shows generally good rank order correlation between the SDC specimens.

Table 5--SDC Papers Lightfastness Category Ratings

Specimen	Arizona/UG	Florida /UG	Florida/VUG	O-SUN Xenon	Ci35 Xenon	CPS+ Xenon
SDC-1	V	V	V	V	V	V
SDC-1	V	V	V	V	V	V
SDC-2	V	V	V	V	V	V
SDC-2	V	V	V	V	V	V
SDC-3	V	V	V	V	V	V
SDC-3	V	V	V	V	V	V
SDC-4	III	III	III	III	III	II
SDC-4	III	III	III	III	III	II
SDC-5	III	-	III	III	III	III
SDC-5	III	-	III	III	III	III
SDC-6	III	-	III	II	III	II
SDC-6	III	-	III	II	III	II
SDC-7	III	-	III	II	III	II
SDC-7	III	-	III	II	III	II
SDC-8	II	III	II	I	II	I
SDC-8	II	III	II	I	II	I

D4303 Lightfastness Category Errors. Table 6 presents the rating discrepancies between the various exposure methods, illustrating how the variability of results between the various exposure locations causes anomalies when D4303 Lightfastness Categories are applied to the specimens. The rating discrepancy data in Table 6 is also expressed in percentages (shown in parentheses).

Table 6 shows how the various six exposure tests related to each other. For example, there was only one rating discrepancy in comparing the Florida Vented Under Glass exposures and the Florida Under Glass exposures. There were 9 rating discrepancies between the Ci35 Xenon exposures and the Arizona Under Glass exposures.

Table 6--Rating Errors Using D4303 Lightfastness Categories

Number of rating discrepancies between different exposure methods.

<u>Exposure</u>	<u>Florida/UG</u>	<u>Florida/VUG</u>	<u>Arizona/UG</u>	<u>CPS+ Xenon</u>	<u>Q-SUN Xenon</u>	<u>Ci35 Xenon</u>
Florida Under Glass	0 (0%)	x	x	x	x	x
Florida Vented UG	1 (7%)	0 (0%)	x	x	x	x
Arizona Under Glass	6 (40%)	6 (40%)	0 (0%)	x	x	x
CPS+ Xenon	3 (20%)	4 (27%)	9 (60%)	0 (0%)	x	x
Q-SUN Xenon	8 (53%)	7 (47%)	8 (53%)	5 (33%)	0 (0%)	x
<u>Ci35 Xenon</u>	<u>3 (20%)</u>	<u>4 (27%)</u>	<u>9 (60%)</u>	<u>2 (13%)</u>	<u>5 (33%)</u>	<u>0 (0%)</u>

In Table 6, the rating discrepancy percentages showed a wide range. The best result in comparing natural and accelerated exposures test to one another still exhibited a 20% percent discrepancy between Florida Under Glass exposures and the CPS+ Xenon exposures. This calls into question the method of assigning Lightfastness Categories to the specimens is not very useful.

Rank Order Correlation. For most materials, it is very difficult to correlate outdoor exposure with laboratory results (X hrs Outdoor exposure = Y hrs Accelerated laboratory exposure). One of the few useful methods is a comparison of relative rank orders. Spearman Rank Order is a statistical measure that provides a value for a set of performance rankings[1]. For example, if two sets of data are being compared, rank order indicates how closely the rankings match one another. Perfect correlation is represented by a value of 1.0. Random correlation is represented by a value of 0. Negative correlation is represented by a value of -1.0. Spearman rank correlation coefficients (rs) are commonly used for relating weathering tests [1].

To illustrate the concept, Table 7 shows a theoretical example of Rank order correlation. Six types of materials (A-F) were subjected to four different tests (Tests 1-4). Test 1 represents a perfect ranking of the six material types (i.e. 1,2,3,4,5 & 6). Material performance rankings in tests 2-4 are then compared and ranked against the rankings in test 1.

In correlating accelerated and real exposure tests, the rank performance of the materials exposed to both environments is compared, and the strength of the association between the tests is established.

Table 7--*Example of Rank Performance*

Material	Rank in Test #1	Rank in Test #2	Rank in Test #3	Rank in Test #4
A	1	1	2	6
B	2	2	6	5
C	3	3	3	4
D	4	4	4	3
E	5	5	1	2
F	6	6	5	1

r_s to Test #1	1.0	0	-1.0
	Perfect Correlation	Random	Negative Correlation

Table 8--*Rank Order Correlations*

Colored Pencil Matrix

Exposure	Florida/UG	Florida/VUG	Arizona/UG	CPS+ Xenon	Q-SUN Xenon	Ci35 Xenon
Florida Under Glass	1.00	x	x	x	x	x
Florida Vented UG	0.99	1.00	x	x	x	x
Arizona Under Glass	0.94	0.93	1.00	x	x	x
CPS+ Xenon	0.96	0.94	0.94	1.00	x	x
Q-SUN Xenon	0.93	0.92	0.95	0.95	1.00	x
Ci35 Xenon	0.95	0.95	0.91	0.94	0.92	1.00

SDC Paper Matrix

Exposure	Florida/UG	Florida/VUG	Arizona/UG	CPS+ Xenon	Q-SUN Xenon	Ci35 Xenon
Florida Under Glass	1.00	x	x	x	x	x
Florida Vented UG	1.00	1.00	x	x	x	x
Arizona Under Glass	0.98	0.99	1.00	x	x	x
CPS+ Xenon	0.98	0.99	0.97	1.00	x	x
Q-SUN Xenon	0.98	0.99	0.96	0.99	1.00	x
Ci35 Xenon	0.98	0.99	0.98	0.97	0.96	1.00

Table 8 shows rank order correlation between the six exposure tests for colored pencils and SDC blue papers. There was excellent rank order correlation between all the exposures. In the colored pencil matrix, the Florida Under Glass exposures and Florida Ventilated Under Glass exposures are in almost perfect agreement with one another (i.e. 0.99). The Q-SUN Xenon appears to be more similar to Arizona (0.95) than to Florida Under Glass (0.93). The CPS+, on the other hand, appears to be more similar to Florida (0.96) than to Arizona (0.94).

The CI35 Xenon correlated well with the CPS+ Xenon (0.94) and the Q-SUN Xenon (0.92). All of the exposures show excellent correlation, with rank orders of 0.91 and higher.

The SDC paper specimens gave similar results. All three xenon exposures correlated nearly perfectly with Florida Under Glass exposures and Florida Ventilated Under Glass exposures, with values of 0.98 and 0.99, respectively.

VII Conclusions

At this time, some conclusions seem apparent:

1. Florida Under Glass exposure tests were very useful for artists' pencils. There were only minor variations between ventilated and unventilated Florida exposures. These could have been caused by temperature or because the exposures were performed at different sites and at slightly different times.

In this test, Florida Under Glass exposures did not need mechanical ventilation to avoid water droplet spotting. The only specimen to exhibit water spotting was exposed in the vented exposure box.

2. Arizona was very useful for exposures of artists' pencils. Arizona produced faster degradation than Florida. Consequently, it is likely that the Arizona exposures could be of a shorter duration.
3. There was excellent rank order correlation between natural and accelerated exposures. Correlation in absolute numbers was poor on some materials, but was very good on others.
4. There was excellent rank order correlation between the various G151/G155 xenon arc exposures. Correlation in absolute numbers and Lightfastness Categories was reasonably good.
5. Relative Humidity did not appear to be a critical parameter in the tests. In the xenon exposures, there was not a noticeable difference between specimens exposed in a humidity-controlled xenon arc test with similar specimens exposed in a xenon arc without controlled humidity.
6. For this application, the "table top" xenon testers were just as useful as the larger xenon arc testers.
7. All of the methods can distinguish rank order lightfastness levels, but the practical use of absolute numbers is dependent on repeatability and reproducibility.
8. The Society of Dyers and Colorists' (SDC) Blue Pigmented Paper No. 4 appears to have promise as a reference material for this application.

9. The blank paper substrates supplied by the Colored Pencil Society of America (CPSA) for color stability testing showed inconclusive results. There was very little yellowing of the substrates. However, some of the substrate specimens were sensitive to moisture resulting from the Florida Under Glass exposure.
10. At least three replicates of each specimen should be used, in order to minimize variability in test results.

VIII Future Work

1. Lightfastness Categories could be useful if exposure variability is addresses. This issue of variability in the test results is a common issue. When ASTM Committee G03 on Weathering and Durability conducted round-robin studies of accelerated weathering testers, the results were similar to the study above. There was significant variability in test results for absolute values. However, there was good rank order correlation [2].

Presently, the repeatability and reproducibility of the various exposure methods is unknown. Variability resulting from specimen preparation and color measurement techniques is also unknown. The practical use of D4303 Lightfastness Categories requires that all these issues be better understood.

2. One research option would be to select a reference material with known durability and expose it along with the test specimens to a predetermined change (within a predetermined range). The test specimen data could be normalized against the reference material's performance.
3. It would be useful if the D01.57.14 Colored Pencil Task Group could determine an appropriate benchmark exposure based on actual, real world service life conditions. Current "real world" exposures in Florida and Arizona may actually be too severe for this study. Compared to the normal service conditions for fine art materials, the Arizona exposure may be too severe because of its high heat, where Florida may also be too severe because of unrealistically high levels of humidity.
4. The idea of a "referee test" may be a useful concept. For example, a xenon-arc tester could be used as a qualifier for colored pencil specimens. However, if a specimen is borderline between two Lightfastness Categories, the particular specimen should be re-tested outdoors under glass in Florida.

Acknowledgements

The authors would like to thank the following for their invaluable assistance: Mark Gottsegen, University of North Carolina, Rhonda Farfan, Colored Pencil Society of America, Joy Turner Luke, Studio 231, David Tee, Cumberland Pencil Co., Jamie Paulin, Sanford Corp., Arjen Wittekoek, Bruynzeel Potlodenfabriek BV, Carol Graham, Society of Dyers and Colourists, Jack Martin, South Florida Test Service,

Michael Crewdson, Q-Lab Weathering Research Service, and Members of the D01.57.14 Colored Pencil Task Group

References

1. Fischer, R. M. "Results of Round Robin Studies of Light- And Water-Exposure Standard Practices," Accelerated and Outdoor Durability Testing of Organic Materials, ASTM STP 1202, Warren D. Ketola and Douglas Grossman, Eds., American Society of Testing and Materials, Philadelphia, 1994.
2. Fischer, R. M. and Ketola, W. D., "The Impact of Recent Research on the Development and Modification of ASTM Weathering Standards," Durability Testing of Nonmetallic Materials, ASTM STP 1294, Robert J. Herling, Ed., American Society for Testing and Materials, 1996.

SERVICE LIFE

Dieter Kockott¹ and Gerhard Manier²

CALCULATION OF THE SPECTRAL IRRADIANCE OF SOLAR RADIATION FOR THE LIFETIME PREDICTION OF POLYMER MATERIALS

Reference: Kockott, D. and Manier, G., “Calculation of the Spectral Irradiance of Solor Radiation for the Lifetime Prediction of Polymer Materials,” *Durability 2000: Accelerated and Outdoor Weathering Testing, ASTM STP 1385*, J. D. Evans and W. D. Ketola, Eds., American Society for Testing and Materials, West Conshohocken, PA, 2000.

Abstract: The calculation program under consideration determines the spectral irradiance of direct solar radiation, diffuse solar radiation and reflected radiation as well as global radiation as a factor of sun position (as determined by geographic location, season and time of day) and meteorological conditions: temperature and relative humidity, O₃ concentration, degree of cloud cover and visibility as well as the spectral ground reflectance. Spectral irradiance levels are calculated for randomly positioned surfaces. The irradiance level is calculated as a function of time of day on the basis of the hourly means for the meteorological parameters as measured by many different weather stations. On this basis, the radiant exposure for a given day is calculated in terms of selectable wavelength ranges. The program also calculates the effective radiant exposure by using the spectral sensitivity of a specific material as a basis for lifetime prediction. The lifetime of a polymer material depends on several external parameters, e.g., solar radiation, temperature and moisture content of the material. The general scope of this paper is restricted to radiation and its effect on lifetime.

Keywords: calculation, global radiation, irradiance, radiant expsoure, lifetime prediction

¹Consultant to Atlas Material Testing Technology, Vogelsbergstr. 27, D-63456 Hanau, Germany.

²Prof., Meteorological Institute University of Darmstadt, Groß-Gerauer Str. 14, D-64331 Weiterstadt, Germany.

Interactions Between Radiation and Polymer Materials

Characterization of the Radiation Striking a Material Sample

The impinging radiation is measured in terms of spectral irradiance E_λ - given in $W/m^2 \cdot nm$. This value indicates the radiant flux per unit of area within a limited wavelength range $\Delta\lambda$ - usually 1 nm - impinging on the material sample. Plotting spectral irradiance E_λ in a number of equally spaced wavelength intervals yields the spectral distribution of the radiation. The irradiance in the wavelength interval lying between λ_1 and λ_2 is then

$$E = \int_{\lambda_1}^{\lambda_2} E_\lambda d\lambda \quad \text{given in } W/m^2 \quad (1)$$

If radiation with the irradiance E acts on the surface of a material for a period of time t , then a specific radiant energy strikes the surface during this period of time. This value is called the radiant exposure H

$$H = \int_{t_1}^{t_2} E dt \quad \text{given in } J/m^2 \quad (2)$$

Characterization of Radiation-Related Aging of a Polymer Material

A portion of the radiation striking a material is absorbed. The absorption ϵ_λ , which generally depends on the wavelength, indicates the ratio of absorbed energy to that striking the material. Most of the absorbed radiation heats up the irradiated material. Only a very small portion of the absorbed radiation causes primary photochemical processes, for example leading to excited states, radicals or chain scission. Absorption of radiation is required for photochemical changes to occur. However, not all the radiation absorbed causes photochemical changes. Therefore, the absorption alone is not sufficient to describe the behaviour of a material with respect to the change in its useful properties as a result of optical radiation. For such a description, the spectral sensitivity s_λ of the material is much more appropriate. This parameter describes the wavelength dependence of a defined change in material properties in a given material as the result of a radiant exposure under otherwise equivalent conditions of exposure. s_λ is a standardized parameter and is dimensionless, whereby the maximum is usually determined as = 1. The spectral sensitivity is a parameter specific to the material and characterizes material behaviour without providing detailed information on the type of degradation processes involved. It is independent of the radiation source used.

The degradation processes are in most cases temperature-dependent. Therefore, s_λ is also generally dependent on temperature. This can be determined experimentally by measuring s_λ at different sample temperatures and under otherwise equivalent conditions of exposure.

Characterization of Effective Radiation on Sample

For a given material and a specific property change, only that part of the radiation is of interest which leads to an actual effect in the material. The effective irradiance E_{eff} thus results from weighting the spectral irradiance E_{λ} with spectral sensitivity s_{λ} , then integrating the result analogously to eq. (1).

$$E_{\text{eff}} = \int_{\lambda_1}^{\lambda_2} E_{\lambda} s_{\lambda} d\lambda \quad (3)$$

The effective radiant exposure H_{eff} is then analogous to eq. (2)

$$H_{\text{eff}} = \int_{t_1}^{t_2} E_{\text{eff}} dt \quad (4)$$

Lifetime Prediction

In first calculatory approximation, the change in a material property $\Delta\psi$ resulting from irradiation is proportional to the effective radiant exposure H_{eff}

$$\Delta\psi \sim H_{\text{eff}} \quad (5)$$

In a comparison of the properties of a material, e.g. at equal effective radiant exposure H_{eff} , but varying spectral irradiance levels E_{λ} , it is assumed that the spectral irradiance levels will not differ by orders of magnitude. Examples from practice [1,2] indicated that eq. (5) is valid for the materials investigated, even if E_{λ} varies up to a factor of 3.

The essential thing is that the other exposure parameters such as temperature and moisture remain unchanged. The influence of temperature can, however, be taken into consideration by means of experimental determination of s_{λ} as dependent on temperature.

If s_{λ} and E_{λ} are known as a function of time t , it is possible to derive, e.g. from the experimentally determined lifetime of a material at location A at a spectral irradiance of $E_{\lambda,A}(t)$, the lifetime of the same material at location B with a spectral irradiance of $E_{\lambda,B}(t)$. That is the reason a knowledge of E_{λ} as a function of daytime and season at the various locations where the material is used is so essential for estimation of aging behaviour. E_{λ} can be determined either experimentally or by calculation.

Calculation of E_{λ} for Different Geographic Locations, Meteorological Conditions and Sample Positions

We describe in this section a program for calculation of solar spectral irradiance. It corresponds to the method of calculation in the VDI guideline 3789, part 3 [3]. The calculation program is designated CESORA (Calculation of Effective Solar Radiation).

Spectral irradiance E_{λ} ($\beta, \alpha; N$) on a randomly positioned surface can be divided into three portions:

$$E_{\lambda}(\beta, \alpha; N) = I_{\lambda}(\beta, \alpha; N) + D_{\lambda}(\beta, \alpha; N) + R_{\lambda}(\beta, \alpha; N) \quad (6)$$

whereby

I_{λ} = spectral direct solar radiation

D_{λ} = spectral diffuse solar radiation

R_{λ} = spectral reflected global radiation

β = angle of elevation of surface normal

α = azimuth of surface normal

N = degree of cloud cover in terms of 1/8th sections of visible sky

Spectral Direct Solar Radiation

Extraterrestrial spectral solar radiation $I_{0\lambda}$, known from measurements taken outside the earth's atmosphere [4-6], is attenuated in the atmosphere by the following influences:

- Scattering at air molecules
- Absorption by ozone, water vapour, carbon dioxide and other gases
- Scattering and absorption by aerosol
- Reflection, scattering and absorption by clouds.

According to Iqbal [7], these influences are described by five transmission functions, whereby clouds are not taken into account:

Scattering at air molecules

$$\tau_R(\lambda) = \exp[-0,008735 \cdot (\lambda/1000\text{nm})^{-4,08} \cdot m \cdot (p/p_0)] \quad (7)$$

$m = f(\gamma)$; γ : solar altitude; p : air pressure

Scattering and absorption by aerosol

$$\tau_a(\lambda) = \exp[-\beta_A \cdot (\lambda/1000\text{nm})^{-\alpha_A} \cdot m_a] \quad (8)$$

$\alpha = 1.3$

$\beta = f(v)$; v = visibility distance

Absorption by water vapour

$$\tau_w(\lambda) = \exp\left\{-0,2385 \cdot \sigma_w(\lambda) \cdot w \cdot m_w / [1 + 20,07 \cdot \sigma_w(\lambda) \cdot w \cdot m_w]^{0,45}\right\} \quad (9)$$

$\sigma_w(\lambda)$ = spectral absorptance

w = water content of atmosphere in cm of precipitated water

$w = f(r, \theta)$; r = relative humidity at height of 2 m, θ = air temperature at height of 2 m

Absorption by ozone

$$\tau_{OZ}(\lambda) = \exp\left[-\sigma_{OZ}(\lambda) \cdot l \cdot m_{OZ}\right] \tag{10}$$

$\sigma_{OZ}(\lambda)$ = spectral absorbance
 l = ozone content in cm NTP, 0.3 cm or from table.

Absorption by other gases

$$\tau_g(\lambda) = \exp\left\{-1,41 \cdot \sigma_g(\lambda) \cdot m \cdot (p / p_0) / \left[1 + 118,93 \cdot \sigma_g(\lambda) \cdot m \cdot (p / p_0)\right]^{0,45}\right\} \tag{11}$$

$\sigma_g(\lambda)$ = spectral absorbance

Direct spectral solar radiation is thus equal to:

$$I_\lambda(\beta, \alpha; 0) = I_{0\lambda} \tau_R \tau_a \tau_w \tau_{OZ} \tau_g \tag{12}$$

Measurements [8] have demonstrated that in mean values covering 1 h of direct solar radiation, the dependence of direct solar radiation from the degree of cloud cover is linear. This measurement result can be transferred to spectral direct solar radiation, that the following holds, dependent on the degree of cloud cover N:

$$I_\lambda(\beta, \alpha; N) = I_\lambda(\beta, \alpha; 0) (1 - N/8) \tag{13}$$

Spectral Diffuse Solar Radiation

Cloudless Sky - The spectral diffuse solar radiation from a cloudless sky $D_\lambda(\beta, \alpha; 0)$ is calculated from the integral value of diffuse solar radiation $D(\beta, \alpha; 0)$ according to VDI 3789, part 2 [9] and a weighting function for wavelength dependence $f_D(\lambda)$ (see [3]).

$$D_\lambda(\beta, \alpha; 0) = D(\beta, \alpha; 0) f_D(\lambda) \tag{14}$$

Spectral diffuse radiation from a cloudless sky results from the scattering of spectral direct solar radiation at air molecules and aerosol.

Due to radiation scattering caused by air molecules, half of the radiation reaches the soil and the other half makes the earth into the familiar "blue planet" as seen from outer space. A common assumption that is not quite accurate holds that this radiation scattering is isotropic, i.e. independent on direction. The radiation from every point in the visible sky would thus be equal.

Radiation scattered by aerosol deviates little from the direction taken by direct solar radiation. It is assumed that the directions correspond. The portion, g , scattered in the

direction of the earth's surface is much greater than $\frac{1}{2}$ and is given by the following formula:

$$g = 1 - \exp(-1.837 \sin \gamma - 0.764) \quad (15)$$

The same transmission functions are required for the calculation of spectral diffuse solar radiation from a cloudless sky as for direct solar radiation.

Sky with Cloud Cover - Under a cloudy sky, $N=8$, spectral direct solar radiation is zero and spectral global radiation is equal to spectral diffuse radiation. Spectral global radiation under a cloudy sky is also calculated from the integral value of global radiation under cloud cover, VDI 3789, part 2 [9], and a wavelength-dependent weighting function $f_w(\lambda)$.

$$D_\lambda(\beta, 8) = G(\beta, 0) f_w(\lambda) \quad (16)$$

Under cloud cover, the global radiation depends only on the zenith angle β , not on the azimuth α . $f_w(\lambda)$ is determined based on the calculated spectral distribution according to Justus and Paris [10].

Partial Cloud Cover - Under a partly cloudy sky, it is assumed that the diffuse solar radiation can be divided into two portions. For the portion $(1 - N/8)$ of an hour, the diffuse radiation is equal to the diffuse radiation under a cloudless sky. For the portion $N/8$ of an hour, clouds cover the sun. The diffuse solar radiation during this time period is not $N/8$, but rather $N/8 f(N)$. $f(N)$ is a function of degree of cloud cover [3] and > 1 . The diffuse solar radiation under partial cloud cover is thus:

$$D(\beta, \alpha; N) = D(\beta, \alpha; 0) (1 - N/8) + D(\beta, \alpha; 8) N/8 f(N) \quad (17)$$

The wavelength dependence is determined by the functions $f_0(\lambda)$ and $f_w(\lambda)$, so that the spectral diffuse solar radiation is expressed by:

$$D_\lambda(\beta, \alpha; N) = D(\beta, \alpha; 0) (1 - N/8) f_0(\lambda) + D(\beta, \alpha; 8) N/8 f(N) f_w(\lambda) \quad (18)$$

Spectral Reflected Global Radiation

For $\beta \neq 0$ the surface receives a portion of the global radiation reflected at the earth's surface:

$$R_\lambda(\beta, \alpha) = \rho(\lambda) G_\lambda(0, \alpha; N) \quad (19)$$

with $\rho(\lambda)$ the spectral reflectance of the ground.

Spectral Irradiance

Spectral irradiance is the sum of the spectral irradiance levels from direct, diffuse and reflected radiation.

The following input parameters are required for the calculation:

- Geographic coordinates:
 - Geographic latitude
 - Geographic longitude
 - Altitude above NN

Date and time

Orientation of irradiated surface

Spectral reflectance of the ground

Meteorological data

- Degree of cloud cover
- Visibility
- Air temperature
- Relative humidity

Ozone concentration

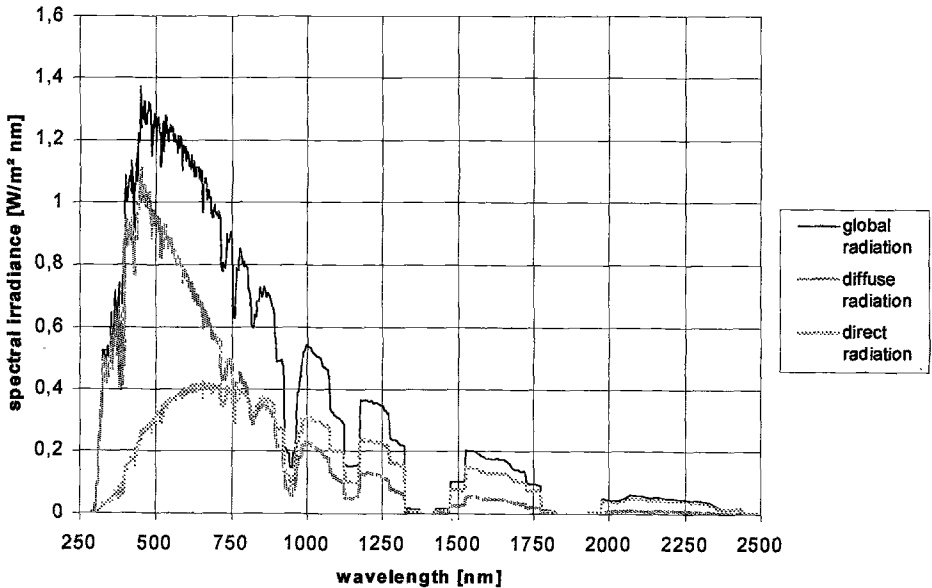


Fig. 1 Spectral irradiance levels for Miami on June, 21, at 12:00 real local time

Figure 1 shows an example of calculation for the parameters indicated. The varying spectral distributions for direct and scattered solar radiation are clearly recognizable. The program CESORA also allows for altering a parameter while the others remain constant. Figure 2 shows an example of this.

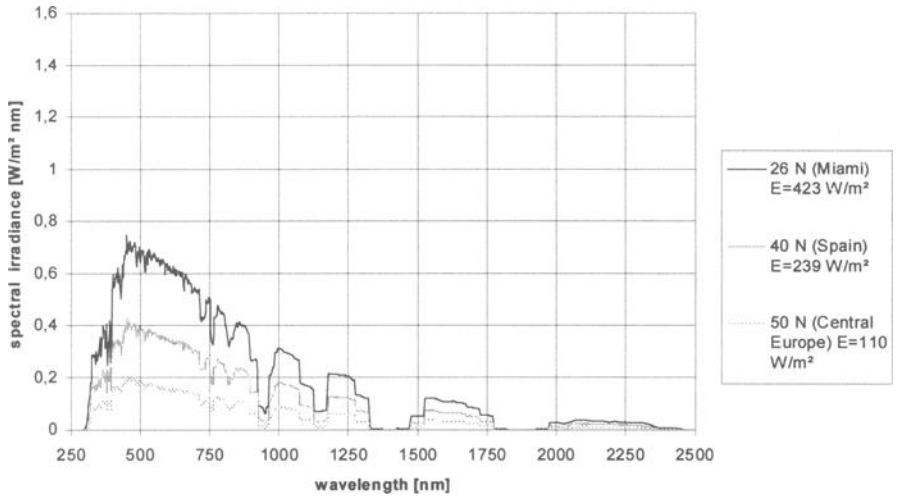
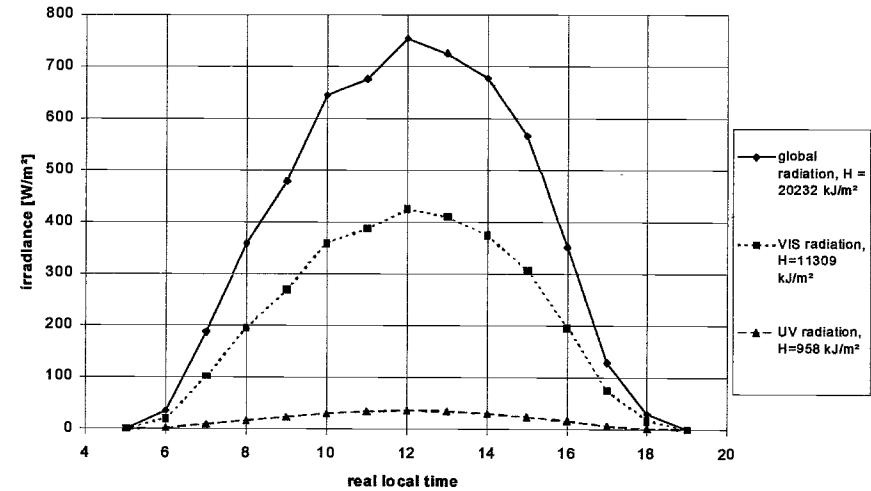


Fig. 2 Spectral global irradiance for three different locations on Dec. 21 at 12:00 real local time

The diurnal variation, e.g. for global radiation, can also be calculated. For this purpose one requires, in addition to the input parameters mentioned, the hourly mean meteorological data during the day under consideration. Figure 3 shows an example of this



time	0	1	2	3	4	5	6	7	8	9	10	11	12	13	14	15	16	17	18	19	20	21	22	23
tem perature	23	23	23	23	23	23	23	29	25	28	30	31	32	33	34	34	33	32	30	28	27	25	24	23
humidity	45	45	45	45	45	50	55	60	70	80	85	90	90	90	85	85	85	80	80	80	70	75	70	70
visibility	3	3	3	3	3	3	3	3	3	3	3	3	3	3	3	3	3	3	3	3	3	3	3	3
cloud cover	3	3	3	3	3	4	3	2	2	3	2	3	2	2	1	0	2	5	4	6	3	1	1	1

Fig. 3 Diurnal variation of global, visible and UV radiation for Miami on June 21, taking into account the meteorological data given on bottom of the diagram

Effective Spectral Irradiance

The effective spectral irradiance is the product of spectral irradiance and spectral sensitivity s_λ (see section 1.3)

$$E_{\lambda,eff}(\beta, \alpha; N) = s_\lambda E_\lambda(\beta, \alpha; N) \tag{20}$$

Figure 4 shows the example of effective spectral irradiance and effective irradiance in terms of discoloration of pigmented PVC [11,12].

Comparison with Other Calculations and Measurements

The method described above for calculation of spectral irradiance levels uses integral irradiance values according to VDI guideline 3789 part 2 [9]. The direct solar radiation is described accurately by the spectral transmittance functions. The aerosol content of the atmosphere is parametrized by the meteorological parameter visibility.

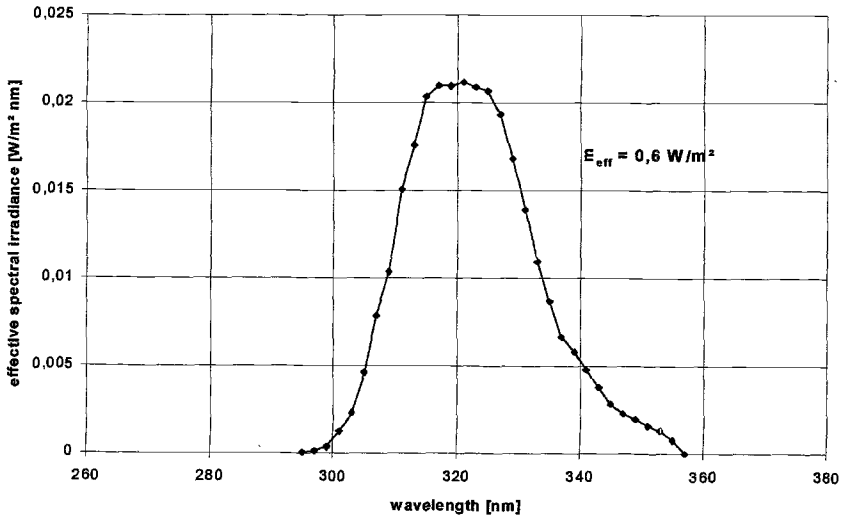


Fig. 4 *Effective spectral irradiance in terms of discoloration of pigmented PVC for Miami on June 21 at 12:00 real local time*

Under a cloudless sky, calculation of global radiation $G(0)$ is according to a formula derived from measurements. Nearly all measured values are within a range of $\pm 5\%$ of the calculated value [10]. As with direct solar radiation, atmospheric aerosol content is parametrized on the basis of visibility for global radiation as well.

Under cloud cover with a degree of coverage of $N=8$, calculation of global radiation $G(N)$ is done with an equation which is also derived from measurements [13]. The standard deviation of the measured hourly means is, due to the wide variability of cloud types and thicknesses, $\pm 25\%$. The error of $G(0)$, which is included in determination of $G(N)$, is much smaller and is negligible compared with the above value $\pm 25\%$.

Other Calculation Models

The main source of error in calculating solar radiation is the diffuse portion. For this reason, only the diffuse portion is compared below with the results of the highly complex calculation model HELIONDA [14]. The calculated values are listed in Table 1.

Table 1 *Irradiance of diffuse solar radiation on an upright wall facing south ($\alpha = 0^\circ$) or north ($\alpha = 180^\circ$), $D(90^\circ, \alpha; 0)$, at noon, calculated with the models HELIONDA and CESORA. γ = solar altitude, $\delta_a(500 \text{ nm})$ = spectral optical thickness of aerosol at a wavelength of 500 nm.*

α	γ	$\delta_a(500 \text{ nm})$	$D(90^\circ, \alpha; 0) / (\text{W/m}^2)$ HELIONDA	$D(90^\circ, \alpha; 0) / (\text{W/m}^2)$ CESORA
0°	41.8°	0.3	135	126
		0.6	178	164
	19.5°	0.3	129	148
		0.6	128	136
180°	41.8°	0.3	40	35
		0.6	73	64
	19.5°	0.3	34	36
		0.6	51	51

The agreement is quite close, with an error of 10% being reached only rarely.

To check relative spectral distribution, the CESORA results are compared with the generally recognized model of Justus and Paris [10], which is also used by CIE (International Commission on Illumination) [15]. The comparison is based on a horizontal surface. It was carried out for a large number of parametric combinations of solar altitude and visibility (atmospheric aerosol content), separately for direct and diffuse solar radiation and for global radiation. Figure 5 shows an example.

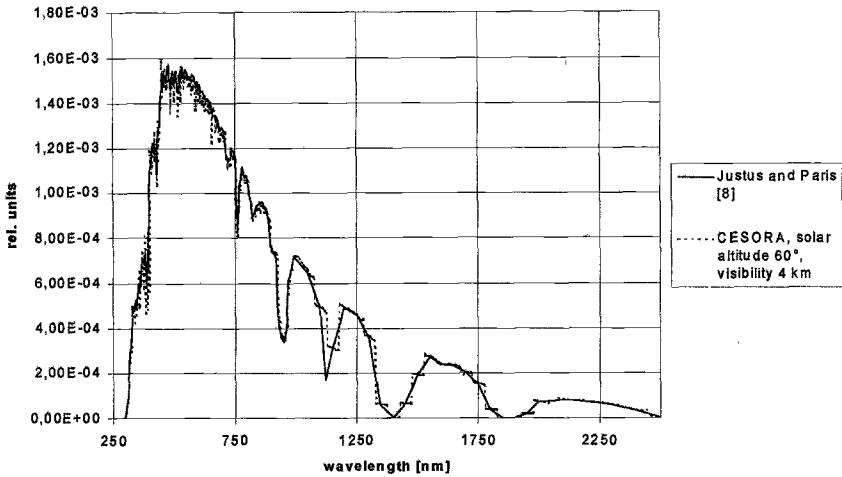


Fig. 5 *Standardized spectral irradiance of global radiation.*

The level of agreement is close. The differences result partly from the differing wavelength intervals in Justus and Paris and CESORA.

Individual Comparisons

Measurements in the Tropics - For purposes of comparison, measurements from Piazena [16] on two days in February in Antofagasta (23°S) were used. For these measurements, the integral values for direct solar radiation and global radiation were determined for the wavelength intervals 308-319 and 313-374 nm. Unfortunately, the article mentions the degree of cloud cover ($N=0$) only, but there is no information on visibility as a parameter for atmospheric aerosol content. The figures in the publication suggest a high visibility. The comparative calculations were therefore carried out for a visibility of 50 km. Table 2 contains the results:

Table 2 *Comparison of measured and calculated irradiance from direct solar radiation and global radiation for the wavelength ranges 308–319 and 313–374 nm. The bold figures are the measured values, the unit being W/m². The double figures indicate differing results on the two different days.*

		313 – 374 nm							
		Solar altitude							
		10	20	30	40	50	60	70	80
Global	radiation	3.6	9.2	15.0	20.3	24.7	28.2	30.7	32.2
		2.5	7.5	14.0	20.0	26.0	31.0	37.0	38.0
Dir. solar	radiation	0.1	2.0	5.7	10.3	15.0	19.1	22.3	24.3
		0.5	2.0	4.0	8.5/10.3	12.5/14.5	15.5/18.5	20/22	24.0
		308 – 319 nm							
		Solar altitude							
		10	20	30	40	50	60	70	80
Global	radiation	0.1	0.4	0.9	1.4	1.8	2.2	2.5	2.6
		0.1	0.3	0.6	1.0	1.4	1.8	2.1	2.4
Dir. solar	radiation	0.0	0.0	0.2	0.5	0.8	1.2	1.5	1.7
		0.03	0.05	0.15	0.3/0.4	0.5/0.7	0.85/1.05	1.05/1.25	1.45

On the whole, the agreement between measurement and calculation is satisfactory, both for the global radiation and for direct solar radiation.

Measurements in a Hot, Dry Climate -AUDI AG of Ingolstadt, Germany was so kind as to provide us with measurement results obtained for an automobile positioned along the north-south axis, facing the equator, on the company's own outdoor weathering grounds in South Africa. The radiation measurement was carried out on Febr. 13, 1997. Figure 6 shows a comparison of measurements taken at various points on the lateral parts of the car with the CESORA calculation. The level of agreement is good.

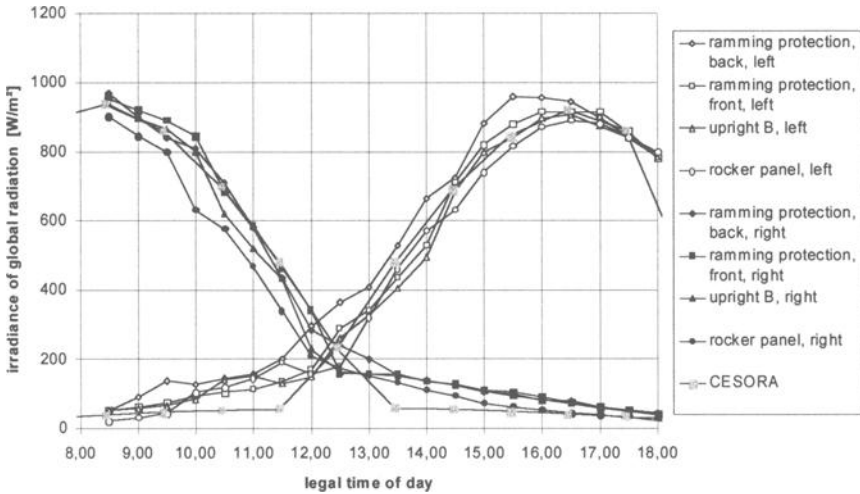


Fig. 6 Data calculated by CESORA compared with data measured in South Africa

Conclusion

The calculation program CESORA is useful for calculating the spectral irradiance of solar radiation in dependence on geographic location, meteorological conditions and sample position. By knowledge of the spectral sensitivity of a polymer material, mathematical lifetime prediction is possible. Comparisons with outdoor weathering results are in preparation.

References

- [1] Stuck, J.W., "Erfahrungen und neue Möglichkeiten bei der Schnellbewitterung", Atlas/DEK-Tagung 22 Oct., 1996, Gelnhausen.
- [2] Boxhammer, J. and Scott, K. P., "A comparison of new and established accelerated weathering devices in aging studies of polymeric materials at elevated irradiances and temperature", 3rd International Symposium on Weatherability of Materials Life Society, Tokyo, 14-16 May, 1997.
- [3] VDI 3789 Blatt 3: Umweltmeteorologie. Wechselwirkungen zwischen Atmosphäre und Oberflächen. Berechnung der spektralen Bestrahlungsstärke im solaren Wellenlängenbereich. Publication forthcoming, 1999.

- [4] Thekaekara, M. P., "Extraterrestrial Solar Spectrum, 3000-6100 Å at 1 Å-Intervals", *Applied Optics*, Vol. 13, 1974, pp. 518-522.
- [5] Neckel, H. and Labs, D., "Improved Data of Solar Spectral Irradiance from 0,33 to 1,25 μ ", *Solar Physics*, Vol. 74, 1981, pp. 231-249.
- [6] Dehne, K. and Kasten, F. "Die Spektren von extraterrestrischer Sonnenstrahlung und Globalstrahlung im UV als Grundlage für Referenz-Sonnentage", *Licht-Forschung* 5, 1983, pp. 85-87.
- [7] Iqbal, M. "An Introduction to Solar Radiation", Academic Press, Toronto, Canada, 1983.
- [8] Kasten, F. "Measurement and Analysis of Solar Radiation Data", *Performance of Solar Energy Converters*. Hrsg. G. Beghin. Reidel, Dordrecht/Niederlande, 1983, pp. 1-64.
- [9] VDI 3789 Blatt 2: Umweltmeteorologie. Wechselwirkungen zwischen Atmosphäre und Oberflächen. Berechnung der kurz- und langwelligen Strahlung, 1994.
- [10] Justus, C.G. and Paris, M.V., "A Model for Solar Spectral Irradiance and Radiance at the Bottom and Top of a Cloudless Atmosphere." *J. Clim. Appl. Meteor.*, Vol. 24, 1985, pp. 193-205.
- [11] Andradý, A.L., Torikai, A. and Fueki, K. "Photodegradation of Rigid PVC Formulations", I. Wavelength Sensitivity to Light-Induced Yellowing by Monochromatic Light", *J. Appl. Polym. Sci.*, Vol. 37, 1989, pp. 935-946.
- [12] Andradý, A.L. and Searle, N.D. "Photodegradation of Rigid PVC Formulations, II. Spectral Sensitivity to Light-Induced Yellowing by Polychromatic Light", *J. Appl. Polym. Sci.*, Vol. 37, 1989, pp. 2789-2802.
- [13] Kasten, F.; K. Dehne, H. D. Behr, U. Bergholter, "Die räumliche und zeitliche Verteilung der diffusen und direkten Sonnenstrahlung in der Bundesrepublik Deutschland", *Forsch. Ber. BMFT-FB-T84-125*, Deutscher Wetterdienst, Hamburg, 1984.
- [14] Thomalla, E., Meteorological Institute of University of Munich, Germany.
- [15] CIE, Technical Report "Solar Spectral Irradiance", Publ. No. CIE 85, 1989.
- [16] Piazena, H., "The Effect of Altitude upon the Solar UV-B and UV-A Irradiance in the Tropical Chilean Andes," *Solar Energy*, Vol. 57, No. 2, 1996, pp. 133-140.

Carl G. Cash¹

Estimating the Durability of Roofing Systems

Reference: Cash, C. G., “Estimating the Durability of Roofing Systems,” *Durability 2000: Accelerated and Outdoor Weathering Testing, ASTM STP 1385*, J. D. Evans and W. D. Ketola, Eds., American Society for Testing and Materials, West Conshohocken, PA, 2000.

Abstract: A method for the estimation of the durability of both steep and low sloped roofing systems is presented. The “thermal load” concept is defined. Each estimate is based on the thermal load at the exposure site, the presence of significant design, workmanship, and materials defects, and the generic roofing system proposed or selected. Examples show how to calculate the mean durability, and the durability adjusted for systemic defects for any of seventeen low- and steep-sloped roofing systems.

Thermal loads for many geographic locations and the thermal sensitivity factors for many roofing systems are provided.

Keywords: durability estimation, low-sloped roofing, roofing, steep-sloped roofing, thermal load, thermal sensitivity

Nomenclature

A	A constant in the Arrhenius equations that is characteristic of the product's failure mechanisms and sample size (years)
APP	Atactic polypropylene
BUR	Built-Up Roofing
CPE	Chlorinated polyethylene
CSPE	Chlorosulfanated polyethylene (Hypalon)
E	The activation energy in the Arrhenius equations (Joule)
EP	Ethylene-propylene rubber
EPDM	Ethylene-propylene-diene rubber
k	A Stefan Boltzmann constant (1.3806×10^{-23} Joules per degree Kelvin)
SBS	Styrene-butadiene-styrene block copolymer
T	Thermal load, mean horizontal surface temperature (Kelvin)
T'	Reference thermal load (Kelvin)
TPO	Thermoplastic polyolefin
t	Durability (years)
t'	Reference durability (years)

¹Carl G. Cash is a Principal and Vice President of Simpson Gumpertz & Heger Inc., Consulting Engineers and Building Pathologists, 297 Broadway, Arlington, MA 02474-5310.

Introduction

Our attempts to predict the performance of roofing systems, based on physical or chemical testing and various accelerated weathering programs has been disappointing because there seems to be no constant relationship between test performance and the service life observed in the field. Some test methods, such as heat aging in an oven, can be useful in comparing the future performance of similar materials, but are seldom reliable in predicting performance differences between the many types of materials sold in the roofing market.

A more practical and accurate method of estimating durability is based on the opinions expressed by the people in the roofing industry. We calculated the values for the activation energy and the Arrhenius constant "A" from empirical data we obtained from two surveys of NRCA members, mostly roofing contractors, conducted in 1995 for steep roofing [1] and 1996 for low-sloped roofing [2]. Using these survey data avoids the very severe problem of defining "failure;" a topic that could occupy much more space and time than is available for this presentation. Computation methods for the thermal load were previously reported [3].

Thermal Load

For this paper, thermal load is defined as the mean temperature of a horizontal surface of a roofing system at a specific location. The mean temperature is used, rather than a time weighted thermal load, as a measure of exposure because the average temperature - time curve follows the geometric figure "companion to a cycloid" and is symmetric about the mean temperature.

We all know that climate is more than temperature. It includes many interrelated factors including, but not limited to rain, wind, radiation, topography, and cloud cover, all of which influence the local temperature. In this concept, temperature is not a cause of deterioration, but rather a measure of total exposure.

We classified the service life responses from our surveys by the thermal load at the headquarters of each respondent. We plotted mean service life responses for each roofing system vs. thermal load, and computed the regression coefficient. These regression coefficients have low outliers, such as 0.74 for SBS polymer modified asphalt roofing and 0.75 for metal roofing. Sixteen other systems have coefficients that range from 0.92 to the 1.00 coefficient of asphalt built-up roofing with glass fiber felts. The average regression coefficient for the entire group, including outliers, is 0.92. This is a remarkable statistic considering the subjective nature of the estimates, the varying experience of the respondents, and supports the idea of using the thermal load as a useful measure of climatic exposure. Table 1 lists the individual regression coefficient, the mean life, and the minimum life for each system in the surveys.

This concept shows, that the mean local temperature of a material on a horizontal surface (the thermal load) is an accurate measure of the local climatic exposure for materials such as roofing systems, with the long service life most of these systems demonstrate. It may not be useful to predict the performance of materials or systems with short service lives because these systems are too sensitive to exposure. The use of temperature as a result of climatic activity, rather than a cause of that activity, probably explains why changes in materials due to outdoor exposure differ significantly from the changes due to oven exposure (where temperature is a cause of change, and which does not have the exposure to radiation and other climatic influences).

Estimating the Mean Durability

To use the Arrhenius rate of reaction [4] equation (1) to calculate the estimated durability, use the empirical constants from our steep- and low-sloped roofing surveys from Table 1 for the roofing systems under consideration.

$$t = A \exp[E/(kT)] \quad [1]$$

Table 1—Arrhenius Constants, Regression Coefficients, Mean and Minimum Lives

Roofing System	E*	A	Regression Coefficient	Mean Life, years	Min. Life
Natural Slate	2.916	0.0459	0.83	60.3	35.2
Clay Tile	4.470	0.0008	0.92	46.7	25.2
Asbestos- Cement Slates	3.172	0.0133	0.97	31.4	17.0
Metal Panels	1.218	1.3216	0.93	26.5	13.8
Coal-Tar Organic BUR	0.657	4.7269	0.95	23.0	12.2
Coal-Tar Glass BUR	1.955	0.1730	0.92	21.9	11.2
Asphalt Glass Shingles	1.891	0.1236	0.79	17.7	8.9
Asphalt-Organic Shingles	2.948	0.0130	0.93	17.5	9.3
Asphalt Glass BUR	0.657	3.3915	1.00	16.7	9.1
SBS Mod. Asphalt	0.288	7.7013	0.74	15.9	8.4
Asphalt Org. BUR	1.074	0.9557	0.93	14.7	7.3
EPDM	2.996	0.0088	0.95	14.2	7.0
PVC	5.544	0.000016	0.95	13.8	6.5
APP Mod. Asphalt	2.163	0.0651	0.92	13.7	7.1
CSPE-CPE	1.939	0.1086	0.99	12.8	6.5
EP-TPO	0.993	1.0556	0.93	12.7	6.0
Polyisobutylene	3.429	0.0212	0.95	10.6	4.8

* Joules x 10⁻²⁰

Appendix 1 provides the thermal load for white, gray, and black horizontal surfaces at many locations throughout the world.

Handling Major Defects

It is necessary to take into account the condition of the system when estimating the durability of an existing roof. Major defects can affect the service life of the system. Major defects are those conditions that have a direct influence on the system's service life. We consider the following as major defects, with the full understanding that there is probably no universal agreement on the conditions we select, and other defects can be added to this list, as appropriate. While it is not listed, human error is a major defect that can be present in any system, but is too difficult to quantify to be useful.

Major Defects:

- Water ponding on the surface. Zero slope in a low-slope system. Less than 25% slope (3 inches per foot) in a system intended for a steep-slope application.
- Lack of secure attachment to the structure.

- Inadequate or severely deteriorated flashing systems.
- Severe blistering, splitting or open laps.

Cut the estimated service life in half for each major defect present. This divides the estimate for the system with one major defect by two, with two major defects by four, with three major defects by eight, etc. This factor for the service life reduction is based solely on the author's experiences with a large number of roofs. While it is unsupported by data, it has been useful in our estimates of service life.

Estimate Calculations

The following examples show:

- How an estimate of mean service life of a proposed system can be calculated,
- How estimated service lives of competing proposed systems can be calculated, and
- How the remaining service life can be calculated, taking into account major defects.

Example 1— Calculating the service life estimate of a new roofing system.

Given: the proposed system is a gray "20-year" asphalt-glass fiber shingle, on a 33% slope, in New Orleans, Louisiana. The thermal load for gray materials at New Orleans is 307 Kelvin (Appendix 1). The activation energy "E" is 1.891×10^{-20} and the test statistic "A" is 0.02136. Using equation 1:

$$t = 0.1236 \exp[1.891 \times 10^{-20} / (1.381 \times 10^{-23} \times 307)] = 10.7 \text{ years}$$

This value suggests that an alternate system be used. Note: Our survey data are for "20-year" shingles, the commodity grade. Shingles with a longer projected service life are available.

Example 2— Calculating the estimated service life of two competing black systems. Given: The proposed roofing systems include properly drained asphalt built-up roofing with glass fiber felts, or an EPDM system, to be installed in Minneapolis, Minnesota. The thermal load for black systems in Minneapolis is 297 Kelvin (Appendix 1). The values for "E" and "A" are: 0.657×10^{-20} , 3.3915 for the BUR and 2.996×10^{-20} , 0.0088 for the EPDM. Substituting in equation 1:

$$\begin{aligned} (\text{BUR})t &= 3.3915 \exp[0.657 \times 10^{-20} / (1.381 \times 10^{-23} \times 297)] = 16.8 \text{ years} \\ (\text{EPDM})t &= 0.0088 \exp[2.996 \times 10^{-20} / (1.381 \times 10^{-23} \times 297)] = 13.1 \text{ years} \end{aligned}$$

These values suggest that the BUR should last 28% longer than the EPDM system.

Example 3— Calculating mean remaining service life of an existing system.

Given: a four year old APP modified asphalt system with gray surfacing in Kansas City, Missouri, with inadequate drainage due to plugged drains. The thermal load in Kansas City is 301. The "E" and "A" for an APP polymer modified asphalt roof is 2.163×10^{-20} , and 0.0651. Substituting in equation 1:

$$\begin{aligned} (\text{APP})t &= 0.0651 \exp[2.163 \times 10^{-20} / (1.381 \times 10^{-23} \times 301)] = 11.1 \text{ years} \\ (11.1/2) - 4 &= 1.6 \text{ years} \end{aligned}$$

This computation suggests the existing roof has a remaining life of about 2 years. Fixing the drains may enable the roof to last for an additional 9 years; probably well worth the effort and expense.

Example 4— Calculating the mean life of a system with many defects. Given: A one-year-old white asphalt-glass felt shingle roof in Buffalo, New York is showing some thermal splits. The slope is 17% and there is no underlayment. The thermal load in Buffalo is 286 (Appendix 1). The “E” and “A” is 1.894×10^{-20} , and 0.1236. Substituting in equation 1:

$$t' = 0.1236 \exp[1.894 \times 10^{-20} / (1.381 \times 10^{-23} \times 286)] = 14.9 \text{ years, if without defects.}$$

$$t = t'/2^3 \text{ (for three major defects)} = 14.9/8 = 1.9 \text{ years}$$

$$1.9 - 1 = 0.9 \text{ years}$$

Of course, with these defects, calculations are hardly necessary.

Acknowledgment

The work for this presentation was supported by the Principals and Associates of Simpson Gumpertz & Heger Inc. of Arlington, Massachusetts and San Francisco, California.

References

- [1] Cash, C. G., “Using Shingles for Steep Sloped Roofing,” Construction Business & Technology Conference & Expo, Providence, RI, Feb. 1997.
- [2] Cash, C. G., “The Relative Durability of Low Sloped Roofing,” *Fourth International Symposium on Roofing Technology*, NRCA-NIST, Gaithersburg, MD, Sept. 1997.
- [3] Cash, C. G., “Estimating the Mean Temperature of Horizontal Surfaces for Predicting the Durability of Thermally Sensitive Materials (Arrhenius Relationship),” *Dealing With Defects in Buildings*, Varenna, Italy, Sept. 1994.
- [4] Nelson, W., *Accelerated Testing*, John Wiley & Sons, New York 1990, p. 76.

Appendix 1—Thermal Loads at Various Locations, Kelvin

Area	Country	City	Black	Gray	White
Africa	Algeria	Alger	324	317	307
	Angola	Luanda	314	309	301
	Botswana	Maun	311	306	297
	Cameroon	Yaounde	313	308	300
	Chad	Faya	325	318	308
	Congo	Albertville	313	308	300
	Dahomey	Cotonou	314	309	301
	Ethiopia	Addis Ababa	300	296	289
	Gabon	Libreville	316	311	303
	Ghana	Accra	315	310	302
	Kenya	Mombasa	318	312	304
	Libia	Benghazi	310	305	297
	Mali	Gao	320	313	305
	Morocco	Rabat	308	303	295
	South Africa	Capetown	306	301	293
Antarctica		McMurdo Station	260	258	254
		South Pole Station	219	220	219
Asia-Far East	China	Guangzhou	314	308	300
		Lanzhou	298	293	285
		Shanghai	309	303	295
	Japan	Kushiro	277	274	268
		Tokyo	304	299	291
	Korea	P'yongyang	299	293	285
		Seoul	301	295	287
	Russia	Dubinka	274	270	264
		Omsk	287	282	275
	Verkhoyansk	269	265	258	
Asia-Middle East	Iran	Tehran	312	306	297
	Iraq	Bagdad	321	314	305
	Isreal	Jerusalem	309	304	296
	Jordan	Amman	310	304	296
	Kuwait	Kuwait	320	314	305
	Lebanon	Beirut	312	307	298
	Oman	Muscat	323	317	308
	Saudi Arabia	Dhahran	324	317	308
	Syria	Damascus	313	307	298
	Turkey	Ankara	304	299	290
	Izmir	312	306	297	
Asia - South	Afghanistan	Kabul	306	300	291
	India	Bangalore	311	305	298
		Calcutta	315	309	301
	Nepal	Katmandu	306	301	293
	Pakistan	Karachi	315	310	301
Asia-Southeast	Burma	Mandalay	317	311	302
	Cambodia	Phnom Penh	319	314	305
	Indonesia	Jakarta	317	311	303
	Malaya	Singapore	319	313	305
	Thailand	Bankok	318	312	304

Appendix 1—Thermal Loads at Various Locations, Kelvin (continued)

Area	Country	City	Black	Gray	White	
Australia	Australia	Adelaide	310	304	296	
		Brisbane	311	305	297	
Tasmania		Sidney	306	301	293	
New Zealand	Tasmania	Hobart	300	296	289	
	New Zealand	Dunedin	297	293	286	
		Wellington	300	295	288	
Central America	Belize		317	311	303	
	Costa Rica	San Jose	309	304	296	
	El Salvadore	San Salvador	316	310	302	
	Guatemala	Guatemala City	308	303	295	
	Honduras	Tela	317	312	303	
Europe	Panama	Balboa Heights	318	312	304	
	Albania	Durres	307	302	294	
	Austria	Vienna	299	294	286	
	Bulgaria	Sofia	301	296	288	
	Cyprus	Nicosia	315	309	300	
	Czech Rep.	Prague	298	293	286	
	Denmark	Copenhagen	298	293	286	
	Finland	Helsinki	294	289	282	
	France	Ajaccio	308	303	295	
		Paris	301	296	289	
	Georgia	Tbilisi	303	298	290	
	Germany	Berlin	298	293	286	
		München(Munich)	296	292	284	
	Gibraltar	Windmill Hill	306	301	294	
	Greece	Athens	311	306	297	
		Crete	310	305	297	
	Hungary	Budapest	302	297	289	
	Iceland	Reykjavik	290	286	280	
	Ireland	Dublin	297	292	286	
	Italy	Genova	307	301	294	
		Palermo	310	305	297	
		Rome	310	304	296	
		Latvia	Riga	295	291	284
		Luxembourg	Luxembourg	299	294	287
	Malta	Valletta	311	305	297	
	Monaco	Monaco	305	300	293	
	Netherlands	Amsterdam	298	293	286	
	Norway	Oslo	296	291	284	
	Poland	Gdansk	296	291	284	
	Portugal	Braganca	303	298	290	
Lisbon		306	301	294		
Romania	Bucharest	303	298	289		
Russia	Arkhangelsk	286	282	275		
	St. Petersburg	293	288	281		
	Moscow	294	290	282		

Appendix 1—Thermal Loads at Various Locations, Kelvin (continued)

Area	State	City	Black	Gray	White	
Europe (Cont.)	Serbia	Belgrade	304	298	291	
		Spain	Barcelona	306	301	293
			Madrid	306	301	293
			Sevilla	314	308	299
			Sweden	Gotenborg	296	291
			Stockholm	295	291	284
			Switzerland	Berne	298	293
		Turkey	Istanbul	305	300	292
		Ukraine	Odessa	300	295	287
		United Kingdom	Belfast	295	291	285
			Edinburgh	296	292	285
			London	300	295	288
			North America	Canada	Alert, NWT	266
			Calgary, Alta	293	288	280
			Charlottetown PEI	293	288	281
		Chatham, NB	293	288	281	
		Churchhill, Man	278	274	267	
		Edmonton, Alta	290	285	278	
		Fort Nelson, BC	287	282	275	
		Gander, Nfld	293	288	281	
		Halifax, NS	295	290	283	
		Montreal, Que	295	290	282	
		North Bay, Ont	294	289	281	
		Ottawa, Ont	296	290	283	
		Port Arthur, Ont	290	285	278	
		Prince George, BC	292	287	280	
		Quebec, Que	293	288	280	
		Regina, Sask	291	286	278	
		Resolute, NWT	266	263	258	
		St. John, NB	291	287	280	
		St Johns, Nfld	293	289	282	
		Saskatoon, Sask	289	285	277	
		Toronto, Ont	298	293	285	
		Vancouver, BC	300	295	288	
		Whitehorse, YT	286	282	275	
		Winnipeg, Man	290	285	277	
		Yellow Knife, NWT	282	277	270	
	Greenland	Angmagssalik	283	279	273	
		Nord	267	264	258	
		Scoresbysund	276	273	268	
	Mexico	Acapulco	319	313	305	
		Guadalajara	306	301	293	
		La Paz	318	312	303	
		Mazatlan	314	309	301	
		Mexico City	303	298	290	
		Monterrey	313	307	299	
		Tampico	315	310	302	

Appendix 1—Thermal Loads at Various Locations, Kelvin (continued)

Area	Country	City	Black	Gray	White
North America (cont.)	United States	Albuquerque, NM	303	298	293
		Anchorage, AK	282	279	276
		Ashville, NC	299	295	291
		Atlanta, GA	302	298	293
		Austin, TX	314	308	299
		Barrow, AK	269	266	260
		Birmingham, AL	311	305	297
		Boise, ID	306	300	292
		Boston, MA	293	292	288
		Brownsville, TX	316	310	301
		Buffalo, NY	299	294	286
		Cheyenne, WY	301	295	287
		Chicago, IL	302	296	288
		Cincinnati, OH	300	295	291
		Concord, NH	293	289	285
		Denver, CO	298	293	289
		El Paso, TX	311	305	296
		Fairbanks, AK	284	279	272
		Fargo, ND	290	286	282
		Hartford, CT	296	292	288
		Honolulu, HI	315	310	302
		Indianapolis, IN	303	298	290
		Jacksonville, FL	307	303	298
		Kansas City, MO	307	301	293
		Las Vegas, NE	316	310	300
		Los Angeles, CA	304	300	292
		Louisville, KY	307	301	293
		Miami, FL	315	310	301
		Minneapolis, MN	297	292	284
		New Orleans, LA	313	307	298
		New York, NY	304	299	291
		Nome, AK	280	276	270
		Oklahoma City, OK	309	303	295
		Phoenix, AZ	313	308	302
		Portland, ME	297	292	285
		Portland, OR	303	298	290
		Sacramento, CA	307	302	297
		Salt Lake City, UT	307	301	292
		San Diego, CA	299	296	292
		San Francisco, CA	301	297	290
		Sault Ste. Marie, MI	294	289	282
		Savannah, GA	306	301	297
Seattle, WA	301	296	289		
Spokane, WA	303	297	289		
Washington, DC	306	301	293		
Wilmington, NC	309	304	295		
Wilmington, DE	299	295	290		
Yuma, AZ	316	310	304		

Appendix 1—Thermal Loads at Various Locations, Kelvin (continued)

Area	Country	City	Black	Gray	White	
North Atlantic & Indian Ocean Islands	Tristan da Cunha	Tristan da Cunha	300	296	289	
	Ascension Is.	Georgetown	317	311	303	
Indian Ocean Islands	Azores	Horta	307	302	295	
	Canary Is.	Las Palmas	305	300	293	
	Cape Verde	Porto da Praia	315	309	302	
	Faeroes	Thorshavn	290	287	280	
	Fernando Po	Santa Isabel	318	312	394	
	Hebrides	Stornoway	294	290	284	
	Reunion Is.	Hellberg	304	299	292	
	Madeira	Funchal	307	302	295	
	Norway	Jan Mayen	281	278	273	
	Novaya Zemlya	Matochkin Shar	274	271	266	
	Seychelles	Port Victoria	317	311	303	
	Mauritius	Royal Albert Ob.	315	309	301	
	Sao Tome	Sao Tome	316	310	302	
	Shetlands	Lerwick	292	288	282	
	Svalbard	Gronfjorden	274	272	266	
	St. Helena	Hutts Gate	303	299	292	
	Pacific Islands	Bonin Islands	Iwo Jima	315	310	302
		Easter Island	Isla de Pascua	309	304	296
		Fiji Islands	Suva	316	311	303
		Marianas Is.	Guam	318	312	304
Mas a Tierra		Juan Fernandez	304	299	292	
Midway Is.			312	307	299	
Okinawa		Naha	315	309	301	
Phoenix Is.		Canton	320	315	306	
Samoa		Pago Pago	319	313	305	
Seymour Is.		Galapagos Is.	317	311	303	
South America	Argentina	Buenos Aires	309	304	296	
		La Quiaca	309	305	298	
		Santa Cruz	303	299	292	
	Bolivia	Concepcion	306	300	292	
		La Paz	305	301	294	
	Brazil	Brasilia	306	301	293	
		Rio de Janeiro	312	307	299	
		Sao Paulo	298	293	285	
	Chile	Santiago	313	308	300	
		Valparaiso	304	299	292	
	Columbia	Bogota	305	300	294	
		Cartagena	304	298	290	
	Equador	Quito	293	289	282	
	Guyana	Georgetown	298	293	285	
	Paraguay	Asuncion	311	305	296	
	Peru	Cusco	293	288	281	
	Surinam	Paramaribo	310	304	296	
	Uruguay	Montevideo	303	298	290	
	Venezuela	Caracas	299	294	287	

Appendix 1—Thermal Loads at Various Locations, Kelvin (continued)

Area	Country	City	Black	Gray	White
South Atlantic Islands	South Georgia	Cumberland Bay	283	280	274
	South Orkneys	Laurie Island	271	268	264
	Falkland Islands	Stanley	290	286	280
West Indies	Bahamas	Nassaau	318	312	304
	Barbados	Bridgetown	317	311	303
	Bermuda	Hamilton	313	308	300
	Cuba	Havana	317	311	303
	Haiti	Port-au-Prince	321	315	306
	Martinique	Fort-de-France	317	311	303
	Puerto Rico	San Juan	311	306	298

P. B. Adams,¹ and H. Ben Tre'²

The Durability of Modern Sculptures Constructed of Glass

Reference: Adams, P. B. and Ben Tre', H., "The Durability of Modern Sculptures Constructed of Glass," *Durability 2000: Accelerated and Outdoor Weathering Testing, ASTM STP 1385*, J. D. Evans and W. D. Ketola, Eds., American Society for Testing and Materials, West Conshohocken, PA, 2000.

Abstract: A large water fountain sculpture has been installed in a city park. The fountain incorporates glass castings whose resistance to environmental effects is not well understood. A study of the glass properties and accelerated environmental tests predict that the sculpture will remain relatively unchanged for 20 years or more.

Keywords: glass, weathering, sculpture, prediction, water, environment

Introduction

The task of the sculptor is more than just fashioning an interesting art object. He is often seeking to create a new and different experience by trying a new material. This can lead to new challenges, as well as new opportunities.

In the mid-1970's, H. Ben Tre' pioneered the use of large-scale glass castings for interior sculpture installations. The glass castings offer the opportunity to create unique interactions with light since thickness and angularity can be dramatically varied to incorporate angles and edges that add aesthetic interest. The large castings permit a variety of inclusions, such as bubbles, glass inhomogeneities and other "foreign" features to be present. The large objects also display fractures and folds in a dramatic manner.

All of these factors can be enhanced, modified or subdued by the character of the surface of a glass casting. It can be polished, sand blasted or pitted. It can be further

¹Glass Consultant, Precision Analytical, 300 S. Madison Ave., Watkins Glen, NY 14841.

²Sculptor, 114 Morris Ave., Providence, RI 02906.

varied by taking advantage of the unique topography created on the surface where the casting contacts the mold, or the mold release material. The sculptor's objective is to control the various factors so as to produce a positive and definitive aesthetic experience for the observer.

If he achieves this goal, he must then assure himself that the sculpture will continue to interest the viewer for many years to come. However, if the object is to be used in an environment substantially harsher than indoors, he has to consider the possibility that it may deteriorate more readily. This could put the viewing experience at risk and the sculpture may fail to provide a positive long-term experience.

This paper addresses some of the issues that arose when glass was used in a new way in a fountain sculpture in Post Office Square in Boston (Fig. 1).

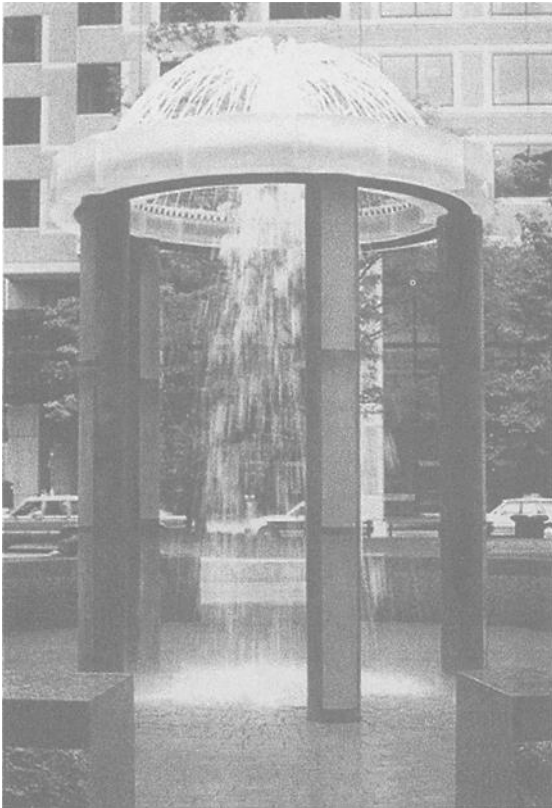


Figure 1 - *Columnar Fountain in Post Office Square*

Description of the Fountain

The fountain structure consists of five columns with a circular crown also constructed of glass. The columns are composed of three one meter sections, each of which includes a glass component, about 15x20x100 cm, that has been backed with bronze.

The glass segments had been reshaped from rough glass castings. The face of the glass that is exposed in the finished column had been formed against a bed of sand. The glass was a borosilicate, presumed to be the same composition as that used in chemically resistant PYREX[®] brand products.

Water, controlled at pH 6 to 8, cascades over the structure about fourteen hours each day for eight months of the year. After 4 or 5 years in service, some observers believed that changes, perhaps pitting, of the glass surface were

occurring. There was a concern that such changes might be an omen of severe appearance degradation and/or structural defects, such as cracks in the glass.

Experimental Program

The general objective of the program was to estimate the practical life of the fountain sculpture. This involved determining whether changes were, in fact, occurring, as well as whether the glass had the inherent capability to withstand the environment for many years.

Tests were therefore done to characterize the glass and to try to induce degradation of the surface by simulating various environmental factors that were most likely to be involved. The general approach and the nature of glass weathering has been documented [1-4].

It was not possible to obtain glass samples from the fountain for testing in the laboratory. Therefore samples were taken from segments that had been manufactured concurrent with those in the fountain, but which had never been exposed to the fountain environment.

Glass Characterization

Surface Appearance - On close inspection, the surface topography is seen to be quite rough (Fig. 2). It is typified by "valleys and hills" on a scale of about 5 to 10 mm.

Superimposed on these are smaller bumps and depressions on a scale of 0.5 mm or less. Some exhibit a clean, pristine glass surface whereas others show a roughened surface that suggests the presence of fine grained deposits. Additionally, some of the "hill tops" have a clear glass flat that under the microscope shows the features of a surface that could have had a small flake chipped from it (Fig. 3).

Bulk Character - For the most part, the glass is clear and colorless. However it contains a variety of inclusions. There are many bubbles, usually in fan-like arrays.

Cords, string-like inhomogeneities, are also present. There are some blade-like inhomogeneities that extend from the surface to a depth as much as 1 cm. They breach the free surface, leaving a line or groove that is visible at the surface (Fig. 4).

Chemical Compositions - The chemical composition of the underlying base glass and its surface, including some of the "deposits" was estimated using the XRED mode of the Scanning Electron Microscope (Table 1). There is no doubt that the base glass is a borosilicate, similar, but not necessarily identical to the glass used in making PYREX Brand chemically resistant glass products. The deposits on the surface have a composition that is consistent with feldspar sand, the release material used when the glass was poured and molded.

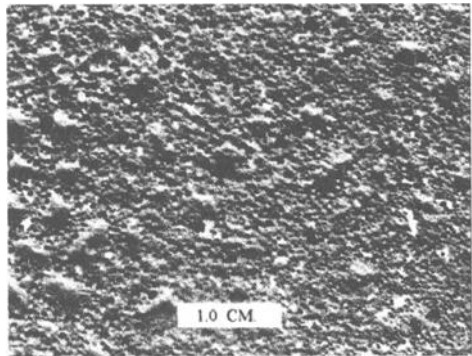


Figure 2 - *Closeup of Surface*

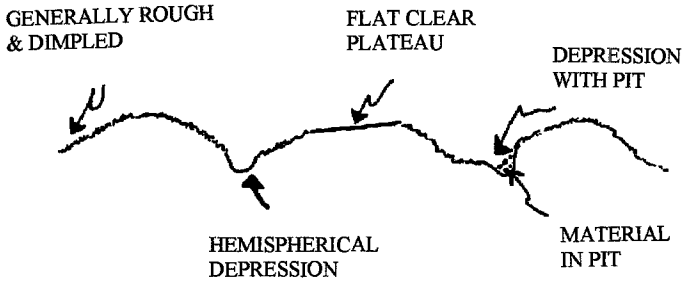


Figure 3 - Schematic Cross-Section Showing Surface Topography

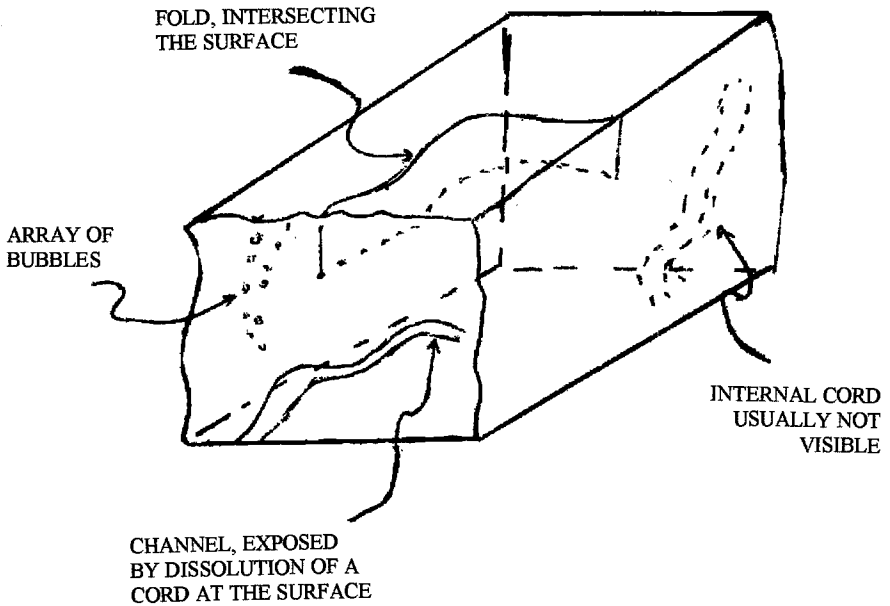


Figure 4 - Schematic View of Internal Features

Table 1 - *Composition of Glass and Mineral Deposits*

Sample	Composition ¹ Metallic Elements	Probable Material
Glass	Si, Al, Na	Borosilicate Glass
Deposit 1	Si, Fe, Zr, Al, Na	Albite Feldspar + Zr & FeO
Deposit 2	Si, Zr, K, Al, Na	Anorthoclase Feldspar + ZrO ₂
Deposit 3	Si, K, Al, Na	Anorthoclase Feldspar

¹Listed in order of decreasing concentration.

Glass Solubility - The glass castings were cooled slowly after being poured into the mold. It is known that a borosilicate glass of the type used here can, if cooled too slowly, undergo phase separation which in turn may increase the solubility of the glass. Tests were therefore done to measure its solubility using the "Test Method for Resistance of Glass Containers to Chemical Attack - Test Method P-AW ASTM C-225". The results show that the base glass is about 8 times more reactive with water than would be expected from a properly manufactured chemically resistant borosilicate glass of the PYREX[®] Brand type (Table 2).

Table 2 - *Solubility Test with ASTM C-225*

Sample Source	Test Results ¹
NO. 1 GLASS SEGMENT	6.9
NO. 2 GLASS SEGMENT	8.5
NORMAL BOROSILICATE GLASS	1.0

¹Results are expressed as ml. of 0.02 N. H₂SO₄ to neutralize the sodium extracted by the test.

Surface Degradation Tests - The first question was the possible reaction with atmospheric factors. It was concluded that agents, such as rain, snow, humidity, temperature changes, pollutants, etc., would be overshadowed by the constant wetting and drying conditions of fountain operation. Thus, it was decided to study the factors that were associated with the fountain itself. Laboratory experiments were designed where the processes could be accelerated, other variables could be introduced, and the effects on the samples could be observed to provide data for prediction of long-term effects [2,3].

Tests were made under static conditions, meaning no interspersed drying time as was the case in the fountain operation. They continued for periods up to 2 months at 60°C to accelerate any reactions. Samples were inspected periodically. The final results when each test was terminated have been assembled (Table 3). Under these conditions of continuous exposure to the solvent, a one month test is estimated to be equivalent to approximately 5

full years in the park. This assumes that the rate of acceleration is about a factor of 2 for every 10°C increase in temperature [2] and takes into consideration the fact that the fountain operates only about half of the year. The tests were done with city water from Post Office Square as well as with deionized water. Acidic water (pH 4) and alkaline water (pH 9) were also used to simulate worst case conditions in the fountain.

Tests were also made under cycling conditions to create alternate wet and dry conditions as occurs in fountain operation (Table 3). Water at 60°C was passed over the sample for 30 minutes, followed by a 30 minute drying period. In this case, a test period of one month was estimated to be equivalent to approximately two and a half full years [2], since the solvent exposure time per day is only half what it was for the static tests.

Neither the dynamic or static tests showed any evidence of the formation of pits, additional to what were present before test. There was some "brightening" of the initial surface so that depressions as well as bumps were more apparent. This is probably due to loss of the roughened character which results from the adhered sand. Some samples seemed to become slightly duller. This could be attributed to leaching, or selective extraction of alkali, from the underlying glass. The effect was more obvious on surfaces that were initially polished. They were iridescent and/or dull in many cases. The tests in mild acid (pH4) and mild alkali (pH9) did not show any effects that were significantly different than the tests in water. Tests in deionized water indicated slightly greater reaction rate than the tests in "Boston water", a result consistent with expectations [2]. The cycling fountain tests did not indicate that the constant wetting and drying was accelerating surface degradation.

Conclusions

The surface as it is formed is extremely uneven, with bumps and depressions. Many of these depressions have a glassy surface and some have material adhered to them. The surface has been modified by adherent and fused material, probably feldspar sand.

Although the glass is inherently somewhat more soluble than a high quality borosilicate, there is no evidence that this lessened resistance is a significant factor in any surface change seen to date at the fountain site.

In spite of the fact that the glass used in the fountain is somewhat imperfect, solution tests show no evidence to indicate that it is being eroded or that pits are being created. Rather, the pits, and the peaks seem to have material adhered that is removed during fountain operation.

The tests are believed to be predictive on a one to one basis up to approximately 5 years. Given the fact that the effects seen are minimal, there should be very little if any significant physical change for a much longer period, the order of 20 years or more. Any long range effects will probably result from the general corrosion of the base glass. This may be exhibited as a change toward a somewhat dulled and "sandblasted" look. There is no reason to believe that the glass will develop cracks or fractures as a direct result of any surface degradation caused by the fountain water reactions.

Table 3 - Surface Degradation Tests at 60°C

Surface Character	Solvent Circulation	Solvent	Appearance at end of test	Test Duration at 60°C (Days)	Equivalent Exposure at 20°C (Yrs)	
Molded	Static	City water	Slightly dulled	26	2	
			No Change	59	5	
			Slightly dulled	59	5	
			Slightly brighter on peaks	70	6	
	Cycle	DI water	City water	Slightly brighter on peaks, in pits	70	6
				Slightly dulled	26	1
		City water	No change	22	1	
			No change	22	1	
			No change	22	1	
Polished	Static	City water	Hazy. Grooved	26	2	
			Slightly hazed	26	2	
			Slight iridescence, haze	59	5	
			Slight haze	59	5	
			No change	59	5	
			Hazy	70	6	
			Iridescent	70	6	
	Cycle	City water	Slight Haze,, Grooved.	26	1	
			Slight Haze	26	1	
			Slight iridescence, haze	22	1	
			Slight iridescence, haze	22	1	
			Slight iridescence, haze	22	1	
			Slight iridescence, haze	22	1	
Molded	Static	Dil. Acid	Slightly brightened	70	6	
		Dil. Alkali	Brighter Peaks, Deposits gone	35	3	
Polished	Static	Dil Acid	Slight iridescence	70	6	
			No change	61	5	
		Dil Alkali	Stained, Iridescent	35	3	

References

- [1] Walters, H.V. and Adams, P.B., "Effects of Humidity on the Weathering of Glass," *Journal of Non-crystalline Solids*, 1975, 19, pp. 183-199.
- [2] Adams, P.B., "Glass Containers for Ultrapure Solutions," *Ultrapurity*, M. Zeif, Ed., Marcel Dekker, NY, 1972, p. 293.
- [3] Adams P.B., "Predicting Corrosion," *Corrosion of Glass, Ceramics and Ceramic Superconductors*, D.E. Clark and B.K. Zoitos, Eds., Chapter 2, Predicting Corrosion. Noyes Publications, Park Ridge, NJ, 1991, pp. 29-50.
- [4] Adams, P.B., "Predicting the Resistance of Inorganic Architectural Materials to Appearance Degradation in Natural and Polluted Environments," *Ceramic Bulletin*, Vol. 61, No.11, Nov. 1982, pp. 1224-1227.